UNIVERSIDADE FEDERAL DE MINAS GERAIS

Escola de Engenharia

Programa de Pós-Graduação em Engenharia Metalúrgica, Materiais e de Minas

Paula Maria Gomes Cunha Leão

BRIQUETES AUTORREDUTORES DE PELLET FEED E BIOCHAR DE BAGAÇO DE CANA-DE-AÇÚCAR PARA USO EM ALTOS-FORNOS: DESEMPENHO DE REDUÇÃO E CARACTERIZAÇÃO ESTRUTURAL AVANÇADA

SELF-REDUCING BRIQUETTES OF PELLET FEED AND SUGARCANE BAGASSE BIOCHAR FOR BLAST FURNACE APPLICATION: REDUCTION PERFORMANCE AND ADVANCED STRUCTURAL CHARACTERIZATION

Belo Horizonte

2026

Paula Maria Gomes Cunha Leão

BRIQUETES AUTORREDUTORES DE PELLET FEED E BIOCHAR DE BAGAÇO DE CANA-DE-AÇÚCAR PARA USO EM ALTOS-FORNOS: DESEMPENHO DE REDUÇÃO E CARACTERIZAÇÃO ESTRUTURAL AVANÇADA

Tese apresentada ao Programa de Pós-Graduação em Engenharia Metalúrgica, Materiais e de Minas da Universidade Federal de Minas Gerais, como requisito parcial para a obtenção do título de Doutora em Engenharia Metalúrgica, Materiais e de Minas.

Orientador: Prof. Dr. Maurício Covcevich Bagatini

Belo Horizonte
2026

Leão, Paula Maria Gomes Cunha.
L437b Briquetes autorredutores de Pellet Feed e Biochar de bagaço de cana-de-açúcar para uso em altos-fornos [recurso eletrônico]: desempenho de redução e caracterização estrutural avançada / Paula Maria Gomes Cunha Leão. – 2026.
1 recurso online (163 f.: il., color.): pdf.

Orientador: Maurício Covcevich Bagatini.
Tese (doutorado) - Universidade Federal de Minas Gerais, Escola de Engenharia.

Inclui bibliografia.
Exigências do sistema: Adobe Acrobat Reader.

1. Engenharia metalúrgica – Teses. 2. Metalurgia extrativa -Teses.
3. Biochar – Teses. 4. Pirólise – Teses. 5. Altos-fornos – Teses.
6. Briquetes (Combustível) – Teses. I. Bagatini, Maurício Covcevich.
II. Universidade Federal de Minas Gerais. Escola de Engenharia. III. Título.

CDU: 669(043)

Ficha catalográfica elaborada pela Bibliotecária Letícia Alves Vieira CRB/6 2337
Biblioteca Prof. Mário Werneck, Escola de Engenharia da UFMG

UNIVERSIDADE FEDERAL DE MINAS GERAIS
ENGENHARIA - COLEGIADO DE PÓS-GRADUAÇÃO EM ENGENHARIA METALÚRGICA MATERIAIS E DE MINAS - SECRETARIA

ATA DE DEFESA DE TESE

Às 14 horas do dia 06 (seis) de fevereiro de 2026, na sala 1010 do Bloco III, localizada no Prédio da Escola de Engenharia da UFMG, realizou-se a sessão pública para a defesa da Tese da aluna **Paula Maria Gomes Cunha Leão**, para a obtenção do grau de Doutora em Engenharia Metalúrgica, Materiais e de Minas, na área de concentração de Metalurgia Extrativa e Meio Ambiente. O presidente da sessão, Prof. Maurício Covcevich Bagatini, orientador da aluna, apresentou a comissão examinadora, composta pelo Prof. Cláudio Batista Vieira - Dr. (UFOP), Prof. Ismael Vemdrame Flores - Dr. (UFRJ), Valdirene Gonzaga de Resende - Drª (VALE S.A.) e Fabrício Vilela Parreira - Dr. (VALE S.A). Em seguida, a candidata fez a apresentação do trabalho que constitui sua Tese de Doutorado, intitulada: **"Briquetes Autorredutores de Pellet Feed e Biochar de Bagaço de Cana-de-Açúcar para Uso em Altos-Fornos: Desempenho de Redução e Caracterização Estrutural Avançada"**. Após a apresentação, os examinadores procederam à arguição da candidata. Concluída essa etapa, a comissão reuniu-se em caráter reservado, sem a presença da candidata e do público, e decidiu por **APROVAR** a Tese de Doutorado. O resultado final foi comunicado publicamente à candidata pelo presidente da sessão. Não havendo mais nada a tratar, o presidente encerrou a sessão e lavrou a presente ata, que, após lida, foi assinada pelos membros da comissão examinadora e pelo coordenador do Programa.

Belo Horizonte, 06 de fevereiro de 2026.

Assinatura dos membros da banca examinadora:

Documento assinado eletronicamente por **Ismael Vemdrame Flores**, **Usuário Externo**, em 20/02/2026, às 09:44, conforme horário oficial de Brasília, com fundamento no art. 5º do Decreto nº 10.543, de 13 de novembro de 2020.

Documento assinado eletronicamente por **Fabricio Vilela Parreira**, **Usuário Externo**, em 20/02/2026, às 10:21, conforme horário oficial de Brasília, com fundamento no art. 5º do Decreto nº 10.543, de 13 de novembro de 2020.

Documento assinado eletronicamente por **Valdirene Gonzaga de Resende**, **Usuária Externa**, em 20/02/2026, às 22:08, conforme horário oficial de Brasília, com fundamento no art. 5º do Decreto nº 10.543, de 13 de novembro de 2020.

Documento assinado eletronicamente por **Claudio Batista Vieira**, **Usuário Externo**, em 21/02/2026, às 21:35, conforme horário oficial de Brasília, com fundamento no art. 5º do Decreto nº 10.543, de 13 de novembro de 2020.

Documento assinado eletronicamente por **Mauricio Covcevich Bagatini**, **Professor do Magistério Superior**, em 23/02/2026, às 17:34, conforme horário oficial de Brasília, com fundamento no art. 5º do Decreto nº 10.543, de 13 de novembro de 2020.

Documento assinado eletronicamente por **Gilberto Rodrigues da Silva**, **Subcoordenador(a)**, em 01/04/2026, às 11:41, conforme horário oficial de Brasília, com fundamento no art. 5º do Decreto nº 10.543, de 13 de novembro de 2020.

A autenticidade deste documento pode ser conferida no site https://sei.ufmg.br/sei/controlador_externo.php?acao=documento_conferir&id_orgao_acesso_externo=0, informando o código verificador **4964219** e o código CRC **174D3107**.

Referência: Processo nº 23072.209339/2026-79 SEI nº 4964219

Dedico esta Tese ao meu esposo João Paulo, aos meus pais Olívio e Maria das Graças, e à minha irmã Maria Olívia.

AGRADECIMENTOS

Agradeço, primeiramente, a Deus pela força e pela determinação concedidas ao longo de toda esta caminhada. Por iluminar meus passos, renovar minhas esperanças e me amparar nos momentos de maior incerteza. Sem Sua presença constante, esta conquista não seria possível. Agradeço, também, por colocar no meu caminho todas as pessoas que contribuíram para a realização deste trabalho.

À minha família, deixo minha profunda gratidão pelo apoio incondicional e pela compreensão nos períodos de ausência. Aos meus pais, Olívio e Maria das Graças, agradeço por não medirem esforços para minha formação. Por cada sacrifício, renúncia, incentivo e cuidado dedicados ao longo de toda a minha trajetória. Carrego comigo os valores e a educação que sempre me transmitiram. À minha irmã, Maria Olívia, agradeço pela parceria e pelas longas horas de conversas e desabafos, que tornaram mais leves os desafios e mais especiais as conquistas. Obrigada por ter "segurado a barra" nos momentos em que eu não pude estar presente.

Ao meu esposo e companheiro de vida, João Paulo, agradeço pelo amor, pela paciência e pela compreensão diante das longas horas de dedicação e de ausência e nos momentos mais desafiadores desta jornada. Agradeço pela força que me ofereceu quando a minha faltou, por ser meu maior incentivador e por me fazer acreditar em mim todos os dias. Seu incentivo diário e sua fé no meu potencial foram fundamentais para que eu chegasse até aqui. Externo também minha gratidão a toda a sua família, em especial aos seus pais, Elísio e Ana.

Às minhas amigas, Joanna, Betina, Maria Mariana, Andressa, Bárbara e Luana, agradeço pela amizade de uma vida inteira. Obrigada pelas palavras de incentivo, pela escuta atenta e pelo acolhimento generoso nos momentos em que esta jornada parecia pesada demais.

Ao meu orientador, Maurício Bagatini, agradeço por acreditar em mim e no meu trabalho, pela oportunidade de crescimento profissional e pela orientação acadêmica. Obrigada por todos os ensinamentos compartilhados, que ultrapassaram as fronteiras deste trabalho, pelos incentivos constantes e por trilhar esta jornada comigo. Aos colegas e professores Ismael Flores e Antônio Marlon, agradeço pela parceria no desenvolvimento de novos projetos.

Aos alunos e ex-alunos do Laboratório de Processo Siderúrgico (LPS), agradeço pela convivência diária, pelas discussões técnicas, pelo apoio mútuo e pela parceria que tornaram esta jornada mais leve e enriquecedora. Aprendi com cada um de vocês muito mais do que poderia imaginar, não apenas sobre ciência e pesquisa, mas também sobre colaboração, dedicação e amizade. Seria impossível citar nomes individualmente, pois cada um contribuiu de maneira única para minha trajetória e deixou sua marca nesta etapa da minha vida acadêmica.

Ao Programa de Pós-Graduação em Engenharia Metalúrgica, Materiais e de Minas (PPGEM) e seus professores, agradeço pela formação sólida e pelo compromisso constante com a qualidade do ensino. Ao coordenador do curso, professor Eduardo Nunes, registro minha sincera gratidão por nunca medir esforços para resolver as questões pendentes, pela dedicação e disponibilidade em nos ouvir e orientar. E, de modo igualmente especial e carinhoso, agradeço a Cida, não apenas pelo auxílio incansável ao longo de toda esta caminhada, mas também pela amizade que nasceu desse convívio e foi marcada por cuidado, generosidade e apoio nos momentos em que mais precisei.

À professora Augusta Isaac, expresso minha gratidão pelo conhecimento compartilhado e pela generosidade com que me guiou em uma área, até então, desconhecida. Obrigada por me incentivar a conquistar novos espaços, por ampliar meus horizontes e por acreditar no meu potencial.

Agradeço a toda a equipe do DEMET e do DEMIN, em especial, a Alexandra Mansur, aos professores Dagoberto Brandão Santos, Andreia Bicalho e Pedro Henrique Pereira e aos técnicos Tiago, Fernando, Diego, Patrícia, Ricardo, Kelly, Leo e Alberto. Foi um privilégio compartilhar este percurso com vocês e aprender diariamente com cada um. Aos amigos Guilherme Otávio, Daisa Alves, Amanda Oliveira e Filipe Tironi, agradeço pela amizade construída, que trouxe respiro aos momentos mais intensos e que levarei comigo para além desta etapa.

À Universidade Federal de Minas Gerais (UFMG), agradeço pela formação recebida e pela infraestrutura que possibilitou o desenvolvimento desta pesquisa e a todos os seus funcionários, que, com sua presença constante, fizeram parte do meu dia a dia durante essa caminhada.

À Coordenação de Aperfeiçoamento de Pessoal de Nível Superior (CAPES), agradeço pelo suporte financeiro que viabilizou a execução deste estudo.

Ao Centro de Desenvolvimento da Tecnologia Nuclear (CDTN), agradeço pelos recursos disponibilizados ao longo deste estudo. Registro meu agradecimento a José Domingos Ardisson, Sergio Reis e Juliana Xavier (Granioter), cuja colaboração na realização das análises laboratoriais foi fundamental para a qualidade e o desenvolvimento deste trabalho. Agradeço, de forma mais que especial, a Adriana Albuquerque, que, de maneira tão generosa, se tornou uma grande incentivadora do meu trabalho, abrindo portas que eu jamais poderia imaginar. Alguém que sempre foi como família se transformou, também, em uma companheira de trabalho e colaboradora, oferecendo apoio e incentivo que marcaram profundamente esta trajetória. Serei eternamente grata a você.

Agradeço à Tecnosulfur, em especial a Álvaro Guimarães e a João Victor Rocha, bem como à equipe dos laboratórios de análises vinculados ao setor de Controle de Qualidade, que gentilmente contribuíram com análises essenciais à realização deste trabalho.

Ao Centro de Tecnologia de Ferrosos (CTF) da Vale S.A., agradeço pela confiança no meu trabalho e pelo apoio técnico e financeiro que contribuíram para o desenvolvimento desta pesquisa. Em especial, aos pesquisadores Fabrício Parreira e Sílvio Maranha, pela dedicação para que esse projeto fosse realizado e por todas as suas contribuições.

À Tecnored Desenvolvimento Tecnológico S.A., em nome do Manoel Gonçalves, agradeço pela parceria e pela colaboração na produção dos briquetes analisados neste estudo, contribuindo de forma decisiva para a concretização deste trabalho.

Aos membros das bancas de qualificação e defesa, deixo meu sincero reconhecimento pela leitura atenta, pelas críticas construtivas e pelas sugestões que enriqueceram significativamente este estudo.

Finalizo este trabalho com a sensação de dever cumprido e com profunda gratidão a todos que compartilharam esta caminhada comigo. Cada gesto, palavra ou apoio recebido foi essencial para a concretização deste sonho.

“Conheça todas as teorias, domine todas as técnicas, mas ao tocar uma alma humana, seja apenas outra alma humana.”

Carl Gustav Jung

RESUMO

O uso de biomassa em briquetes autorredutores constitui uma alternativa promissora para reduzir o consumo de combustíveis fósseis e as emissões de CO_2 na indústria siderúrgica. Esta Tese tem como objetivo investigar o desempenho de redução e de resistência mecânica de briquetes autorredutores contendo *pellet feed* e biochar de bagaço de cana-de-açúcar, visando sua aplicação como carga complementar em altos-fornos. No Artigo 1, avaliou-se a influência da temperatura de pirólise do biochar (250, 400 e 550 °C) sobre o comportamento dos briquetes produzidos em escala laboratorial, enquanto o Artigo 2 investigou a evolução estrutural desses aglomerados, ampliando a compreensão dos fenômenos ocorridos durante a redução. A caracterização da biomassa bruta e dos biochars obtidos revelou aumento da área superficial e da porosidade com a elevação da temperatura de pirólise, bem como a decomposição dos principais componentes da biomassa e a degradação progressiva da estrutura carbonizada. Através de ensaios interrompidos, todos os briquetes demonstraram elevado desempenho de redução até 950 °C, embora o uso de biochar pirolisado a 550 °C (B550) tenha resultado em maior grau de metalização, alcançando 86% a 1250 °C em comparação com o valor de 28% em B250. A resistência mecânica dos briquetes diminuiu com o aumento da temperatura de aquecimento, atingindo valores mínimos a 950 °C (após a isoterma). A partir dessa temperatura, observou-se um comportamento de inchamento catastrófico em B400 e B550, fortemente influenciado pela formação de *whiskers* de ferro, sendo mais pronunciado nos briquetes com biochars obtidos em temperaturas de pirólise mais elevadas. A contração volumétrica observada em todos os briquetes a 1250 °C foi relacionada à sinterização das partículas de ferro metálico e à formação de escória, de modo que a redução interna uniforme apresentada em B400 contribuiu para a maior resistência em altas temperaturas. Tais resultados foram sustentados por análises combinadas de MEV e micro-CT. No Artigo 3, briquetes contendo 5%, 10% e 15% em massa de biochar pirolisado a 400 °C foram produzidos em escala piloto e testados sob diferentes condições de temperatura e atmosfera representativas da zona granular do alto-forno. Ferro metálico foi identificado a 950 °C, com intensificação da metalização com o aumento da temperatura e do teor de biochar. A atmosfera redutora externa favoreceu a formação de ferro nos aglomerados; entretanto, evidenciou-se maior eficiência de redução promovida pelo carbono sólido do biochar. Em comparação com cargas tradicionais como sinter e pelota, os briquetes apresentaram desempenho de redução consideravelmente superior. Briquetes com 10% de biochar (B10) exibiram maior resistência em altas temperaturas, proporcionando o melhor equilíbrio entre eficiência de redução e integridade mecânica. A menor resistência observada em B05 e B15 foi relacionada, respectivamente, à baixa metalização e à presença de carbono residual associada ao acúmulo de gases nos briquetes. Essa Tese demonstra que as condições de pirólise do biochar e sua proporção nos briquetes impactam significativamente o desempenho metalúrgico e mecânico desses aglomerados, contribuindo para o avanço do conhecimento relacionado ao uso de biochar como agente redutor e para o desenvolvimento de rotas siderúrgicas mais sustentáveis.

Palavras-chave: biochar; pirólise; briquete autorredutor; redução; resistência mecânica; alto-forno; sustentabilidade.

ABSTRACT

The use of biomass in self-reducing briquettes constitutes a promising alternative to reduce fossil fuel consumption and CO_2 emissions in the iron and steel industry. This Thesis aims to investigate the reduction and mechanical strength performance of self-reducing briquettes containing pellet feed and sugarcane bagasse biochar for application as a complementary burden in blast furnaces. In Article 1, the influence of biochar pyrolysis temperature (250, 400, and 550 °C) on the behavior of laboratory-scale briquettes was evaluated, while Article 2 investigated the structural evolution of these agglomerates, expanding the understanding of the phenomena occurring during reduction. Characterization of the raw biomass and the resulting biochars revealed an increase in surface area and porosity with increasing pyrolysis temperature, as well as decomposition of the main biomass components and progressive degradation of the carbonized structure. Based on interrupted experiments, all briquettes exhibited high reduction performance up to 950 °C, although the use of biochar pyrolyzed at 550 °C (B550) resulted in a higher metallization degree, reaching 86% at 1250 °C compared to 28% for B250. The mechanical strength of the briquettes decreased with increasing heating temperature, reaching minimum values at 950 °C after the isothermal stage. Above this temperature, a catastrophic swelling behavior was observed in B400 and B550, strongly influenced by the formation of iron whiskers, and was more pronounced in briquettes produced with biochars obtained at higher pyrolysis temperatures. The volumetric shrinkage observed in all briquettes at 1250 °C was associated with the sintering of metallic iron particles and slag formation, so that the more uniform internal reduction observed in B400 contributed to higher strength at elevated temperatures. These results were supported by combined SEM and micro-CT analyses. In Article 3, briquettes containing 5%, 10%, and 15% by mass of biochar pyrolyzed at 400 °C were produced at pilot scale and tested under different temperature and atmospheric conditions representative of the blast furnace granular zone. Metallic iron was detected at 950 °C, with metallization intensifying as temperature and biochar content increased. The external reducing atmosphere favored iron formation in the agglomerates; however, higher reduction efficiency was predominantly driven by the solid carbon from the biochar. Compared with conventional burdens such as sinter and pellets, the briquettes exhibited considerably superior reduction performance. Briquettes containing 10% biochar (B10) showed the highest mechanical strength at elevated temperatures, providing the best balance between reduction efficiency and mechanical integrity. The lower strength observed in B05 and B15 was associated, respectively, with low metallization and with the presence of residual carbon combined with gas accumulation within the briquettes. This Thesis demonstrates that the biochar pyrolysis conditions and its proportion in the briquettes significantly affect the metallurgical and mechanical performance of these agglomerates, contributing to the advancement of knowledge related to the use of biochar as a reducing agent and to the development of more sustainable steelmaking routes.

Keywords: biochar; pyrolysis; self-reducing briquette; reduction; mechanical strength; blast furnace; sustainability.

LISTA DE FIGURAS

LISTA DE TABELAS

LISTA DE ABREVIATURAS E SIGLAS

ASTM - American Society for Testing and Materials

ATR - Attenuated Total Reflectance

B05 - Briquete com 5% de biochar

B10 - Briquete com 10% de biochar

B15 - Briquete com 15% de biochar

B250 - Briquete com biochar obtido após pirólise a 250 °C

B400 - Briquete com biochar obtido após pirólise a 400 °C

B550 - Briquete com biochar obtido após pirólise a 550 °C

BET - Brunauer-Emmett-Teller

BF - Blast furnace/Alto-forno

BOF - Basic oxygen furnace

CAPES - Coordenação de Aperfeiçoamento de Pessoal de Nível Superior

CDTN - Centro de Desenvolvimento da Tecnologia Nuclear

CNPq - Conselho Nacional de Desenvolvimento Científico e Tecnológico

C/O - Razão entre carbono fixo do agente redutor e oxigênio redutível do minério de ferro

D_{inf} - Diâmetro inferior

DRX/XRD - Difração de raios X

D_{sup} - Diâmetro superior

DTG - Análise termogravimétrica derivada

EBSD - Detector de elétrons retroespalhados

EDS - Espectroscopia de energia dispersiva

EDXRF/XRF - Fluorescência de raios X

ETD - Detector de elétrons secundários

Fa - Faialita

Fe/Fe^0 - Ferro metálico

FEA - Forno elétrico a arco

Fe_T/Total Fe - Ferro total

FTIR - Espectroscopia de infravermelho por transformada de Fourier

GEE/GHG - Gases de efeito estufa

H - Hematita

LOI - Perda por ignição

M - Magnetita

MEV/SEM - Microscopia eletrônica de varredura

Micro-CT - Microtomografia computadorizada de raios X

N/A - Não medido

N/D - Não detectado

O_{red} - Oxigênio redutível

Q - Quartzo

RDI - Índice de degradação sob redução

RI - Índice de redutibilidade

SFCA - Silico-ferrita de cálcio e alumina

TGA - Análise termogravimétrica

W/FeO - Wustita

SUMÁRIO

1. INTRODUÇÃO, OBJETIVOS E ESTRUTURA DA TESE

1.1. Introdução

No atual contexto industrial, as políticas governamentais e exigências ambientais têm se tornado cada vez mais restritivas, especialmente no que se refere à demanda energética e às emissões de gases de efeito estufa (GEE), entre os quais o CO_2 se destaca pela maior intensidade de emissão (Sun et al., 2020). A siderurgia, por sua vez, configura-se como um setor intensivo no consumo de recursos primários e de energia, além de ser responsável por emissões significativas de gases poluentes e particulados (Zhang et al., 2021; Chen et al., 2025), contribuindo com aproximadamente 7–9% das emissões globais de GEE (Kim et al., 2022). Esse impacto está particularmente associado à rota integrada a alto-forno e conversor a oxigênio (BF-BOF), responsável por cerca de 70% da produção mundial de aço bruto (World Steel Association, 2025) e reconhecida como a etapa dominante em termos de intensidade das emissões de CO_2 no processo siderúrgico (Wei et al., 2025). A produção de ferro-gusa em altos-fornos impacta de forma expressiva o balanço global de carbono, devido à forte dependência de combustíveis fósseis empregados nos processos termoquímicos de alta temperatura, como carvão mineral e coque metalúrgico (Munir et al., 2023). Diante desse cenário, alternativas que viabilizem a substituição parcial ou total desses combustíveis por fontes de energia e matérias-primas mais limpas despontam como estratégias promissoras para a descarbonização da siderurgia.

Entre esses recursos, a biomassa destaca-se como uma matéria-prima potencialmente neutra em carbono, uma vez que o CO_2 liberado durante sua combustão tende a ser compensado pelo CO_2 capturado da atmosfera durante seu crescimento (Suopajärvi et al., 2018; Orre et al., 2021). No entanto, características intrínsecas da biomassa bruta, como elevado teor de umidade, baixa densidade, baixo teor de carbono fixo e reduzido poder calorífico, limitam sua aplicação direta na indústria siderúrgica, além de representarem desafios logísticos e de eficiência energética. Ademais, sua natureza fibrosa dificulta a fragmentação em partículas menores e mais uniformes, necessárias para diversas aplicações subsequentes (Li et al., 2025). Nesse contexto, processos de conversão termoquímica da biomassa, como torrefação e pirólise, têm sido amplamente empregados (Khasraw et al., 2024), resultando em produtos com propriedades mais adequadas ao uso metalúrgico (Jayasekara et al., 2023). Após essa etapa de tratamento,

forma-se um material carbonáceo sólido denominado biochar, caracterizado por elevado teor de carbono e baixos teores de oxigênio e hidrogênio (Lehmann et al., 2021). Do ponto de vista ambiental, de acordo com Mathieson et al. (2011), Mandova et al. (2018) e Nwachukwu et al. (2021), produtos derivados da biomassa apresentam potencial para reduzir entre 32% e 58% as emissões de CO_2 na rota integrada BF-BOF. Entre as possibilidades de aplicação, com base na substituição direta dos materiais, destacam-se: injeção nas ventaneiras dos altos-fornos (19–25%); uso como combustível sólido na sinterização (5–15%); produção de aglomerados autorredutores para altos-fornos e cargas pré-reduzidas para BOF (4–7%); substituição de coque em altos-fornos (3–7%); componente de misturas de carvão para coqueria (1–5%); e uso como agente recarburante na fabricação do aço (0,04%). Na rota empregando forno elétrico a arco (FEA), as aplicações incluem a substituição do carbono da carga, do agente espumante da escória e do recarburante do aço (Mathieson et al., 2011).

Avanços tecnológicos têm sido incorporados à operação em altos-fornos, entre os quais se destaca a evolução da composição da carga empregada nesses reatores. Aglomerados autorredutores, produzidos a partir da mistura entre óxidos de ferro e agentes redutores carbonáceos, têm sido amplamente investigados devido às elevadas taxas de redução, podendo exibir velocidades superiores às observadas nos processos tradicionais (Mourão e Takano, 2003), aliadas a uma maior flexibilidade no emprego de matérias-primas. Sua estrutura favorece o contato íntimo entre os reagentes, o que, em altas temperaturas, acelera as reações de gaseificação e de redução dos óxidos de ferro, resultando em elevada pressão parcial de gases redutores em seu interior (Noldin Jr., 2002). Esse efeito pode se refletir em uma maior eficiência na zona de preparação do alto-forno e na redução do consumo de combustível (Kowitwarangkul et al., 2014; Gandra et al., 2023).

Em contrapartida, os principais desafios associados a esses aglomerados estão relacionados à resistência mecânica em altas temperaturas, especialmente à manutenção da integridade durante o aquecimento e a redução (Mourão e Takano, 2003; Narita et al., 2015). Outro aspecto crítico é a suscetibilidade ao inchamento, um fenômeno comumente observado nesses aglomerados, capaz de provocar uma expansão volumétrica significativa, resultando na fragmentação e desintegração da matriz sólida e, consequentemente, na perda de resistência (Umadevi et al., 2016; Purohit et al., 2025). Esse comportamento compromete a integridade física dos

aglomerados e pode afetar negativamente sua eficiência metalúrgica, constituindo uma limitação relevante à sua aplicação.

Com base no exposto, de um lado, a biomassa desponta como uma fonte de carbono neutra e renovável, alinhada a práticas mais sustentáveis na siderurgia; de outro, os briquetes autorredutores apresentam vantagens relevantes, sobretudo por favorecerem uma maior eficiência de redução. Nesse contexto, a incorporação de biomassa como agente redutor nesses briquetes combina benefícios ambientais às vantagens metalúrgicas dos aglomerados autorredutores, configurando-se como uma alternativa promissora para uso em altos-fornos (Suopajärvi et al., 2018). Entretanto, o desempenho desses aglomerados também pode ser fortemente dependente da natureza, da reatividade e da proporção da biomassa empregada nas misturas autorredutoras. Características como composição elementar, teor de carbono fixo e voláteis, porosidade e a estrutura carbonácea formada após pirólise exercem um papel determinante no comportamento dos briquetes, podendo afetar simultaneamente sua capacidade de redução e sua integridade estrutural.

Apesar dos avanços recentes no estudo da autorredução, na utilização de diferentes fontes de biomassa em briquetes autorredutores e na investigação isolada de fenômenos como redução e cinética reacional, o efeito da temperatura de pirólise da biomassa nesses aglomerados permanece pouco explorado, especialmente quando associado ao comportamento de autorredução e à resistência mecânica em altas temperaturas. Essa lacuna evidencia a necessidade de estudos que integrem esses parâmetros de maneira sistemática, permitindo uma compreensão mais abrangente do emprego da biomassa pirolisada (biochar) em briquetes autorredutores. Nesse contexto, esse trabalho propôs-se a avaliar o desempenho de redução e de resistência mecânica de briquetes autorredutores contendo biochar como agente redutor para uso como carga em altos-fornos. Briquetes com biochars pirolisados em diferentes temperaturas e em teores variáveis foram avaliados em diferentes escalas de produção (laboratorial e piloto) e em condições distintas de aquecimento e atmosfera. O bagaço de cana-de-açúcar foi utilizado como fonte de carbono, por se tratar de um subproduto do processamento agrícola amplamente disponível, com geração anual estimada entre 279 e 300 milhões de toneladas em escala mundial (Periyasamy et al., 2024).

Considerando a multiplicidade de fatores que governam o desempenho desses aglomerados, desde a caracterização das matérias-primas, definição dos aglomerantes empregados e formulação das misturas autorredutoras, até mecanismos de redução em altas temperaturas, torna-se essencial a realização de estudos experimentais capazes de elucidar esses fenômenos e de identificar as condições mais favoráveis que viabilizem o uso de biochar em briquetes autorredutores e sua aplicação em processos de produção de ferro. Uma análise detalhada revela-se particularmente interessante no cenário atual, especialmente diante do crescente interesse pelo uso de fontes renováveis de carbono e pelo desenvolvimento de tecnologias mais sustentáveis na indústria siderúrgica, bem como na aplicação de briquetes como carga em altos-fornos.

1.2. Objetivos

1.2.1. Objetivo geral

A presente Tese tem como objetivo avaliar o desempenho de redução e de resistência mecânica de briquetes autorredutores produzidos a partir de *pellet feed* e biochar de bagaço de cana-de-açúcar como agente redutor, visando à aplicação como carga ferrosa complementar em altos-fornos.

1.2.2. Objetivos específicos

- Caracterizar a biomassa bruta e os biochars obtidos após pirólise em diferentes temperaturas, analisando as transformações decorrentes do processo termoquímico;

- Avaliar a influência da temperatura de pirólise da biomassa e do teor de biochar no comportamento de redução, no grau de metalização e na resistência mecânica dos briquetes;

- Avaliar a influência da atmosfera no desempenho de redução e de resistência mecânica dos briquetes, identificando a contribuição relativa dos gases redutores da atmosfera externa e do carbono sólido proveniente do biochar;

- Investigar o comportamento estrutural dos briquetes durante a redução em altas temperaturas, analisando os fenômenos de inchamento e contração, bem como as alterações morfológicas e os mecanismos envolvidos;

- Determinar as condições ideais de processamento da biomassa e de composição dos briquetes, visando o equilíbrio entre eficiência de redução e estabilidade estrutural para aplicação em altos-fornos.

1.3. Estrutura da Tese

A presente Tese é organizada em 8 capítulos distintos e estruturada a partir de 3 artigos científicos, que, ao se articularem, compõem o conteúdo central desta pesquisa. O Capítulo 1, que inclui a introdução, os objetivos e a estrutura da tese, tem como principal função contextualizar o tema no cenário científico e tecnológico atual, evidenciando sua relevância, identificando lacunas de conhecimento e apresentando o escopo do estudo.

O Capítulo 2 corresponde ao artigo intitulado "*Influence of biomass pyrolysis temperature on the performance of self-reducing briquettes for use in blast furnaces*" (Leão et al., 2026), publicado no periódico internacional *Biomass and Bioenergy* (Qualis A1). Nesse primeiro estudo, briquetes autorredutores produzidos em escala laboratorial a partir de *pellet feed* e biochar de bagaço de cana-de-açúcar pirolisado a 250, 400 e 550 °C foram avaliados sob o regime térmico representativo de um alto-forno, com o objetivo de investigar como a temperatura de pirólise do biochar afeta o desempenho de redução e de resistência mecânica desses aglomerados. Os parâmetros de processamento adotados na produção laboratorial dos briquetes foram previamente estabelecidos e otimizados com base em ensaios preliminares, considerando as principais variáveis de produção: mistura (tempo e condições), compactação (pressão e tempo) e cura (temperatura e tempo). Inicialmente, realizou-se a caracterização da biomassa bruta e dos biochars obtidos em diferentes temperaturas, desempenhando um papel importante na compreensão das transformações químicas e estruturais relacionadas à pirólise. Os briquetes foram submetidos a ensaios interrompidos sob condições não isotérmicas, com temperatura máxima de 1250 °C e atmosfera de N_2, monitorando-se a evolução dos produtos de redução, bem como as alterações na resistência mecânica e na microestrutura dos briquetes em diferentes estágios de aquecimento, por meio da combinação das técnicas de termogravimetria, análises química e gasosa, ensaios de resistência à compressão e microscopia eletrônica de varredura. Embora diversos estudos tenham abordado aspectos isolados do processo de pirólise da biomassa e do comportamento de redução de briquetes autorredutores, a interação entre a temperatura de pirólise, as propriedades do biochar e a evolução concomitante da redução e da resistência mecânica em altas temperaturas ainda não foi totalmente explorada. Este estudo buscou preencher essa lacuna, ao avaliar, de forma sistemática, a influência dessas variáveis sobre o desempenho global de briquetes autorredutores em condições termoquímicas relevantes para aplicações siderúrgicas.

O Capítulo 3 apresenta o manuscrito do artigo intitulado "*Structural behavior of self-reducing briquettes containing biochar pyrolyzed at different temperatures*", submetido ao periódico internacional *Journal of Materials Research and Technology* (Qualis A1). Esse estudo configura-se como uma continuidade direta do trabalho apresentado no capítulo anterior, ao ampliar a abordagem inicialmente centrada no desempenho global de redução e de resistência mecânica de briquetes autorredutores contendo biochar pirolisado em diferentes temperaturas. Nessa segunda etapa, o escopo da investigação foi expandido para incluir uma avaliação da evolução estrutural dos briquetes ao longo dos diferentes estágios de redução, fornecendo uma análise detalhada do processo e dos fenômenos associados. Ensaios interrompidos em altas temperaturas, combinados com técnicas complementares de caracterização (difração de raios X, microscopia eletrônica de varredura e microtomografia de raios X), estabeleceram uma correlação direta entre as transformações macro- e microestruturais e o desempenho metalúrgico e mecânico dos briquetes. Com base na metodologia empregada, esse estudo explorou a micro-CT como uma nova ferramenta para a análise e caracterização de briquetes autorredutores, evidenciando o potencial e as limitações associadas à técnica. Essa abordagem possibilitou uma análise abrangente dos comportamentos de inchamento e contração, os quais puderam ser investigados em profundidade em razão de sua relação intrínseca com a redutibilidade e a resistência.

O Capítulo 4 corresponde ao manuscrito do artigo intitulado "*Reduction and mechanical strength performance of self-reducing briquettes with different biochar contents*", submetido ao periódico internacional *Mineral Processing and Extractive Metallurgy Review* (Qualis A1). Nesse terceiro estudo, a investigação concentrou-se em avaliar o efeito do teor de biochar sobre o desempenho de redução e de resistência mecânica de briquetes autorredutores contendo *pellet feed* e bagaço de cana-de-açúcar obtido a 400 °C. Essa condição (temperatura) de pirólise foi previamente definida com base nos estudos anteriores, que evidenciaram o desempenho superior desses briquetes, fundamentando, assim, sua seleção para a produção em escala piloto. Para avaliação do comportamento de redução, briquetes contendo 5%, 10% e 15% em massa de biochar foram submetidos a diferentes estágios de aquecimento sob atmosfera redutora representativa do alto-forno (N_2/CO/CO_2), tendo seu desempenho comparado ao de cargas tradicionalmente empregadas nesses reatores, como sinter e pelota. Adicionalmente, investigou-se a influência de uma atmosfera inerte (N_2), com o objetivo de avaliar a contribuição relativa dos gases redutores externos e do carbono sólido proveniente do biochar

sobre a eficiência de redução dos briquetes, refletindo a reatividade do biochar empregado. Os ensaios realizados possibilitaram uma avaliação abrangente dos mecanismos e fenômenos associados à perda de massa, transformações de fases, metalização, evolução de gases, resistência à compressão e microestrutura dos briquetes. Dessa forma, esse artigo complementa o conjunto das investigações conduzidas nos estudos anteriores, consolidando uma abordagem integrada sobre o uso de biochar em briquetes autorredutores.

O Capítulo 5 apresenta as considerações finais derivadas dos estudos conduzidos nos Capítulos 2 a 4, integrando os resultados obtidos em cada etapa de investigação e destacando suas implicações e contribuições para o campo de estudo.

O Capítulo 6 é dedicado às contribuições originais do estudo para o conhecimento científico; o Capítulo 7 apresenta o conjunto de publicações produzidas ao longo do desenvolvimento da presente Tese; e o Capítulo 8 reúne as recomendações e sugestões para trabalhos futuros, apontando possíveis linhas de investigação capazes de aprofundar e expandir os resultados obtidos neste estudo, bem como explorar novas abordagens e aplicações em contextos operacionais mais próximos da escala industrial.

Por fim, os Apêndices A, B e C contêm informações complementares ao estudo, incluindo imagens macroscópicas das seções transversais dos briquetes produzidos em escala piloto, cálculos de perda de massa teórica e fração reagida (que permitiram a análise comparativa entre os resultados experimentais e os valores teóricos), bem como a comparação entre os ensaios conduzidos em macrotermobalança e termobalança convencional.

1.4. Referências

Chen, M., Jiang, P., Li, M., Zhao, G., Lin, H., Mu, L., Lau, L.C., Zhu, J., 2025. When crop straw meets CO_2-intensive process industries in China: The potential of CO_2 mitigation and techno-economic analysis. Biomass and Bioenergy 196, 107755. https://doi.org/10.1016/j.biombioe.2025.107755.

Gandra, B.F., Paula Junior, G.E., Bagatini, M.C., Osório, E., 2023. Analysis of self-reducing composites with different iron ore-carbon ratio. Journal of Materials Research and Technology 26, 6433–6445. https://doi.org/10.1016/j.jmrt.2023.08.289.

Jayasekara, A.S., Brooks, B., Steel, K., Koshy, P., Hockings, K., Tahmasebi, A., 2023. Microalgae blending for sustainable metallurgical coke production - Impacts on coking behaviour and coke quality. Fuel 344, 128130. https://doi.org/10.1016/j.fuel.2023.128130.

Khasraw, D., Martin, C., Herbert, J., Li, Z., 2024. A comprehensive literature review of biomass characterisation and application for iron and steelmaking processes. Fuel 368, 131459. https://doi.org/10.1016/j.fuel.2024.131459.

Kim, J., Sovacool, B.K., Bazilian, M., Griffiths, S., Lee, J., Yang, M., Lee, J., 2022. Decarbonizing the iron and steel industry: A systematic review of sociotechnical systems, technological innovations, and policy options. Energy Research & Social Science 89, 102565. https://doi.org/10.1016/j.erss.2022.102565.

Kowitwarangkul, P., Babich, A., Senk, D., 2014. Reduction behavior of self-reducing pellet (SRP) for low height blast furnace. Steel Research International 85(11), 1501–1509. https://doi.org/10.1002/srin.201300399.

Leão, P.M.G.C., Zicker, T.B., Ferreira, N.H.A., Ardisson, J.D., Bagatini, M.C., 2026. Influence of biomass pyrolysis temperature on the performance of self-reducing briquettes for use in blast furnaces. Biomass and Bioenergy 206, 108691. https://doi.org/10.1016/j.biombioe.2025.108691.

Lehmann, J., Cowie, A., Masiello, C.A., Kammann, C., Woolf, D., Amonette, J. E., Cayuela, M. L., Camps-Arbestain, M., Whitman, T., 2021. Biochar in climate change mitigation. Nature Geoscience 14(12), 883–892. https://doi.org/10.1038/s41561-021-00852-8.

Li, Y., Liu, P., Dong, L., Lang, P., Lei, T., 2025. Evolution of oxygen-containing functional groups during torrefaction and its effect on pyrolysis behaviors and hydrogen production from different lignocellulosic biomasses. Applications in Energy and Combustion Science 24, 100421. https://doi.org/10.1016/j.jaecs.2025.100421.

Mandova, H., Leduc, S., Wang, C., Wetterlund, E., Patrizio, P., Gale, W., Kraxner, F., 2018. Possibilities for CO_2 emission reduction using biomass in European integrated steel plants. Biomass and Bioenergy 115, 231–243. https://doi.org/10.1016/j.biombioe.2018.04.021.

Mathieson, J.G., Rogers, H., Somerville, M.A., Jahanshahi, S., Ridgeway, P., 2011. Potential for the use of biomass in the iron and steel industry. In: Chemeca 2011: Engineering a Better World: Sydney Hilton Hotel, NSW, Australia, 18-21 September 2011. Barton, A.C.T.: Engineers Australia, 1065–1076.

Mourão, M.B., Takano, C., 2003. Self-reducing pellets for ironmaking: reaction rate and processing. Mineral Processing and Extractive Metallurgy Review 24(3–4), 183–202. https://doi.org/10.1080/714856821.

Munir, M.T., Saqib, N.U., Li, B., Naqvi, M., 2023. Food waste hydrochar: An alternate clean fuel for steel industry. Fuel 346, 128395. https://doi.org/10.1016/j.fuel.2023.128395.

Narita, C.Y., Mourão, M.B., Takano, C., 2015. Development of composite briquettes of iron ore and coal hardened by heat treatment. Ironmaking & Steelmaking 42(7), 548–552. https://doi.org/10.1179/1743281214y.0000000260.

Noldin Jr., J.H., 2002. Contribuição ao estudo da cinética de redução de briquetes auto-redutores. 130p. Dissertação (Mestrado em Engenharia Metalúrgica). Rio de Janeiro: Pontifícia Universidade Católica do Rio de Janeiro.

Nwachukwu, C.M., Wang, C., Wetterlund, E., 2021. Exploring the role of forest biomass in abating fossil CO_2 emissions in the iron and steel industry - the case of Sweden. Applied Energy 288, 116558. https://doi.org/10.1016/j.apenergy.2021.116558.

Orre, J., Ökvist, L.S., Bodén, A., Björkman, B., 2021. Understanding of blast furnace performance with biomass introduction. Minerals 11(2), 157. https://doi.org/10.3390/min11020157.

Periyasamy, S., Adego, A.A., Kumar, P.S., Desta, G.G., Zelalem, T., Karthik, V., Isabel, J.B., Jayakumar, M., Sundramurthy, V.P., Rangasamy, G., 2024. Influencing factors and environmental feasibility analysis of agricultural waste preprocessing routes towards biofuel production - A review. Biomass and Bioenergy 180, 107001. https://doi.org/10.1016/j.biombioe.2023.107001.

Purohit, S., Pownceby, M.I., Guiraud, A., 2025. Sticking and swelling of iron ore pellets: Mechanisms and controlling factors. Journal of Sustainable Metallurgy 11(1), 67–87. https://doi.org/10.1007/s40831-024-01000-3.

Sun, W., Wang, Q., Zheng, Z., Cai, J., 2020. Material-energy-emission nexus in the integrated iron and steel industry. Energy Conversion and Management 213, 112828. https://doi.org/10.1016/j.enconman.2020.112828.

Suopajärvi, H., Umeki, K., Mousa, E., Hedayati, A., Romar, H., Kemppainen, A., Wang, C., Phounglamcheik, A., Tuomikoski, S., Norberg, N., Andefors, A., Öhman, M., Lassi, U., Fabritius, T., 2018. Use of biomass in integrated steelmaking - Status quo, future needs and comparison to other low-CO_2 steel production technologies. Applied Energy 213, 384–407. https://doi.org/10.1016/j.apenergy.2018.01.060.

Umadevi, T., Kumar, A., Karthik, P., Srinidhi, R., Manjini, S., 2016. Characterisation studies on swelling behaviour of iron ore pellets. Ironmaking & Steelmaking 45(2), 157–165. https://doi.org/10.1080/03019233.2016.1250043.

Wei, R., Peng, Z., Wang, J., Xue, Q., Zuo, H., 2025. Waste crayfish shell addition improves mechanical strength and reducibility of hematite briquettes. Biomass and Bioenergy 201, 108107. https://doi.org/10.1016/j.biombioe.2025.108107.

World Steel Association, 2025. World Steel in Figures. https://worldsteel.org/data/world-steel%20in-Figures/world-steel-in-Figures-2025/. Accessed 25 Sep. 2025.

Zhang, X., Jiao, K., Zhang, J., Guo, Z., 2021. A review on low carbon emissions projects of steel industry in the world. Journal of Cleaner Production 306, 127259. https://doi.org/10.1016/j.jclepro.2021.127259.

2. ARTIGO 1: INFLUENCE OF BIOMASS PYROLYSIS TEMPERATURE ON THE PERFORMANCE OF SELF-REDUCING BRIQUETTES FOR USE IN BLAST FURNACES

Paula Maria Gomes Cunha Leão[a]*, Taís Birchal Zicker[a], Nícolas Henrique Alves Ferreira[a], José Domingos Ardisson[b], and Maurício Covcevich Bagatini[a]

[a] *Laboratory of Ironmaking Processes (LPS), Department of Metallurgical and Materials Engineering, Federal University of Minas Gerais (UFMG), Av. Antônio Carlos, 6627, Escola de Engenharia, 31270-901, Belo Horizonte, MG, Brazil*

[b] *Laboratory of Mössbauer Spectroscopy, Department of Nanotechnology, Nuclear Technology Development Center (CDTN/CNEN), Av. Antônio Carlos, 6627, 31270-901, Belo Horizonte, MG, Brazil*

* Corresponding author

Abstract

The use of different biomass sources in self-reducing briquettes is considered a sustainable and promising alternative for introducing renewable carbon into blast furnaces. However, the influence of pyrolysis conditions on their reduction behavior and mechanical strength remains poorly understood. This study investigated how biomass pyrolysis temperature affects the performance of briquettes produced from pellet feed and sugarcane bagasse obtained at different temperatures (250, 400, and 550 °C). Sugarcane bagasse and its pyrolyzed products exhibited distinct surface areas, functional groups, and microstructures. Self-reducing briquettes with 15% by mass of the different biochars were subjected to the high-temperature interrupted tests under non-isothermal conditions up to 1250 °C. All briquettes presented a high reduction performance up to 950 °C (blast furnace preparation zone), where the briquettes with biomass pyrolyzed at 550 °C resulted in a greater mass loss and a higher metallization degree. Interrupted tests showed that the briquettes reached a minimum compressive strength at 950 °C, followed by an increase at higher temperatures. Although B550 achieved the highest reduction degree, B400 exhibited the highest strength at high temperature, as a result of the swelling phenomena and phase formation that impacted the briquette strength. Microstructural analysis revealed the coalescence and sintering of metallic iron particles at 1250 °C, as well as

the formation of wustite and fayalite phases, and a slag matrix resulting from the interaction of briquette components at high temperature. These findings demonstrate that the pyrolysis temperature strongly influences both the reduction efficiency and the high-temperature mechanical stability of self-reducing briquettes.

Keywords: biomass pyrolysis; briquette; self-reduction; mechanical strength; metallization; blast furnace.

Graphical Abstract

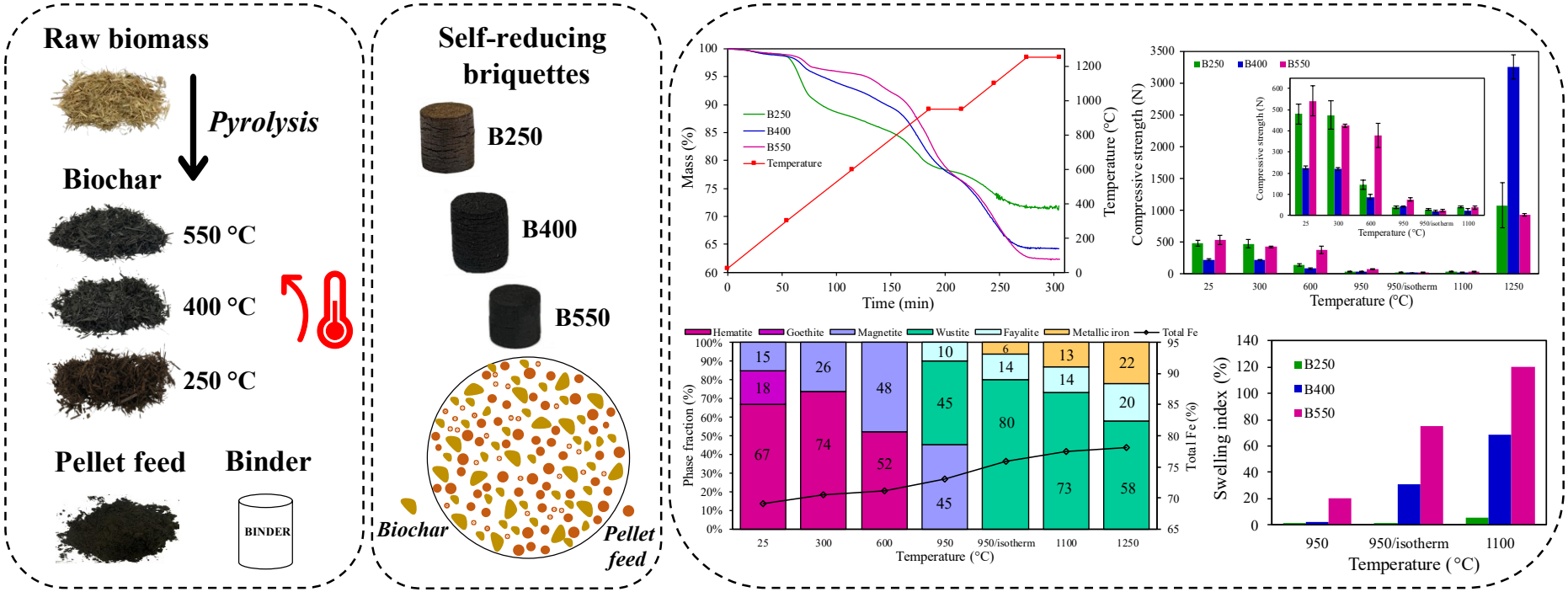

2.1. Introduction

The iron and steelmaking industry faces growing challenges related to energy consumption and greenhouse gas (GHG) emissions, largely due to its intensive reliance on fossil fuels [1]. It is estimated that 7–9% of the total anthropogenic CO_2 emissions are attributed to this industrial sector [2]. In this context, strategies for decarbonization have been increasingly explored [3,4]. According to Ahmed [5], the use of carbonaceous materials from renewable sources in blast furnaces represents one of the most effective strategies to address these environmental concerns. Their application in these reactors aims to reduce fuel consumption, decreasing dependence on coal and coke, and mitigating CO_2 emissions generated by the use of fossil-based reducing agents. Biomass is a renewable resource, considered neutral in CO_2 emissions, and abundantly available, so many studies have explored its potential for use in different stages of steelmaking [6-14]. To convert raw biomass into materials with properties and characteristics required for metallurgical applications, such as higher fixed carbon content and greater calorific value, pre-treatment routes like torrefaction and pyrolysis are often employed [10,15]. The treatment temperature has a significant influence on the chemical composition, yield, and textural and structural properties of the biochar derived by the process [16].

The use of different biomass sources in self-reducing briquettes is considered a sustainable and promising alternative for introducing renewable carbon into blast furnaces [17]. In these agglomerates, the reducing agent is added directly to the mixture, ensuring close contact between the ferrous and carbonaceous sources. This configuration can increase the reduction rate in the blast furnace preparation zone (where drying, preheating, and prereduction of the burden by the ascending gas occur, and carbon practically does not react), as well as reduce fuel consumption and improve the reactor's efficiency and productivity [18,19]. The reduction degree of the agglomerates can be significantly affected by factors such as the temperature of the reaction system, the carbon source employed, and its specific characteristics. Liu et al. [20] investigated pellets composed of iron concentrate and carbonized agricultural residues, used as a substitute for pulverized coal. The experimental results showed that increasing the temperature favored the reduction process up to 1200 °C, achieving a reduction degree of 92.17%. Beyond this point, no substantial improvement was observed. A qualitative analysis of the reduction of iron ore and coke breeze briquettes containing different pre-treated biomasses was conducted by El-Tawil et al. [21]. In the study, low-temperature torrefied sawdust was

recommended for use in briquettes due to its higher volatile matter content and lower catalyst component content. Consequently, at elevated temperatures, the release of volatiles contributes to the reduction process. In another study, Rosso Neto et al. [22] evaluated the effect of biochar particle size on the reduction of self-reducing briquettes and reported that smaller particle sizes lead to faster reaction rates. Through thermogravimetric analysis, Zuo et al. [23] explored the reduction behavior of iron oxide using biomass char (waste wood), comparing it with coal and coke. These authors concluded that biomass increased the reduction rate and that higher C/O molar ratios intensified the self-reduction reactions. They also concluded that the utilization of iron ore-biomass agglomerates in blast furnaces tends to reduce the temperature of the thermal reserve zone and fuel consumption, while increasing the reducibility of the burden. The reactivity of different carbonaceous materials (charcoal, coal, blast furnace coke, and petroleum coke) was also studied by Bagatini et al. [24]. Experiments involving self-reducing mixtures composed of mill scale and various reducing agents indicated a faster rate of self-reduction for charcoal. This behavior was associated with the presence of highly reactive carbon compared to fossil-based reducers [25].

However, the use of self-reducing briquettes in blast furnaces has limitations regarding their mechanical strength when charged at the top of these reactors, especially at high temperatures, during which devolatilization and consumption of the reducing agent occur. When evaluating the high-temperature strength of self-reducing briquettes containing blast furnace dust, Ye et al. [26] observed a decrease in mechanical strength as the degrees of reduction and metallization increased at temperatures below 1100 °C. According to Takano and Mourão [27], the strength of self-reducing agglomerates typically reaches its minimum between 900 and 1000 °C, after which the sintering of the formed iron leads to a subsequent increase in mechanical strength. The proportion of carbonaceous material in self-reducing briquettes also influences their mechanical properties. In the study by Gandra et al. [28], lower strength indices were observed in briquettes with higher contents of petcoke as a reducing agent. Similarly, high levels of swelling can lead to a loss of strength of the agglomerates during heating, and commonly occur in the final stage of the reduction process. As indicated by the literature, the causes of swelling include the formation of iron whiskers and iron carbides during the iron reduction stage, the presence of alkalis and basic oxides, the ore gangue content, the carbon deposition, the composition of the reducing gas, the growth of metallic iron within the molten slag, as well as

the increase in internal pressure caused by the rapid formation of gases at the reaction interface [27,29–34].

Despite the existence of studies related to the use of biomass in self-reducing mixtures, the influence of biomass pyrolysis temperature on the reducibility and mechanical strength of cold-bonded briquettes has not been fully explored. Previous investigations have overlooked the interplay between pyrolysis temperature, biochar properties (beyond fixed carbon and volatile matter), and concurrent reducibility/strength evolution at high temperatures. Thus, this study aimed to evaluate the reduction behavior and mechanical strength of self-reducing briquettes produced from sugarcane bagasse treated at different temperatures (250, 400, and 550 °C) when subjected to thermal regimes that represent the blast furnace, investigating the influence of biomass pyrolysis temperature on these properties. Initially, a characterization of the raw biomass and biochars was carried out, playing an important role in understanding the chemical and structural transformations related to the pyrolysis process. Then, self-reducing briquettes were examined by monitoring the evolution of reduction products during heating and changes in strength and microstructure, through a combination of thermogravimetry, chemical and gas analysis, and mechanical testing.

2.2. Materials and methods

2.2.1. Raw materials

A Brazilian hematite-goethite pellet feed was used as the iron source in the briquettes, with a predominant particle size below 212 μm (95% by mass). Table 2.1 presents the corresponding chemical composition, determined using an ARL™ QUANT'X energy-dispersive X-ray fluorescence (EDXRF) spectrometer (Thermo Scientific™). The total reducible oxygen content was calculated from the chemical analysis. As a reducing agent, sugarcane bagasse supplied by a local sugar-alcohol industry was employed due to its high availability. This biomass is among the most abundant lignocellulosic materials in Brazil [35]. The sugarcane bagasse was used after pyrolysis treatment at 250, 400, and 550 °C (Figure 2.S1 of the Supplementary Material). These temperatures were selected based on the thermal decomposition stages of biomass components: hemicellulose (220–315 °C), cellulose (315–400 °C), and lignin, which decomposes over a wide temperature range (150–900 °C) [36]. The pyrolysis process was

carried out on a laboratory scale using a vertical resistive electric furnace equipped with a stainless-steel reactor tube, in which the samples were heated in a graphite crucible. In these tests, 15 g of dried raw biomass (105 °C for 3 h) were subjected to a constant N_2 atmosphere (flow rate of 1.5 L/min) and heated at a rate of 10 °C/min to the target temperatures, followed by an isothermal period of 2 h. The temperature was continuously monitored using a K-type furnace thermocouple. The characterization of the raw biomass and produced biochars is presented in Table 2.2. Proximate analysis was performed using a LECO TGA 701 thermogravimetric analyzer following ASTM D7582-15, while ultimate analysis was carried out with a LECO CS230 carbon and sulfur elemental analyzer. The increase in pyrolysis temperature resulted in decreasing the volatile matter and increasing the fixed carbon content.

Table 2.1. Chemical composition of pellet feed (% by mass).

Fe	SiO_2	Al_2O_3	MgO	MnO	Co	P_2O_5	Cl	LOI	O_{red}
63.23	5.19	2.59	0.63	0.55	0.44	0.27	0.23	2.47	27.17

LOI: loss on ignition; O_{red}: reducible oxygen

Table 2.2. Proximate and ultimate analyses (% by mass) of raw biomass and biochars after treatment at different temperatures (dry basis).

Pyrolysis temperature (°C)	Fixed carbon	Volatile matter	Ash	Total carbon
Raw biomass	16.89	81.25	1.92	41.27
250	22.96	74.31	2.72	56.54
400	65.69	26.39	7.93	74.85
550	76.21	15.18	8.60	93.24

As an inorganic binder in briquette production, aqueous sodium silicate (a viscous liquid) was used due to its high thermal stability and excellent adhesive properties, making it suitable for applications that require mechanical strength. Additionally, it offers advantages such as low cost and wide availability. The main characteristics include a SiO_2/Na_2O mass ratio of 2.17, 47.14% solid content, and 52.86% moisture.

2.2.2. Biomass characterization

To understand the influence of biomass pyrolysis temperature on its properties and behavior in the self-reducing briquettes, the raw biomass and biochars obtained after treatment at different temperatures were characterized using various analytical techniques. The surface area was

measured by the Brunauer-Emmett-Teller (BET) isotherm method, employing a Quantachrome NOVA 2200 instrument, utilizing N_2 as the adsorbate and a relative pressure of P/P_O (ratio between the adsorption pressure and the atmospheric pressure of N_2) below 0.3. For that, samples with particle size below 0.5 mm were used and degassed at 120 °C in a vacuum condition for 2 h.

The Fourier Transform Infrared (FTIR) spectroscopy was used to characterize the functional groups of the biomass samples, with a focus on identifying the decomposition process of their components as a function of temperature. The analysis was carried out on a Bruker Alpha spectrometer, using the Attenuated Total Reflectance (ATR) module with a diamond crystal. The spectra were collected in the mid-infrared region from 4000 to 400 cm^{-1}, with a spectral resolution of 4 cm^{-1} and a total number of 128 scans per sample.

The microstructure was investigated using a FEI Inspect S50 scanning electron microscope (SEM) coupled with a Genesis EDS spectrometer, operating with an acceleration voltage of 10 kV. The samples were positioned on a support using double-sided adhesive carbon tape and subjected to metallic coating with gold.

Thermogravimetric analysis (TGA) was conducted to investigate the thermal decomposition of the raw biomass and the resulting biochars during heating. The samples were ground to a particle size below 75 μm. The experiments were performed using an SDT Q600 thermobalance (TA Instruments Co.), by heating approximately 5 mg of sample in a cup-type alumina crucible up to 1000 °C at a heating rate of 10 °C/min and a flow rate of 100 mL/min of N_2.

2.2.3. Production of self-reducing briquettes

Before briquetting, the pellet feed was dried at 105 °C for 12 h, and the biochars were crushed to a particle size between 0.053 and 0.5 mm (with 85% by mass having a size larger than 0.106 mm). The briquetting mixtures were composed of mass percentages of 75% pellet feed, 15% treated biomass (biochar), and 10% sodium silicate, with a total mixture moisture of 12% by mass. The raw materials were manually homogenized in a suitably sized container (500 mL) for 15 min to ensure a uniform mixture before the subsequent processing steps. Cylindrical briquettes were individually produced using a steel die (internal diameter of 10 mm) and a

Bovenau hydraulic press (maximum nominal load of 15 tons) with an applied load of 2 tons for 3 min. Curing was subsequently performed in a muffle furnace at 200 °C for 2 h. Considering the proportion of raw materials and their respective chemical compositions (fixed carbon of the reducing agent and reducible oxygen of the ore), the C/O molar ratios obtained were 0.23, 0.64, and 0.75 for briquettes with biochars after treatment at 250 °C (B250), 400 °C (B400), and 550 °C (B550), respectively. Due to differences in the chemical composition of the different biochars, variations were observed in the C/O mass and molar ratios of briquettes containing the same reducing agent content. The final dimensions of the produced briquettes were 10 mm in diameter, with the average height varying according to the biochar used: B250 - 11.3 mm, B400 - 12.3 mm, and B550 - 10.0 mm.

2.2.4. High-temperature interrupted tests with self-reducing briquettes

The high-temperature tests were conducted to elucidate the mechanical and reduction behavior of the briquettes during heating according to the thermal regime of the blast furnace [34]. The apparatus used in these tests (illustrated in Figure 2.S2 of the Supplementary Material) comprises a vertical resistive furnace (maximum temperature of 1600 °C and molybdenum disilicide ($MoSi_2$) heating element), an alumina reaction tube (70 mm diameter), a stainless-steel basket (40 mm diameter), and a Kanthal DS wire (FeCrAl alloy/0.404 mm diameter) for sample suspension on a Shimadzu electronic balance, model UW620H (precision ± 0.001 g), with an RS232C output for real-time data acquisition and automatic recording. Coupled to the furnace, a Gasboard 3100 gas analyzer (Cubic-Ruiyi) enabled the continuous analysis of CO and CO_2 during the tests. A K-type thermocouple was employed to measure the sample temperature.

The tests were performed with batches of 6 briquettes in the basket under an inert N_2 atmosphere, with an upward gas flow rate of 3 L/min and a heating rate of 5 °C/min from room temperature (25 °C) up to 1250 °C, with an isothermal plateau of 30 min at 950 °C representing the thermal reserve zone of the blast furnace. Interrupted tests at 300, 600, 950 (before and after the isothermal plateau), and 1100 °C were conducted by rapid cooling under N_2 atmosphere, with the samples being moved to the upper region of the alumina tube, outside the furnace heating zone. All tests were carried out in duplicate with continuous measurements of mass, temperature, and gas composition.

2.2.5. Characterization of self-reducing briquettes

The chemical characterization of the samples was carried out by the Mössbauer spectroscopy technique, enabling the identification and quantification of the ferrous compound. The spectra were acquired using a conventional spectrometer (Wissenschaftliche Elektronik GmbH) with constant acceleration and a ^{57}Fe source in a Rh matrix maintained at room temperature. Sample holders containing absorbers with approximately 10 mg of Fe/cm² were used in the measurements. The quantitative analysis was performed using a specific computational method, the Normos™ 90 program, developed at the Applied Physics Laboratory of the University of Duisburg, Germany, utilizing the Fortran programming language. The total iron content was calculated considering the iron content in each detected phase. With these results, it was possible to obtain the metallization degree of the briquettes, calculated by the mass percentage ratio of metallic iron and total iron. The samples were also subjected to carbon analysis using a LECO CS230 carbon and sulfur elemental analyzer.

The mechanical strength of the briquettes was determined through compressive tests in the axial direction before and after the tests (after cooling). Five briquettes were individually tested for each condition, subjected to progressive pressure in a Shimadzu universal machine model AGS-X 300 kN, with a constant cross-head speed of 0.01 mm/s up to sample rupture.

For microstructural analysis via SEM, the samples were cut in the direction of the mechanical load application, embedded in polymeric resin, and prepared by grinding (120, 240, 320, 400, 600, and 1000 grit) and polishing (9, 3, and 1 μm, and diamond paste) steps. The images were acquired using the FEI Inspect S50 equipment coupled with a Genesis EDS spectrometer, operating with an acceleration voltage of 20 kV.

2.3. Results and discussion

2.3.1. Biomass characterization

2.3.1.1. BET analysis of biomass

The surface area and porosity characteristics of the biochars after treatment at different temperatures are presented in Table 2.3. An increase in surface area and total pore volume was

observed with higher pyrolysis temperatures, most pronounced in the sample pyrolyzed at 550 °C. This behavior may be related to the progressive thermal degradation of the biomass organic matter. With the increase in pyrolysis temperature, there is a greater loss of volatiles and the release of substances that decompose or clog the pore structure. This results in a greater pore formation, which increases the surface area of the biochar, influencing the yield and porosity of the product [37]. On the other hand, the average pore diameter decreased after pyrolysis at higher temperatures, which is associated with the increased formation of micro and nanopores during the pyrolysis process at higher temperatures. Similar patterns have been observed in various studies in the literature [37–41].

Table 2.3. Surface area and porosity characteristics of biochars after treatment at different temperatures.

Pyrolysis temperature (°C)	Specific surface area (m^2/g)	Total pore volume (mm^3/g)	Average pore diameter (Å)
250	0.58	1.90	130.52
400	2.44	4.04	66.35
550	114.58	75.86	26.48

2.3.1.2. FTIR analysis of biomass

The FTIR spectra (Figure 2.1) were collected to evaluate the structural evolution of the functional groups in biomass as a function of treatment temperature. Structural changes can be observed from the onset of pyrolysis, through mechanisms such as fragmentation, depolymerization, and cross-linking reactions of macromolecular components [42].

In the raw biomass and the biochar treated at 250 °C, peaks associated with O–H stretching from hydroxyl groups (3330–3280 cm^{-1}) and C–H stretching vibrations of aliphatic groups (2930–2890 cm^{-1}) were identified [43,44]. Additionally, several bands between 1700 and 400 cm^{-1} were detected, corresponding to the functional groups of hemicellulose, cellulose, and lignin. Peaks near 1700–1650 cm^{-1} were associated with the C=O carbonyl group due to the presence of hemicellulose [45]. In the 1440–1300 cm^{-1} range, they are related to the C–H stretching vibrations of cellulose and hemicellulose chains, and at 1250–1148 cm^{-1}, they represent C–O–C bonds from these components [46,47]. At a wavelength close to 1020–1030 cm^{-1}, the peaks correspond to C–O deformation and stretching bonds [48]. Bands

between 700 and 900 cm^{-1} and 400 and 700 cm^{-1} can be attributed, respectively, to C–H bonds of aromatic groups in lignin and to C–C stretching vibrations [36].

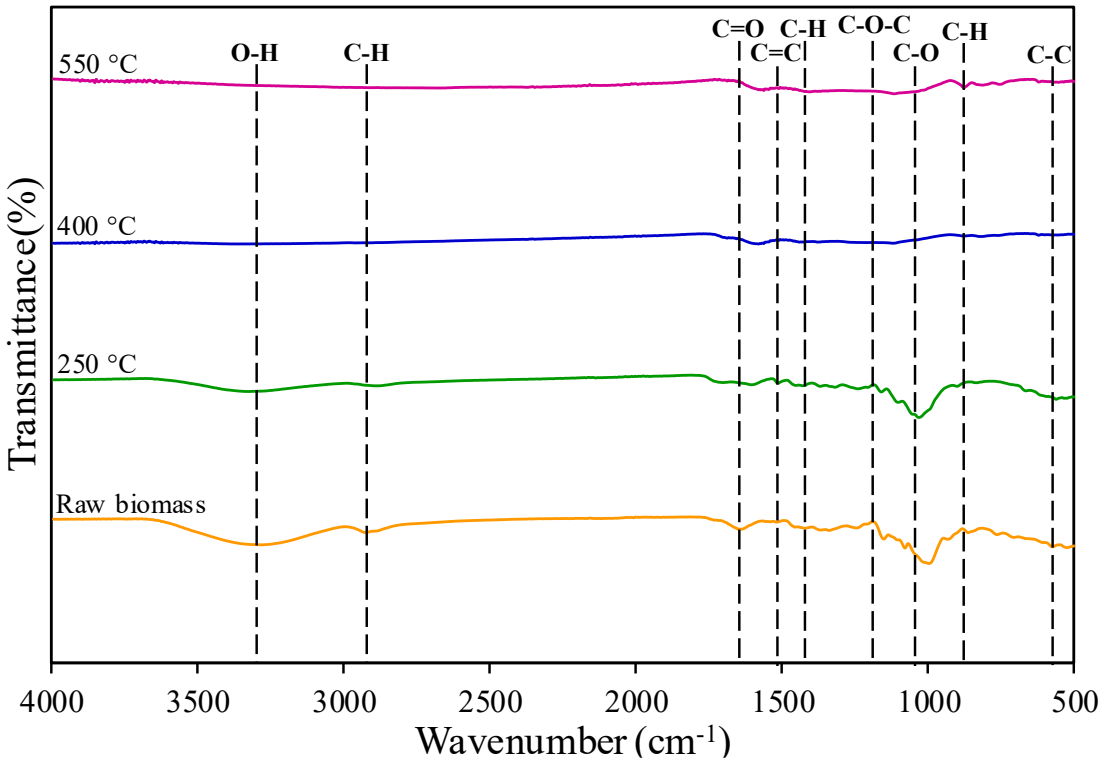

Figure 2.1. FTIR spectra of raw biomass and biochars after treatment at different temperatures.

With increasing pyrolysis temperature, the absorption peaks of some functional groups gradually weakened or even disappeared, reflecting the degradation or transformation of functional groups. This process results in a decrease in aliphatic components and the formation of condensed ring structures. Additionally, bands between 1700 and 400 cm^{-1} showed a lower transmittance intensity. In the range of 1440–1417 cm^{-1}, peaks associated with C–H stretching vibrations of cellulose disappeared, as a consequence of its thermal decomposition [49]. According to Li and Chen [43], the disappearance of O–H and C–H bonds in biomass pyrolyzed at higher temperatures (in this study, 400 and 550 °C) is attributed to the breakage of hydroxyl groups of aliphatic groups. Kloss et al. [50] stated that the removal of these bonds is closely associated with an increase in pore numbers. After pyrolysis at 550 °C, almost no functional groups were found in the produced biochar. The disappearance of these compounds may be specifically related to the total decomposition of hemicellulose and cellulose and the removal of volatile matter at higher temperatures. However, between 1605–1500 cm^{-1}, C=C peaks were

identified, whose presence was also noted in other samples, associated with aromatic rings due to the presence of lignin [51].

Overall, the analyzed spectra demonstrated a clear distinction between the functional groups present in each biochar, influenced by thermal decomposition. This difference is mainly reflected in the permanence of the lignin functional groups and the disappearance of the groups associated with cellulose and hemicellulose, indicating a reduction in oxygen and hydrogen content. Figure 2.1 highlights that the biomass pyrolysis process resulted in the decomposition of compounds containing C–O, O–H, and C=O bonds, while compounds with C–H and C=C bonds were maintained.

2.3.1.3. Microstructural and morphological analysis of biomass

The micrographs obtained by SEM at different magnifications are shown in Figure 2.2. It was observed that the pyrolysis temperature strongly influenced the microstructure of the different biochars obtained. The raw biomass exhibited a continuous surface, similar to the biochar derived from biomass treated at 250 °C. Under these conditions, a slightly porous structure was observed, with the presence of disconnected pores, associated with an incomplete carbonization at low temperature.

After pyrolysis at 400 °C, the biochar particles appeared more fibrous, which can be attributed to cellulose, whose proportion became predominant in relation to hemicellulose. The biochar produced at 550 °C presented a disordered and extensively degraded structure, with its fibrous character reduced, resulting in a greater surface area (as indicated in Table 2.3). The thermal degradation of the main biomass components and the significant release of volatile matter that occurs at this temperature may be responsible for the presented structure.

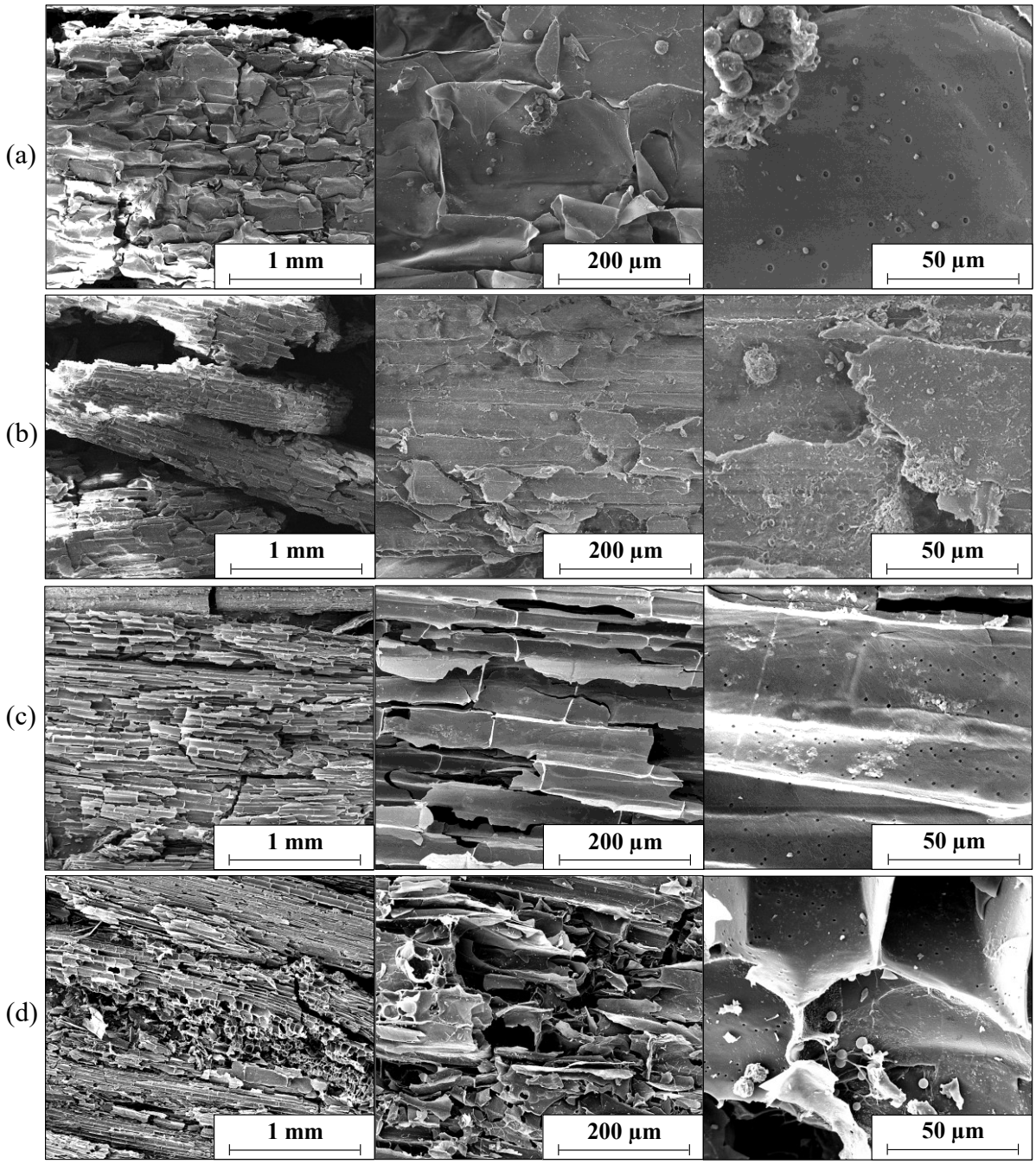

Figure 2.2. SEM images showing the surface microstructure of (a) raw biomass and biochars after treatment at (b) 250 °C, (c) 400 °C, and (d) 550 °C.

2.3.1.4. Thermogravimetric analysis of biomass

Figure 2.3 presents the TGA and DTG curves of the raw biomass and its pyrolyzed products. The thermogravimetric analysis allowed for the association of mass loss with moisture loss, degradation of the main components remaining in each biomass, and the volatilization process.

The results observed in this study were very consistent with thermogravimetric analyses of different biomasses [38,45,47,52–54].

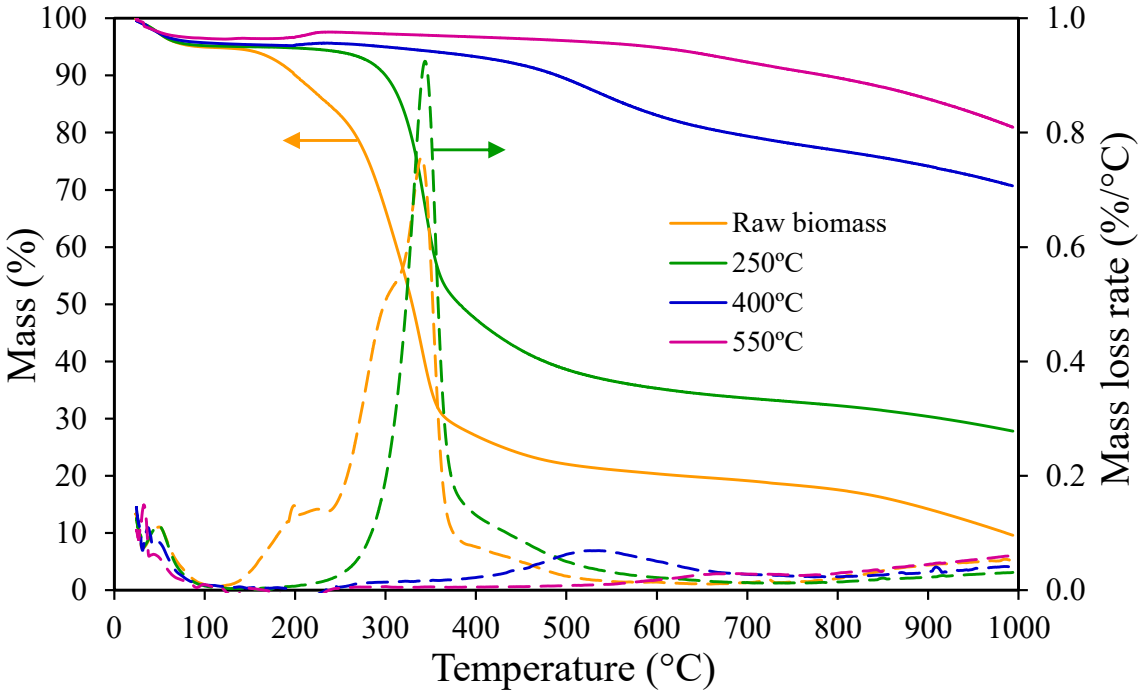

Figure 2.3. TGA and DTG curves of the raw biomass and biochars after treatment at different temperatures.

It was possible to identify a distinct thermal behavior between the samples, with the curves corresponding to the raw biomass and the biochar after treatment at 250 °C showing an intense mass loss in the range of 200 to 400 °C. This behavior was expected since the other samples were subjected to a previous heat treatment at higher temperatures. Therefore, they had already experienced part of the volatile matter decomposition during the pyrolysis process. Through the analysis of the DTG curves, the highest intensity peaks were attributed to the degradation of hemicellulose and cellulose. According to El-Tawil et al. [55] and Najafi et al. [56], two prominent peaks can be observed in the DTG curves of different biomasses. The main peak is associated with cellulose decomposition, while a first shoulder at a lower temperature corresponds to hemicellulose degradation, as also seen in raw biomass. Biochars pyrolyzed at 400 and 550 °C did not exhibit pronounced or well-defined peaks, possibly due to the predominance of lignin as the main organic component, which decomposes slowly and gradually. Combined with the other findings, these results highlight the influence of pyrolysis

temperature on biomass properties during heat pre-treatment, playing a key role in altering its chemical composition, structure, and thermal behavior.

2.3.2. Performance of self-reducing briquettes at high temperatures

2.3.2.1. Mass loss of self-reducing briquettes

The mass loss of the briquettes resulting from tests up to 1250 °C is shown in Figure 2.4. For the briquettes, the results indicated a progressive increase in mass loss with increasing temperature. Up to 300 °C, mass loss was similar for all samples and was attributed to the release of intrinsic moisture from the agglomerates and the partial dehydration of goethite ore (as indicated by the thermogravimetric analysis of the pellet feed shown in Figure 2.S3 of the Supplementary Material) and sodium silicate. Above 300 °C, the mass loss was associated with the final portion of sodium silicate decomposition and, primarily, with the devolatilization of the biomass. B250 exhibited a substantially greater mass loss in this interval due to the nature and higher volatile matter content remaining from the treatment at 250 °C (see Table 2.2).

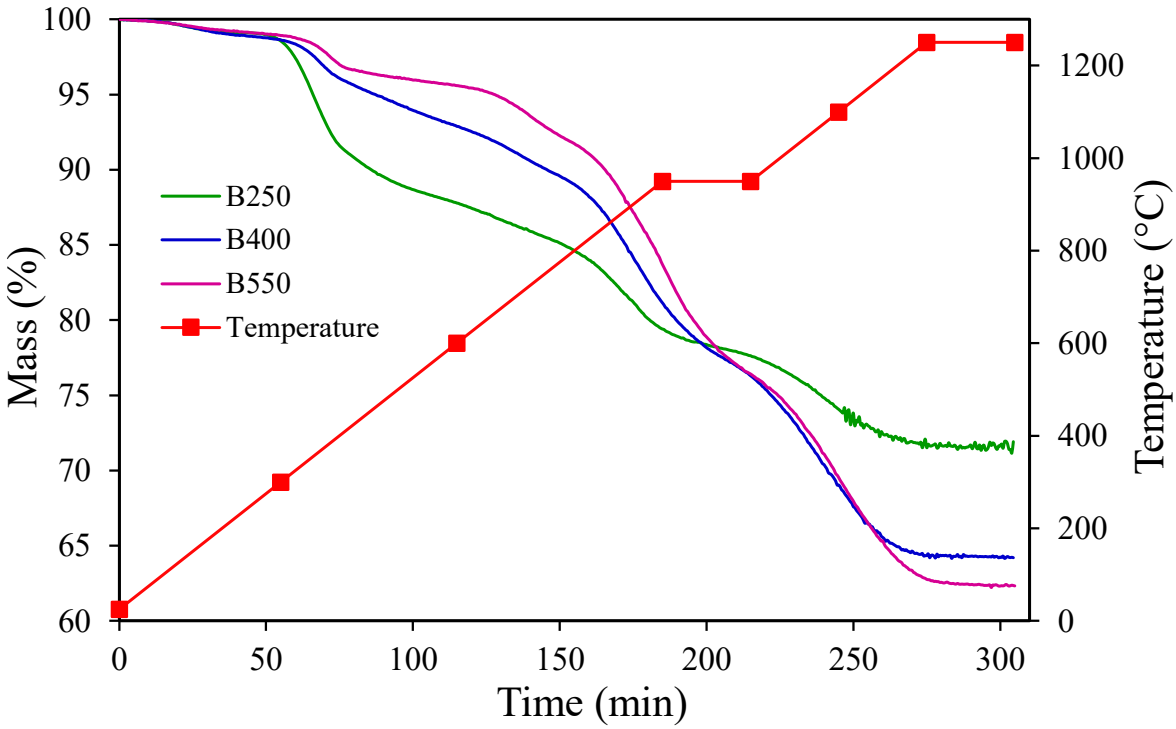

Figure 2.4. Mass loss of briquettes with biochars after treatment at different temperatures.

At 950 °C, the briquettes presented a considerable increase in mass loss. This phenomenon must be mainly related to the beginning of carbon gasification (Boudouard reaction) and iron oxides reduction by CO, although a small fraction can be linked to the remaining volatile matter decomposition. The self-reduction reactions, represented by Equations 2.1 and 2.2, are associated with the increase in partial pressure of CO inside the briquettes, resulting from carbon consumption in the gasification reaction, which occurs at temperatures above 800 °C [31]. There is a consensus among several researchers, from the early studies of Fruehan [18] to the most recent ones, such as Bagatini et al. [34], that the global self-reduction reaction is a solid-solid process that proceeds through gaseous intermediates (CO and CO_2) formed within the agglomerates by parallel reactions. After 30 min of isothermal plateau at 950 °C, a continuous increase in mass loss was observed, probably as a result of the continuation of the self-reduction reactions.

$$C_{(s)} + CO_{2(g)} = 2CO_{(g)} \quad (2.1)$$

$$Fe_xO_{y(s)} + CO_{(g)} = Fe_xO_{y-1(s)} + CO_{2(g)} \quad (2.2)$$

In this interval, B550 showed a greater mass loss compared to the other briquettes, which is possibly related to the greater availability of carbon for reaction, according to the C/O molar ratio (Section 2.3). A greater amount of carbon favors the gasification reaction and the self-reduction mechanism, increasing the potential for CO_2 regeneration within the agglomerates and, consequently, enhancing the reduction degree [57]. When briquettes reached 1250 °C, the mass remained constant for all the briquettes, indicating that the reagents (C or O) were consumed, limiting the reactions. Overall, the thermogravimetric behavior of the briquettes was consistent with their respective compositions (primarily volatile matter, carbon, and reducible oxygen).

2.3.2.2. Gas analysis of self-reducing briquettes

Figure 2.5 shows a projection of the CO/CO_2 data on the Chaudron equilibrium diagram, obtained from the quantitative analysis of the gas volumes generated during the high-temperature tests with the gas analyzer, as described in Section 2.4. This diagram illustrates how the partial pressure of CO, expressed as the $PCO/(PCO+PCO_2)$ ratio, and temperature

affect the chemical equilibrium of iron oxide phases in the system—that is, the temperature conditions under which the partial pressure of CO is sufficient to stabilize a given oxide phase.

Up to 700 °C, the partial pressure of CO of gases evolved from the briquettes was zero, except for a small interval associated with B250, resulting from the biomass devolatilization. In these briquettes, although there is an increase in the volume of CO produced, the amount of CO_2 generated is higher, which justifies the decrease in the partial pressure of CO at temperatures above 300 °C. From 700 °C onwards, with the increase in temperature, a trend of increasing partial pressure of CO was observed. This fact is likely related to the occurrence of carbon gasification, which is favored by a progressive increase in temperature. According to the gas analysis data for all the briquettes, the CO concentration increased with temperature, where the iron oxides reduction becomes thermodynamically feasible, promoting the progressive reduction of hematite to magnetite at around 700 °C, magnetite to wustite at 800 °C, and finally, wustite to metallic iron at 950 °C.

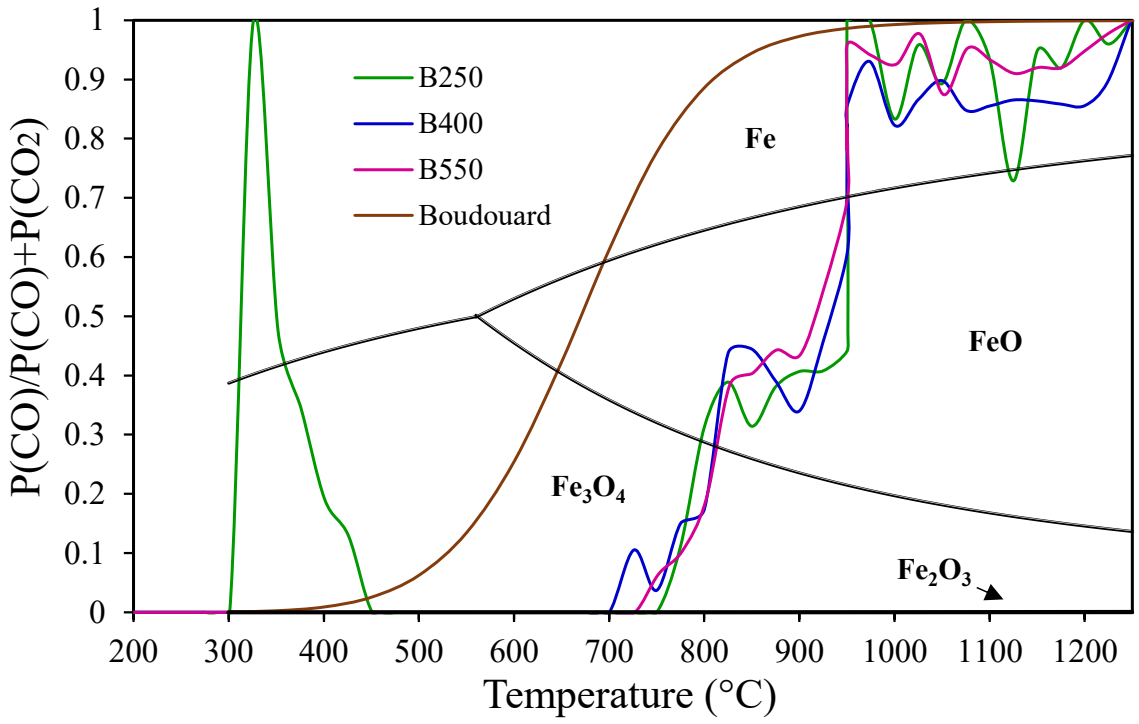

Figure 2.5. Chaudron equilibrium diagram for briquettes with biochars after treatment at different temperatures.

As observed in Figure 2.5, from 950 °C onwards, the PCO/(PCO+PCO_2) ratio of the gas generated by the reactions induced by briquette heating is higher than that associated with the reduction of wustite to metallic iron and lower than the gasification (Boudouard) curve. The

results demonstrate that the partial pressure of the reducing gases was thermodynamically enough to promote the reduction of wustite to metallic iron. From this temperature, there is CO available for reduction, indicating thermodynamic conditions favoring metallic iron formation, and if this does not occur, it is due to reduction barriers. Thus, it cannot be stated that carbon gasification is the only reaction controlling the global kinetics of self-reduction.

In this work, gas analysis demonstrated that all the biochars are highly reactive and that the carbon reactivity is similar among the samples treated at different temperatures. For all the briquettes evaluated, the gasification reaction exhibited high kinetics, with a strong potential for CO_2 regeneration, ensuring that the partial pressure of CO remained high from 950 °C onwards. Therefore, under the conditions of this study, the reduction proved to be the reaction-limiting step.

2.3.2.3. Chemical characterization and metallization of self-reducing briquettes

The ferrous phases identified in the briquettes by Mössbauer spectroscopy are presented in Figure 2.6, along with their proportion in each sample. At room temperature, hematite was the predominant phase in all the briquettes, although magnetite and goethite were also identified, reflecting the ferrous raw material used in these agglomerates (pellet feed). In the tests at 600 °C, goethite was no longer detected for any sample due to its decomposition into hematite, which begins at around 250 °C (as indicated in Figure 2.S3 of the Supplementary Material). Additionally, a greater presence of magnetite was observed compared to the previous conditions, indicating the partial reduction of hematite. This transition was more pronounced in the B250 briquettes, possibly as a result of reduction by volatiles, as this biochar has a higher volatile matter content, which is released at lower temperatures. According to Bagatini et al. [44] and Das et al. [58], volatiles can have significant potential as a reducing agent and play an important role in self-reducing mixtures at temperatures below 800 °C.

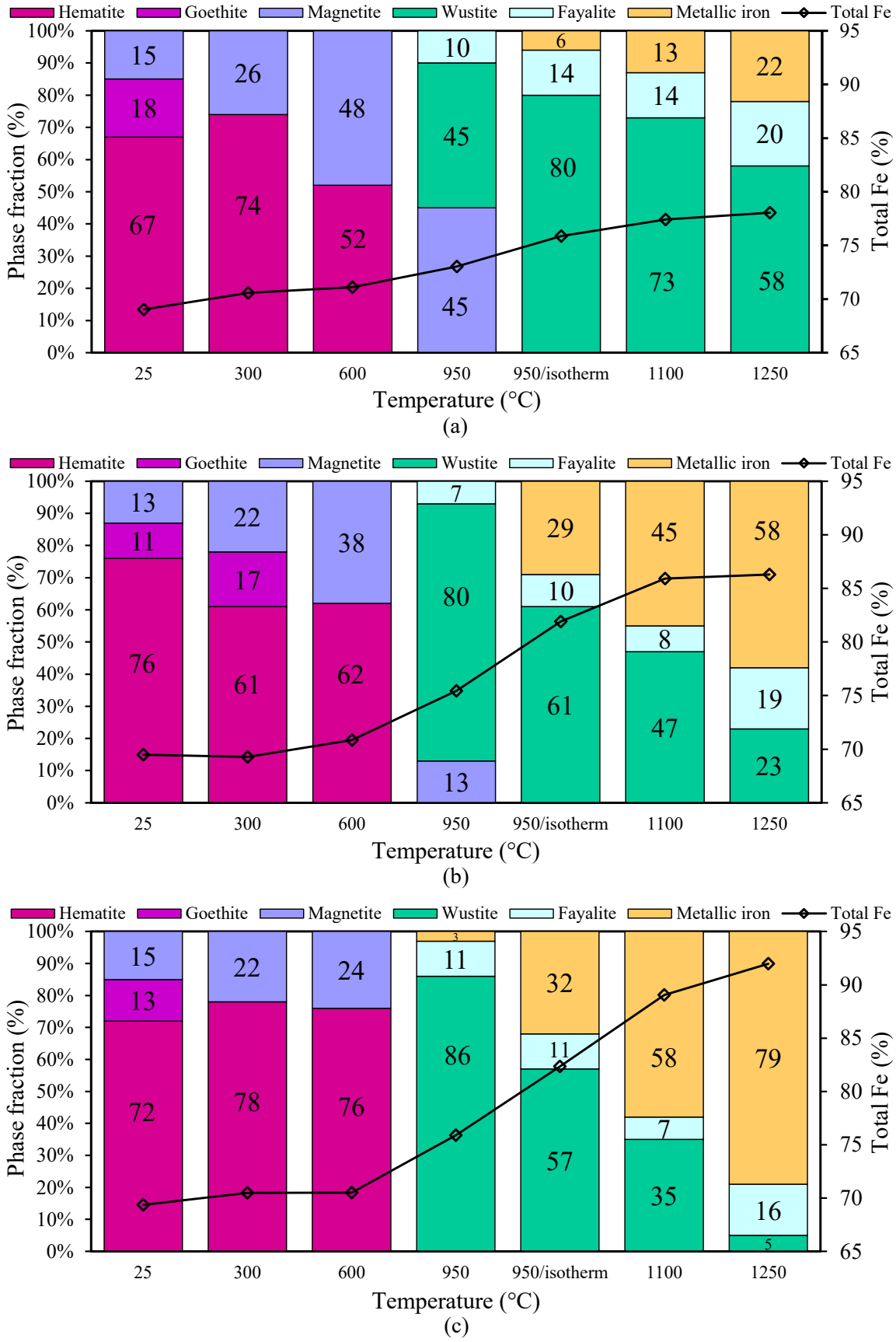

Figure 2.6. Chemical analysis of ferrous phases obtained by the Mössbauer spectroscopy technique: (a) B250, (b) B400, and (c) B550.

At 950 °C, hematite was no longer detected, indicating that this phase was completely reduced. In B250 and B400, the phases magnetite, wustite, and fayalite were identified, pointing to the progress of the reduction process. For B550, wustite was the predominant phase, accompanied by fayalite and the emergence of metallic iron in lower proportions. It is noted that, for this sample, no more magnetite was detected. These results indicate that the mass loss related to self-reduction up to 950 °C occurred primarily due to the reduction of hematite and magnetite to wustite, as well as the associated carbon consumption. After 30 min of isothermal plateau at 950 °C, the magnetite was completely reduced, and metallic iron was identified in all samples. This phase showed a higher proportion as the temperature increased to 1100 °C, due to the enhanced carbon gasification and the increasingly thermodynamically favorable conditions for the reduction of wustite to metallic iron.

After heating to 1250 °C, the highest percentage of metallic iron was achieved, where the higher the biomass pyrolysis temperature, the higher the reduction progress. This behavior is likely related to the greater availability of fixed carbon for the iron oxides reduction, as previously discussed. The fayalite identified in all briquettes results from the presence of reagents with high silica (SiO_2) content, formed through the partial association of wustite (FeO) with the SiO_2 (Equation 2.3) present in the iron ore and sodium silicate used as a binder. It is noted that fayalite reduced more slowly than wustite, which was also observed in other studies [59,60].

$$2FeO_{(s)} + SiO_{2(s)} = Fe_2SiO_{4(s)} \quad (2.3)$$

From the Mössbauer results, data concerning the total iron content of the briquettes are illustrated in Figure 2.6. Up to 600 °C, no significant differences were found between the briquettes studied. However, after this temperature, a continuous increase in the total iron content was observed, attributed to the evolution of volatiles, the reduction of iron oxides, and carbon gasification. In this context, the briquettes with biochar pyrolyzed at 550 °C exhibited higher total iron content.

The reduction efficiency of the briquettes was also evaluated through the carbon and metallization analyses (Figure 2.7). It can be first noted that the higher the biomass pyrolysis temperature, the higher the carbon content in the samples, which is consistent with the chemical analysis of the biochars that compose each briquette (see Table 2.2). The proportion of carbon

in samples increased up to 300 °C, which can be attributed to the partial decomposition of the iron ore and binder. However, from this temperature and for all the briquettes studied, a decrease in carbon content was observed as a function of temperature and time, which reflects its progressive consumption due to the devolatilization (up to around 600 °C) and gasification (mainly from 900 °C) stages. When higher temperatures (1250 °C) were reached, the intensified reactions of iron oxide reduction and carbon gasification promoted the complete consumption of carbon in the briquettes. These results elucidated that the mass stability and the complete reduction of samples were limited by the availability of carbon. On the other hand, the metallization degree of the briquettes increased from 950 °C and advanced progressively with the temperature, achieving the highest value (86%) at 1250 °C for B550. Therefore, it is evident that the increasing fixed carbon content provides advantages for the iron oxide reduction and higher iron formation in the briquettes.

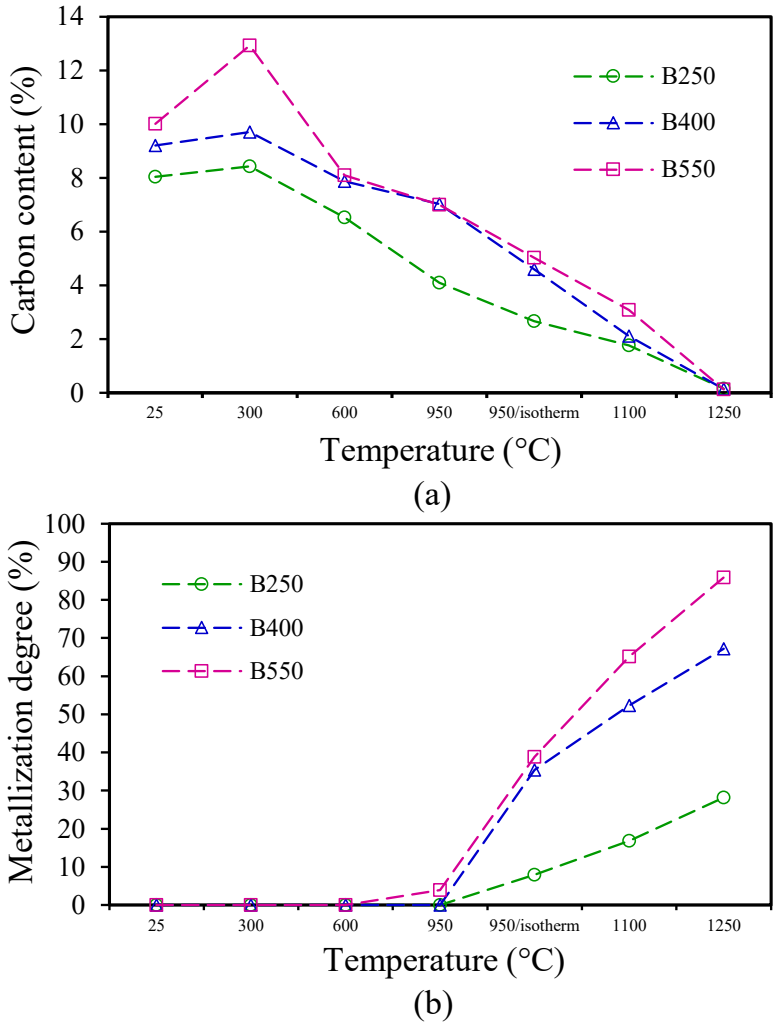

Figure 2.7. (a) Carbon content and (b) metallization degree of briquettes with biochars after treatment at different temperatures.

Nevertheless, considering the use in blast furnaces and the operational parameters of this reactor, all the briquettes exhibited higher performance in terms of reduction and metallization in the preparation zone (up to approximately 950 °C). Once the briquettes achieve the elaboration zone blast furnace in a more reduced state, it leads to lower fuel consumption in this reactor. In this context, B550 obviously would promote greater fuel savings, as it achieved the highest metallization degree among the briquettes tested.

2.3.2.4. Mechanical strength of self-reducing briquettes

Figure 2.8 shows the compressive strength of briquettes before and after the interrupted tests. At room temperature, B550 exhibited higher strength, which may be associated with the phenomena resulting from the thermal decomposition of biomass components during pyrolysis. In the biochar produced after pyrolysis at 550 °C, there was greater degradation of its components, where hemicellulose and cellulose were completely degraded (Figure 2.2). This resulted in a reduced fibrous character and, therefore, lower elasticity, contributing to a more cohesive structure in the briquettes. According to Narita et al. [61], the elastic recovery of a material can generate cracks in its structure, reducing its strength. Another reason may be related to the greater surface area in this biochar (Table 2.3) as a consequence of greater devolatilization. Thus, the binder's action within the internal structure of the briquettes is enhanced, allowing for greater cohesion. On the other hand, the compressive strength values found for B400 were lower than B250. In biomass treated at 250 °C, the components are in a more uniform proportion, despite the partial degradation of hemicellulose. After pyrolysis at 400 °C, the proportion of cellulose, the most fibrous component of the biomass, becomes predominant, concentrating fibrous material in the briquettes and resulting in lower strength.

After interrupted tests, a decrease in the mechanical strength of the briquettes was observed as the temperature increased, reaching a minimum value at 950 °C after a 30-min isotherm. Up to 600 °C, this drop is likely linked to the thermal decomposition of sodium silicate and the evolution of volatile matter gas from the biomass, as indicated by the mass loss results. In this temperature range, the decrease in strength was more pronounced for B250, which has a higher volatile content. The lower strength at 950 °C may be related to continued devolatilization and self-reduction reactions. The release of gases resulting from these reactions increases the internal pressure in the briquettes, contributing to the weakening of their structure [34]. On the

other hand, after heating at 1250 °C, a significant increase in the strength of the briquettes was noted. According to the literature [27,34,59], this phenomenon may be associated with the formation of metallic iron in the agglomerates and sintering of reduced iron particles, as well as the presence of a liquid phase (slag), resulting in a more cohesive structure.

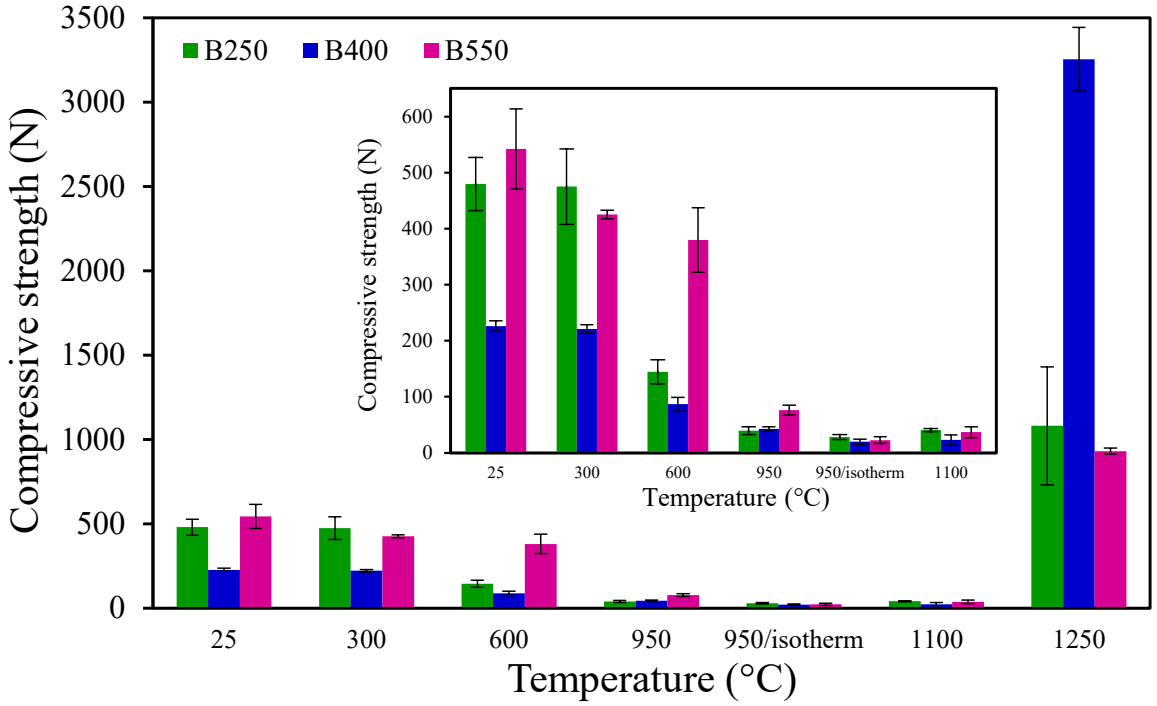

Figure 2.8. Compressive strength of briquettes at different heating stages, highlighting the results from tests interrupted up to 1100 °C.

The external appearance of the briquettes after interrupted tests at different temperatures is shown in Figure 2.9a. Horizontal cracks are observed on the surface of the samples, which must be associated with the one-dimensional compaction characteristic of the production method. These cracks intensified during heating due to the formation and release of internal gases (devolatilization and self-reducing reactions), as well as the volume expansion related to phase transitions of internal iron compounds. Among the briquettes studied, B550 exhibited the most extensive crack propagation, especially after the tests at 950 and 1100 °C, during which swelling also increased significantly. With the increase in temperature to 1250 °C, all the briquettes exhibited a reduction in volume. As also reported by Wei et al. [4], the briquettes shrank after reaching their maximum expansion, indicating that the reduction resulted in a greater formation of the metallic iron phase. This shrinkage can be justified by the greater

sintering of the iron particles, the formation of liquid/slag, and the mass loss of carbon and oxygen from the system [31,62].

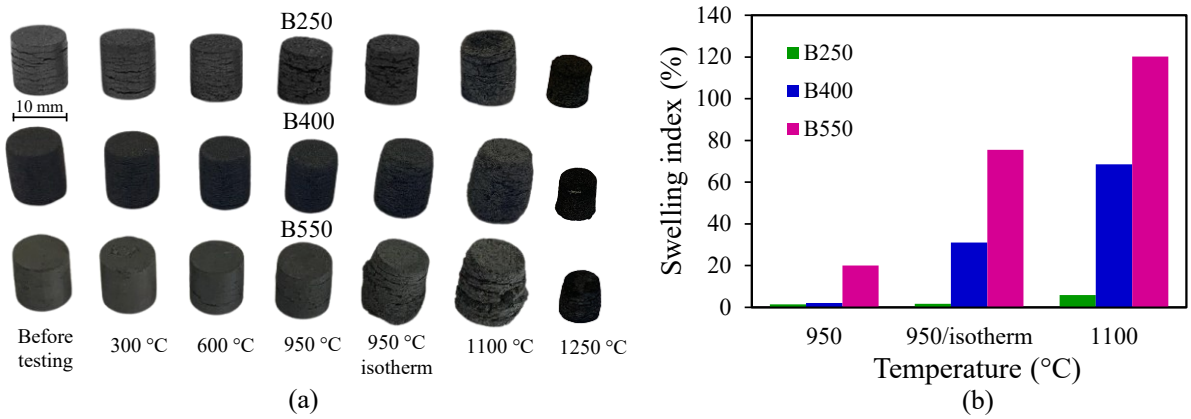

Figure 2.9. (a) Visual appearance and (b) swelling index of briquettes after interrupted tests.

The magnitude of swelling of the briquettes was determined based on the expansion volume relative to the initial sample, determined by the swelling index (Figure 2.9b). The results reveal a clear trend in the swelling behavior with increasing biomass pyrolysis temperature. Furthermore, they indicate that swelling depends on both temperature and reduction time, as also reported by Kumar et al. [31]. B400 and B550 exhibited significant swelling, particularly after the plateau at 950 °C, reaching maximum levels at 1100 °C. However, this behavior was more pronounced in the briquettes containing biomass pyrolyzed at 550 °C. In contrast, B250 maintained its physical and geometrical integrity throughout the analyzed temperature range, despite the decrease in strength up to 950 °C, characterized by minimal swelling indices (< 20%), which are considered acceptable [27].

It was observed that the swelling of the briquettes occurred mainly during the reduction to wustite and metallic iron, as also reported in previous studies in the literature [32,33,63]. According to Takano and Mourão [27], the swelling of pellets containing charcoal begins at approximately 30% of the overall reaction, during the transition from wustite to metallic iron, followed by a shrinkage of the agglomerates. Based on the main factors associated with swelling, the compositional characteristics of the briquettes and their components may explain the different swelling magnitudes among the agglomerates studied. The greatest variation in volume in B550 may be attributed to the more intense generation and release of gases within the briquette structure, which contributed to the development of internal cracks. The high fixed

carbon content promotes faster gasification, leading to increased internal pressure and, consequently, more pronounced swelling. Additionally, the ash content in the biochars also increased with the pyrolysis temperature, which may also influence the observed swelling behavior. On the other hand, the higher the volatile matter content, the higher the porosity of the briquettes during heating due to gas evolution. Thus, a more porous matrix facilitates the release of internally generated gases, reducing internal pressure and mitigating swelling.

After testing at 1250 °C, an inverse trend was observed in the compressive strength of the briquettes, with B400 showing the highest strength. This behavior is thought to be linked to swelling phenomena and the formation of specific phases, such as liquid slag and metallic iron, at this temperature. The abnormal or "catastrophic" swelling exceeding 20% in B550 after interrupted tests at 950 and 1100 °C may have negatively impacted their structural cohesion under high-temperature conditions. Mantovani and Takano [30] associated the decrease in mechanical strength with the swelling phenomenon within this temperature range. Conversely, B250 exhibited a lower reduction compared to B400, indicating less metallic iron formation and, consequently, lower mechanical strength.

2.3.2.5. Microstructural analysis of self-reducing briquettes

The microstructure of the briquettes before testing and after heating to 1250 °C was evaluated via SEM. The briquettes tested at 950 and 1100 °C were not analyzed concerning their microstructure due to their very low mechanical strength, which made the samples' preparation for SEM analysis unfeasible.

Figure 2.10 presents an overview of the internal structure of the briquettes before testing (100x magnification), where the components are homogeneously dispersed and consist of particles of different sizes and shapes incorporated in a single matrix (dark region). A better interpretation of the microstructure of these agglomerates was obtained from the EDS analysis, performed at random points on the samples and representing their main regions. The briquettes are composed of phases rich in iron and oxygen, which correspond to the hematite, magnetite, and goethite oxides (A), and quartz particles (dark gray - B) distributed in a matrix of embedding resin and biochar (black - C). In these images, the biochar, predominantly formed by carbon and oxygen, was easily distinguished, with emphasis on its fibrous and porous structure.

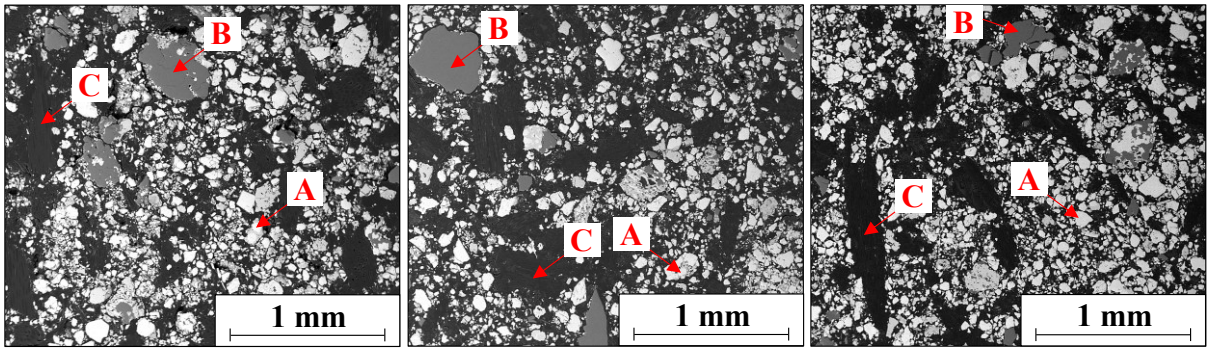

(a) (b) (c)

Figure 2.10. SEM microstructure of briquettes before testing: (a) B250, (b) B400, and (c) B550. A (light shades of gray): hematite, magnetite, and goethite; B (dark gray): quartz; and C (black): resin, biochar, and pore.

After testing at 1250 °C (Figure 2.11), the formed microstructure revealed a denser distribution of small particles, which can result from the coalescence and sintering between the iron metallic grains to each other. Completely reduced iron (white - D), particles rich in iron and oxygen corresponding to wustite (light gray - E), and particles formed by iron, oxygen, and silicon representing fayalite (intermediate gray - F) were identified by EDS analysis. In addition, analyses of the dark gray regions (G) indicated the presence of iron, oxygen, silicon, and considerable amounts (> 1%) of sodium, aluminum, potassium, magnesium, and other trace elements. This phase may be associated with the formation of liquid from different components of the briquettes (pellet feed, biochar ash, and binder) in a matrix defined as slag, resulting from the high-temperature process. As the reduction progressed, small metallic iron particles aggregated to form larger ones, which subsequently separated from the slag [26]. Finally, the darker regions (black - H) represent a porous matrix composed of resin and small amounts of residual biochar (since the carbon was consumed throughout the tests) present in the briquettes.

The influence of biomass pyrolysis temperature on the microstructure of the briquettes was also investigated. In B250, the presence of metallic iron was significantly lower, with a predominant proportion of wustite, which is consistent with the chemical analysis via Mössbauer spectroscopy (Figure 2.6). On the other hand, briquettes produced with biochar pyrolyzed at higher temperatures exhibited greater amounts of metallic iron in their structure. In this condition, the metallic iron particles agglutinated and connected more intensely. As an indication of the reduction mechanism, in B400 (Figure 2.11d) and B550, an external layer of the wustite phase surrounding the iron particles was observed.

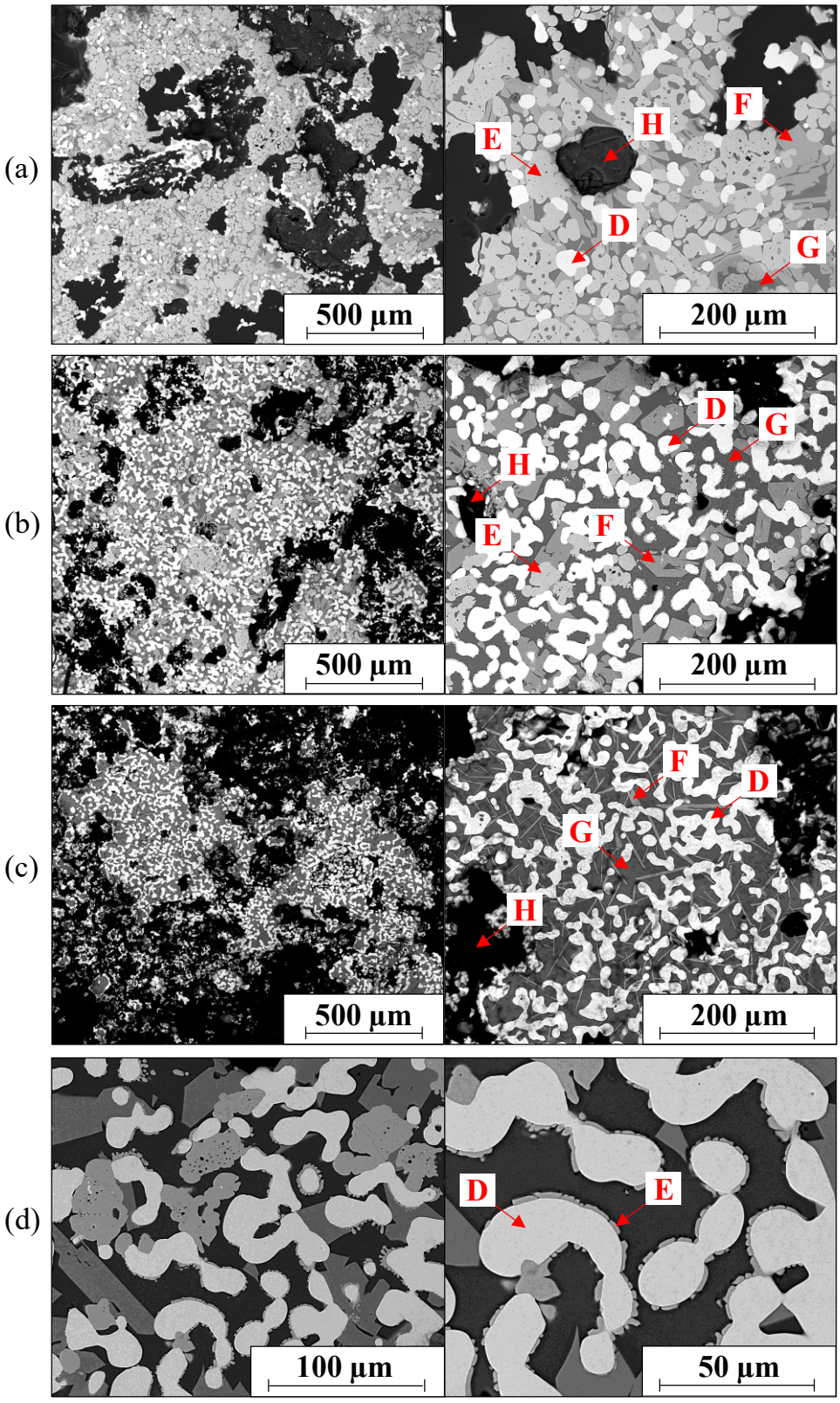

Figure 2.11. SEM microstructure of briquettes after heating to 1250 °C: (a) B250, (b) B400, and (c) B550. (d) SEM microstructure of B400, indicating the advancement of the reduction of wustite into metallic iron. D (white): metallic iron; E (light gray): wustite; F (intermediate gray): fayalite; G (dark gray): slag; and H (black): resin, biochar, and pore.

2.4. Conclusions

In this study, self-reducing briquettes produced from pellet feed and sugarcane bagasse pyrolyzed at different temperatures were evaluated under the thermal regime representative of a blast furnace, investigating the influence of biomass pyrolysis temperature on the reduction behavior and mechanical strength of these agglomerates.

Initially, the results indicated that pyrolysis temperature has a significant influence on the characteristics and physicochemical properties of biochars obtained by thermal pre-treatment. As the temperature increased, volatile release intensified, and the biochars exhibited higher surface area and total pore volume. This temperature effect was also reflected in the permanence of the lignin functional groups and the disappearance of groups associated with hemicellulose and cellulose, as well as in the distinct thermogravimetric behavior observed among the samples. These modifications were directly reflected in the performance of the evaluated briquettes. Thus, controlling pyrolysis conditions is a critical factor in tailoring biomass-derived biochars for metallurgical applications.

From high-temperature tests, mass loss and reduction degree of the briquettes increased with temperature, accompanied by a decrease in carbon content. Metallic iron was detected in all samples at 950 °C, although the use of biomass pyrolyzed at 550 °C resulted in a higher metallization degree, reaching 86% at 1250 °C, due to the greater availability of fixed carbon for self-reducing reactions. Through gas analysis, it was concluded that the biochars are highly reactive and that carbon reactivity is similar among the samples treated at different pyrolysis temperatures. Sufficient CO is available to reduce wustite to metallic iron, and the reduction is the reaction-limiting step. Among all the briquettes, B550 exhibited the highest mechanical strength at room temperature. However, interrupted tests revealed a decrease in compressive strength during heating for all samples, reaching a minimum at 950 °C, followed by an increase at higher temperatures, due to the sintering of the reduced iron particles. The strength of the briquettes after high-temperature heating was directly influenced by swelling behavior, indicating that excessive expansion during heating compromises structural integrity. Therefore, controlling this phenomenon is essential to ensure the mechanical performance of the briquettes.

Considering the operational parameters of the blast furnace, all the briquettes presented a high performance in terms of reduction and metallization degree in the preparation zone, which could result in lower fuel consumption, especially concerning B550. However, B400 exhibited the highest strength at high temperatures (1250 °C), where the concomitant phenomena of lower swelling and the formed phases promoted a more stable structure, less susceptible to degradation. For application in these reactors, where mechanical integrity at high temperatures (> 1100 °C) is critical, biochar pyrolyzed at 400 °C appears to be more suitable, despite slightly lower metallization compared to briquettes produced with biochar treated at 550 °C. Although pyrolysis at 550 °C maximizes reduction, it compromises mechanical strength due to the occurrence of swelling.

Acknowledgments

The authors express gratitude to Coordination for the Improvement of Higher Education Personnel - Brazil (CAPES-PROEX) and National Council for Scientific and Technological Development - Brazil (CNPq) for accomplishment and support of this work.

2.5. References

[1] R.Q. Wang, L. Jiang, Y.D. Wang, C. Font-Palma, V. Skoulou, A.P. Roskilly, Woody biomass waste derivatives in decarbonised blast furnace ironmaking process, Renew. Sustain. Energy Rev. 199 (2024) 114465. https://doi.org/10.1016/j.rser.2024.114465.

[2] J. Kim, B.K. Sovacool, M. Bazilian, S. Griffiths, J. Lee, M. Yang, J. Lee, Decarbonizing the iron and steel industry: A systematic review of sociotechnical systems, technological innovations, and policy options, Energy Res. Soc. Sci. 89 (2022) 102565. https://doi.org/10.1016/j.erss.2022.102565.

[3] R. Lundmark, E. Wetterlund, E. Olofsson, On the green transformation of the iron and steel industry: Market and competition aspects of hydrogen and biomass options, Biomass Bioenergy 182 (2024) 107100. https://doi.org/10.1016/j.biombioe.2024.107100.

[4] R. Wei, Z. Peng, J. Wang, Q. Xue, H. Zuo, Waste crayfish shell addition improves mechanical strength and reducibility of hematite briquettes, Biomass Bioenergy 201 (2025) 108107. https://doi.org/10.1016/j.biombioe.2025.108107.

[5] H. Ahmed, New trends in the application of carbon-bearing materials in blast furnace iron-making, Minerals 8 (2018) 561. https://doi.org/10.3390/min8120561.

[6] E. Mousa, C. Wang, J. Riesbeck, M. Larsson, Biomass applications in iron and steel industry: An overview of challenges and opportunities, Renew. Sust. Energy Rev. 65 (2016) 1247–1266. https://doi.org/10.1016/j.rser.2016.07.061.

[7] S.S. Rath, D.S. Rao, A. Tripathy, S.K. Biswal, Biomass briquette as an alternative reductant for low grade iron ore resources, Biomass Bioenergy 108 (2018) 447–454. https://doi.org/10.1016/j.biombioe.2017.10.045.

[8] H. Suopajärvi, K. Umeki, E. Mousa, A. Hedayati, H. Romar, A. Kemppainen, C. Wang, A. Phounglamcheik, S. Tuomikoski, N. Norberg, A. Andefors, M. Öhman, U. Lassi, T. Fabritius, Use of biomass in integrated steelmaking - Status quo, future needs and comparison to other low-CO_2 steel production technologies, Appl. Energy 213 (2018) 384–407. https://doi.org/10.1016/j.apenergy.2018.01.060.

[9] Y. Liu, Y. Shen, Modelling and optimisation of biomass injection in ironmaking blast furnaces, Prog. Energy Combust. Sci. 87 (2021) 100952. https://doi.org/10.1016/j.pecs.2021.100952.

[10] D. Khasraw, C. Martin, J. Herbert, Z. Li, A comprehensive literature review of biomass characterisation and application for iron and steelmaking processes, Fuel 368 (2024) 131459. https://doi.org/10.1016/j.fuel.2024.131459.

[11] H. Sheng, Y. Yang, W. Zhan, Z. He, J. Liu, L. Gao, Exploring the effects of biomass utilization on the metallurgical performance and formation mechanisms of iron ore pellets, J. Anal. Appl. Pyrolysis 186 (2025) 106977. https://doi.org/10.1016/j.jaap.2025.106977.

[12] J.O. Brotto, D. Danaci, P.S. Fennell, J.S. Salla, H.J. José, R.F.P.M. Moreira, Enhancing low-carbon iron and steel production with torrefied biomass, Biomass Bioenergy 193 (2025) 107558. https://doi.org/10.1016/j.biombioe.2024.107558.

[13] L. Yi, X. Shen, Y. Shu, H. Zhang, Y. Zhang, H. Zhang, G. Li, T. Jiang, Application of biomass in low-carbon ironmaking: Iron ore reduction self-driven by the biogas recirculation, J. Clean. Prod. 521 (2025) 146208. https://doi.org/10.1016/j.jclepro.2025.146208.

[14] S. Reis, P.J. Holliman, C. Martin, Evaluation of the effect of a biomass fuel source on the thermal properties of iron ore sinter, Fuel 381 (2025) 133172. https://doi.org/10.1016/j.fuel.2024.133172.

[15] C.-M. Wiklund, M. Helle, H. Saxén, Economic assessment of options for biomass pretreatment and use in the blast furnace, Biomass Bioenergy 91 (2016) 259–270. https://doi.org/10.1016/j.biombioe.2016.05.033.

[16] J. Solar, F. Hippe, A. Babich, B.M. Caballero, I. de M. Rodríguez, C. Barriocanal, A. López-Urionabarrenechea, E. Acha, Conversion of injected forestry waste biomass charcoal in a blast furnace: Influence of pyrolysis temperature, Energy Fuels 35 (2021) 529–538. https://doi.org/10.1021/acs.energyfuels.0c03040.

[17] H. Tang, L. Ma, Z. Liu, Z. Guo, Charging biochar composite briquette in blast furnace for reducing CO_2 emissions: Combined numerical and experimental investigations, Metall. Mater. Trans. B 53 (2022) 2248–2261. https://doi.org/10.1007/s11663-022-02525-2.

[18] R.J. Fruehan, The rate of reduction of iron oxides by carbon, Metall. Mater. Trans. B 8 (1977) 279–286. https://doi.org/10.1007/bf02657657.

[19] P. Kowitwarangkul, A. Babich, D. Senk, Reduction behavior of self-reducing pellet (SRP) for low height blast furnace, Steel Res. Int. 85 (2014) 1501–1509. https://doi.org/10.1002/srin.201300399.

[20] Z. Liu, X. Bi, Z. Gao, W. Liu, Carbothermal reduction of iron ore in its concentrate agricultural waste pellets, Adv. Mater. Sci. Eng. 2018 (2018) 2138268. https://doi.org/10.1155/2018/2138268.

[21] A.A. El-Tawil, H.M. Ahmed, L.S. Ökvist, B. Björkman, Self-reduction behavior of bio-coal containing iron ore composites, Metals 10 (2020) 133. https://doi.org/10.3390/met10010133.

[22] L. Rosso Neto, C.H. Borgert, F.F. Grillo, J.R. Oliveira, J.L. Coletti, T.E.A. Frizon, M.V.G. Zimmermann, E. Junca, Sustainable steel production: Evaluating the reduction kinetics of iron ore self-reducing briquettes with eucalyptus charcoal, J. Clean. Prod. 457 (2024) 142426. https://doi.org/10.1016/j.jclepro.2024.142426.

[23] H.-B. Zuo, Z.-W. Hu, J.-L. Zhang, J. Li, Z.-J. Liu, Direct reduction of iron ore by biomass char, Int. J. Miner. Metall. Mater. 20 (2013) 514–521. https://doi.org/10.1007/s12613-013-0759-7.

[24] M.C. Bagatini, V. Zymla, E. Osório, A.C.F. Vilela, Carbon gasification in self-reducing mixtures, ISIJ Int. 54 (2014) 2687–2696. https://doi.org/10.2355/isijinternational.54.2687.

[25] S. Kittivinitchnun, P. Kowitwarangkul, E. Mousa, A. Babich, Non-isothermal reduction kinetics model of self-reducing iron ore pellets, ISIJ Int. 64 (2024) 1503–1516. https://doi.org/10.2355/isijinternational.ISIJINT-2024-107.

[26] L. Ye, J. Zhang, J. Yu, R. Xu, H. Dang, Evolution behavior and kinetic analysis of vacuum-extruded iron-rich dust briquette in blast furnace, J. Clean. Prod. 433 (2023) 139753. https://doi.org/10.1016/j.jclepro.2023.139753.

[27] C. Takano, M.B. Mourão, Self-reducing pellets for ironmaking: Mechanical behavior, Miner. Process. Extr. Metall. Rev. 24 (2003) 233–252. https://doi.org/10.1080/714856823.

[28] B.F. Gandra, A.F.L. Oliveira, M.C. Bagatini, E. Osório, Iron ore-petcoke briquettes as complementary burden for blast furnaces, J. Mater. Res. Technol. 35 (2025) 1556–1564. https://doi.org/10.1016/j.jmrt.2025.01.123.

[29] R.C. Nascimento, M.B. Mourão, J.D.T. Capocchi, Kinetics and catastrophic swelling during reduction of iron ore in carbon bearing pellets, Ironmak. Steelmak. 26 (1999) 182–186. https://doi.org/10.1179/030192399677040.

[30] M.C. Mantovani, C. Takano, The strength and the high temperature behaviors of self-reducing pellets containing EAF dust, ISIJ Int. 40 (2000) 224–230. https://doi.org/10.2355/isijinternational.40.224.

[31] M. Kumar, S. Nath, S.K. Patel, Studies on the reduction-swelling behaviors of hematite iron ore pellets with noncoking coal, Miner. Process. Extr. Metall. Rev. 31 (2010) 256–268. https://doi.org/10.1080/08827508.2010.508826.

[32] M. Iljana, O. Mattila, T. Alatarvas, V.-V. Visuri, J. Kurikkala, T. Paananen, T. Fabritius, Dynamic and isothermal reduction swelling behaviour of olivine and acid iron ore pellets under simulated blast furnace shaft conditions, ISIJ Int. 52 (2012) 1257–1265. https://doi.org/10.2355/isijinternational.52.1257.

[33] L. Yi, Z. Huang, T. Jiang, L. Wang, T. Qi, Swelling behavior of iron ore pellet reduced by H_2-CO mixtures, Powder Technol. 269 (2015) 290–295. https://doi.org/10.1016/j.powtec.2014.09.018.

[34] M.C. Bagatini, T. Fernandes, R. Silva, D.F. Galvão, I.V. Flores, Mill scale and flue dust briquettes as alternative burden to low height blast furnaces, J. Clean. Prod. 276 (2020) 124332. https://doi.org/10.1016/j.jclepro.2020.124332.

[35] D. Bueno, C. de Freitas, M. Brienzo, Enzymatic cocktail formulation for xylan hydrolysis into xylose and xylooligosaccharides, Molecules 28 (2023) 624. https://doi.org/10.3390/molecules28020624.

[36] H. Yang, R. Yan, H. Chen, D.H. Lee, C. Zheng, Characteristics of hemicellulose, cellulose, and lignin pyrolysis, Fuel 86 (2007) 1781–1788. https://doi.org/10.1016/j.fuel.2006.12.013.

[37] S.S. Sahoo, V.K. Vijay, R. Chandra, H. Kumar, Production and characterization of biochar produced from slow pyrolysis of pigeon pea stalk and bamboo, Cleaner Eng. Technol. 3 (2021) 100101. https://doi.org/10.1016/j.clet.2021.100101.

[38] W. Li, K. Yang, J. Peng, L. Zhang, S. Guo, H. Xia, Effects of carbonization temperatures on characteristics of porosity in coconut shell chars and activated carbons derived from carbonized coconut shell chars, Ind. Crops Prod. 28 (2008) 190–198. https://doi.org/10.1016/j.indcrop.2008.02.012.

[39] M.R. Snowdon, A.K. Mohanty, M. Misra, A study of carbonized lignin as an alternative to carbon black, ACS Sustain. Chem. Eng. 2 (2014) 1257–1263. https://doi.org/10.1021/sc500086v.

[40] R. Khanna, M. Ikram-ul-Haq, R. Rajarao, R. Cayumil, A. Rawal, V. Sahajwalla, P.S. Mukherjee, Novel multidimensional carbons from structural transformations of waste lignin: A low temperature pyrolysis investigation, Fuel Process. Technol. 166 (2017) 312–321. https://doi.org/10.1016/j.fuproc.2017.06.013.

[41] A. Tomczyk, Z. Sokołowska, P. Boguta, Biochar physicochemical properties: Pyrolysis temperature and feedstock kind effects, Rev. Environ. Sci. Biotechnol. 19 (2020) 191–215. https://doi.org/10.1007/s11157-020-09523-3.

[42] G.I. Ngene, B. Bouesso, M.G. Martínez, A. Nzihou, A review on biochar briquetting: Common practices and recommendations to enhance mechanical properties and environmental performances, J. Clean. Prod. 469 (2024) 143193. https://doi.org/10.1016/j.jclepro.2024.143193.

[43] S. Li, G. Chen, Thermogravimetric, thermochemical, and infrared spectral characterization of feedstocks and biochar derived at different pyrolysis temperatures, Waste Manage. 78 (2018) 198–207. https://doi.org/10.1016/j.wasman.2018.05.048.

[44] M.C. Bagatini, T. Kan, T.J. Evans, V. Strezov, Iron ore reduction by biomass volatiles, J. Sustain. Metall. 7 (2021) 215–226. https://doi.org/10.1007/s40831-021-00337-3.

[45] G. Dall'Osto, D. Mombelli, A. Pittalis, C. Mapelli, Biochar and other carbonaceous materials used in steelmaking: Possibilities and synergies for power generation by direct carbon fuel cell, Biomass Bioenergy 177 (2023) 106930. https://doi.org/10.1016/j.biombioe.2023.106930.

[46] C.G. Mothé, I.C. Miranda, Characterization of sugarcane and coconut fibers by thermal analysis and FTIR, J. Therm. Anal. Calorim. 97 (2009) 661–665. https://doi.org/10.1007/s10973-009-0346-3.

[47] A.K. Varma, P. Mondal, Physicochemical characterization and pyrolysis kinetic study of sugarcane bagasse using thermogravimetric analysis, J. Energy Resour. Technol. 138 (2016) 052205. https://doi.org/10.1115/1.4032729.

[48] L. Yi, N. Zhang, H. Hao, L. Wang, H. Xiao, G. Li, Z. Liang, Z. Huang, T. Jiang, Synergetic conversion laws of biomass and iron ore for syngas and direct reduced iron co-production, J. Clean. Prod. 363 (2022) 132387. https://doi.org/10.1016/j.jclepro.2022.132387.

[49] R. Xie, Y. Zhu, H. Zhang, P. Zhang, L. Han, Effects and mechanism of pyrolysis temperature on physicochemical properties of corn stalk pellet biochar based on combined characterization approach of microcomputed tomography and chemical analysis, Bioresour. Technol. 329 (2021) 124907. https://doi.org/10.1016/j.biortech.2021.124907.

[50] S. Kloss, F. Zehetner, A. Dellantonio, R. Hamid, F. Ottner, V. Liedtke, M. Schwanninger, M.H. Gerzabek, G. Soja, Characterization of slow pyrolysis biochars: Effects of feedstocks and pyrolysis temperature on biochar properties, J. Environ. Qual. 41 (2012) 990–1000. https://doi.org/10.2134/jeq2011.0070.

[51] W. Liao, X. Zhang, S. Ke, J. Shao, H. Yang, S. Zhang, H. Chen, The influence of biomass species and pyrolysis temperature on carbon-retention ability and heavy metal adsorption property during biochar aging, Fuel Process. Technol. 240 (2023) 107580. https://doi.org/10.1016/j.fuproc.2022.107580.

[52] L. Chen, X. Wang, H. Yang, Q. Lu, D. Li, Q. Yang, H. Chen, Study on pyrolysis behaviors of non-woody lignins with TG-FTIR and Py-GC/MS, J. Anal. Appl. Pyrolysis 113 (2015) 499–507. https://doi.org/10.1016/j.jaap.2015.03.018.

[53] Z. Chen, M. Hu, X. Zhu, D. Guo, S. Liu, Z. Hu, B. Xiao, J. Wang, M. Laghari, Characteristics and kinetic study on pyrolysis of five lignocellulosic biomass via thermogravimetric analysis, Bioresour. Technol. 192 (2015) 441–450. https://doi.org/10.1016/j.biortech.2015.05.062.

[54] W.-H. Chen, B.-J. Lin, Y.-Y. Lin, Y.-S. Chu, A.T. Ubando, P.L. Show, H.C. Ong, J.-S. Chang, S.-H. Ho, A.B. Culaba, A. Pétrissans, M. Pétrissans, Progress in biomass torrefaction: Principles, applications and challenges, Prog. Energy Combust. Sci. 82 (2021) 100887. https://doi.org/10.1016/j.pecs.2020.100887.

[55] A.A. El-Tawil, H.M. Ahmed, L.S. Ökvist, B. Björkman, Devolatilization kinetics of different types of bio-coals using thermogravimetric analysis, Metals 9 (2019) 168. https://doi.org/10.3390/met9020168.

[56] H. Najafi, A.G. Sani, M.A. Sobati, Thermogravimetric and thermo-kinetic analysis of sugarcane bagasse pith: A comparative evaluation with other sugarcane residues, Sci. Rep. 14 (2024) 2076. https://doi.org/10.1038/s41598-024-52500-x.

[57] S. Mishra, Review on reduction kinetics of iron ore-coal composite pellet in alternative and sustainable ironmaking, J. Sustain. Metall. 6 (2020) 541–556. https://doi.org/10.1007/s40831-020-00299-y.

[58] D. Das, A. Anand, S. Gautam, V.K. Rajak, Assessment of utilization potential of biomass volatiles and biochar as a reducing agent for iron ore pellets, Environ. Technol. 45 (2022) 158–169. https://doi.org/10.1080/09593330.2022.2102936.

[59] B.F. Gandra, G.E. Paula Junior, M.C. Bagatini, E. Osório, Analysis of self-reducing composites with different iron ore-carbon ratio, J. Mater. Res. Technol. 26 (2023) 6433–6445. https://doi.org/10.1016/j.jmrt.2023.08.289.

[60] C.S. Nguyen, T.H. Nguyen, S.L. Nguyen, A.H. Bui, Study on the reducibility of iron ore pellets at high temperature, Vietnam J. Sci. Technol. Eng. 63 (2021) 3–7. https://doi.org/10.31276/VJSTE.63(4).03-07.

[61] C.Y. Narita, M.B. Mourão, C. Takano, Development of composite briquettes of iron ore and coal hardened by heat treatment, Ironmak. Steelmak. 42 (2015) 548–552. https://doi.org/10.1179/1743281214Y.0000000260.

[62] G. Wang, J. Wang, Q. Xue, Kinetics of the volume shrinkage of a magnetite/carbon composite pellet during solid-state carbothermic reduction, Metals 8 (2018) 1050. https://doi.org/10.3390/met8121050.

[63] A. Kemppainen, M. Iljana, E.-P. Heikkinen, T. Paananen, O. Mattila, T. Fabritius, Reduction behavior of cold-bonded briquettes under simulated blast furnace conditions, ISIJ Int. 54 (2014) 1539–1545. https://doi.org/10.2355/isijinternational.54.1539.

2.6. Supplementary material

Figure 2.S1. Visual aspect of (a) raw biomass and biochars after pyrolysis treatment at (b) 250 °C, (c) 400 °C, and (d) 550 °C.

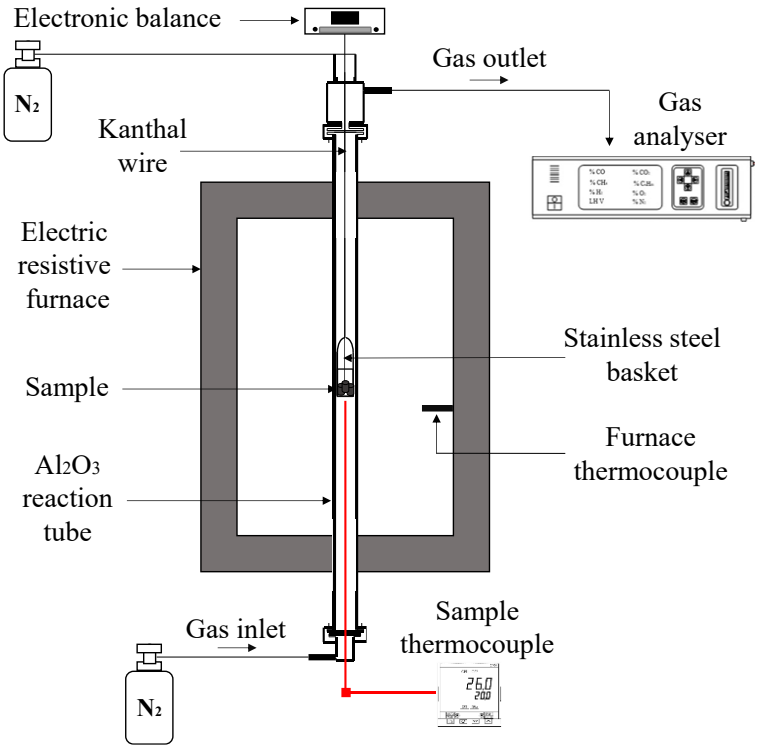

Figure 2.S2. Schematic representation of the apparatus used in the high-temperature interrupted tests.

The thermogravimetric analysis of the pellet feed used in the composition of the briquettes is presented in Figure 2.S3. The total mass loss comprises the elimination of physically bound water due to van der Waals forces and hydrogen bonding (up to 200 °C); the dehydration of goethite, associated with the loss of hydroxyl groups (up to 340 °C); and the dehydroxylation of clay minerals present in the pellet feed (above 400 °C).

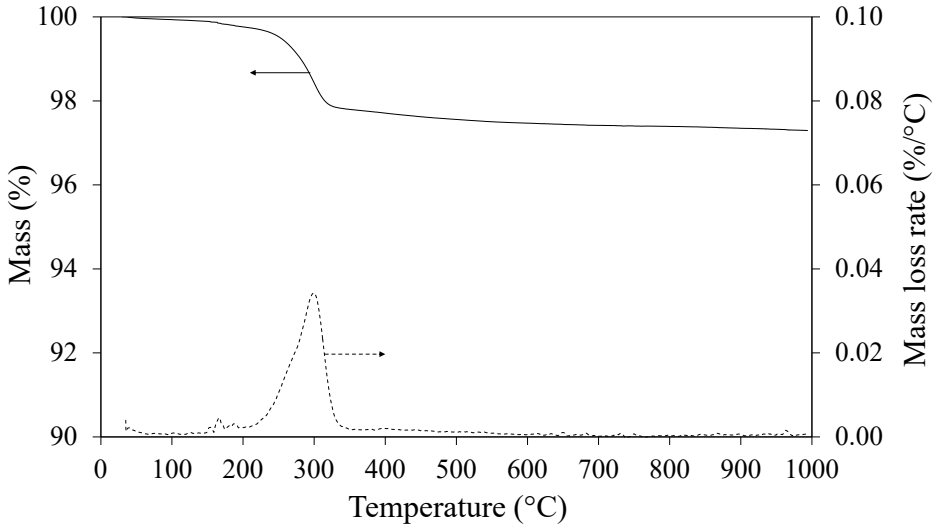

Figure 2.S3. Thermogravimetric curves of pellet feed.

3. ARTIGO 2: STRUCTURAL BEHAVIOR OF SELF-REDUCING BRIQUETTES CONTAINING BIOCHAR PYROLYZED AT DIFFERENT TEMPERATURES

Paula Maria Gomes Cunha Leão*, Isabela Giovana de Oliveira, Augusta Isaac, Maurício Covcevich Bagatini

Department of Metallurgical and Materials Engineering, Federal University of Minas Gerais (UFMG), Av. Antônio Carlos, 6627, Escola de Engenharia, 31270-901, Belo Horizonte, MG, Brazil

* Corresponding author

Abstract

This study investigated the structural evolution at different reduction stages of self-reducing briquettes produced from pellet feed and 15% by mass of sugarcane bagasse biochar pyrolyzed at 250, 400, and 550 °C. Interrupted tests conducted at 950 and 1250 °C, combined with XRD, SEM, and micro-CT characterization techniques, enabled a comprehensive analysis of the reduction process, as well as swelling and shrinkage behavior, and established a direct correlation between structural transformations and metallurgical and mechanical performance of briquettes. XRD analysis revealed the presence of metallic iron in all briquettes from 950 °C onward, with B550 showing the highest reduction performance. At 950 °C, the briquettes exhibited low mechanical strength, mainly associated with intensified self-reduction reactions and swelling within this temperature range, strongly influenced by the formation of metallic iron whiskers. The more pronounced swelling observed in B550 can also be attributed to the combined effects of increased internal pressure due to intense gas generation, a higher reduction degree, and the elevated ash content of the biochar produced at 550 °C. In contrast, B250 maintained its physical and geometrical integrity. After heating to 1250 °C, all briquettes exhibited volumetric shrinkage and increased mechanical strength, ascribed to the sintering of metallic iron particles and the formation of a liquid slag phase. This shrinkage was more pronounced in B400, due to enhanced metallic iron sintering and more uniform reduction of the briquettes, which promoted a more consolidated structure and resulted in the highest mechanical strength among the evaluated samples.

Keywords: biochar; self-reducing briquette; reduction; swelling; shrinkage; X-ray microtomography.

Graphical Abstract

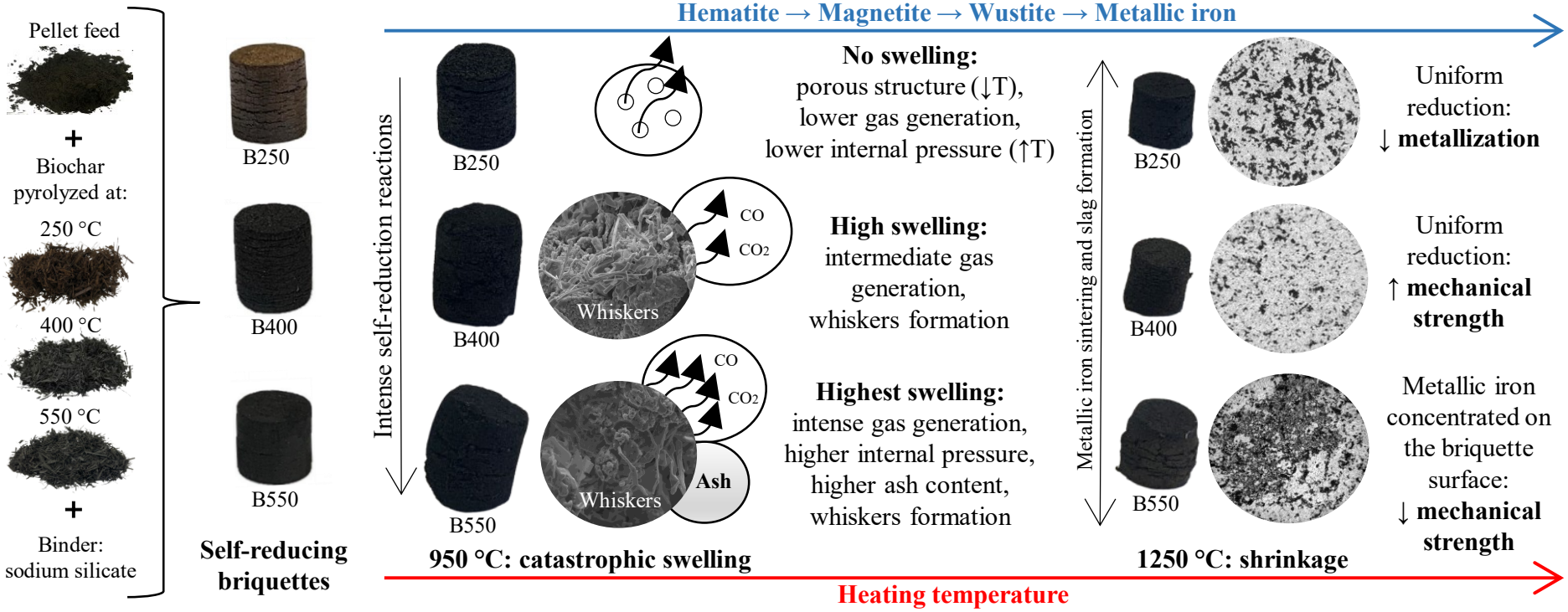

3.1. Introduction

Due to the intensive use of fossil fuels, the iron and steelmaking industry contributes substantially to the global greenhouse gas (GHG) emissions [1]. Among the stages of the steelmaking process, the carbothermic reduction of iron ore accounts for a significant share of energy consumption and CO_2 emissions [2]. Considering that the blast furnace is part of the dominant steelmaking route (BF-BOF), responsible for approximately 70% of global crude steel production [3], the central role of this process in efforts to mitigate the environmental impact of the sector becomes evident.

Biomass is a renewable source of carbon with the potential to reduce fossil fuel consumption in ironmaking. However, raw biomass presents drawbacks such as high moisture, low fixed carbon content, reduced calorific value, and low density, which limit its direct application in the iron and steelmaking industry. Consequently, thermochemical conversion processes are required to produce a solid-derived fuel (biochar) with high carbon content [4–6]. On the other hand, the thermochemical treatment decreases the mechanical strength of raw biomass, limiting the direct coke replacement in blast furnaces.

A promising strategy for incorporating the solid-derived fuel from pyrolyzed biomass in ironmaking is the use of self-reducing briquettes [7–9]. Composed mainly of iron-bearing materials and carbon-based reducing agents, these agglomerates are recognized for their high efficiency in iron oxide reduction [10]. However, the reduction process is often accompanied by structural changes and disintegration of the briquettes, compromising their performance at high temperatures [11,12]. This drop in mechanical strength is detrimental to stable blast furnace operation, as it reduces bed permeability and increases fuel consumption [13], making mechanical strength one of the main barriers to the application of these agglomerates [14].

Swelling is an important metallurgical phenomenon, defined by the extent of volume change in the agglomerates during reduction [15]. Catastrophic swelling, characterized by a volume increase exceeding 20% [16], is generally attributed to (i) the formation of metallic iron whiskers, (ii) phase transformations, (iii) internal stress caused by an uneven reduction rate, and (iv) carbon deposition [17–19]. The effects of gangue [20], additives [21–23], basicity [24–26], and reducing atmosphere [19,27,28] have been extensively investigated, highlighting their

influence on the extent of swelling in these agglomerates. However, the precise mechanism governing swelling is not fully understood and may vary according to the composition, reduction conditions, and the microstructure formed during the process. As reduction progresses at high temperatures, the agglomerates may undergo a decrease in volume, characterizing the shrinkage phenomenon that follows swelling. This behavior is commonly attributed to the sintering of metallic iron and the formation of molten slag, which promote particle coalescence, pore closure, and microstructural densification [11,29].

Understanding the phenomena and reaction mechanisms governing the reduction and structural behavior of the self-reducing agglomerates is essential for their industrial implementation. This requires detailed studies and the combined use of characterization techniques capable of elucidating the underlying processes, their interactions, and the factors that influence both reduction efficiency and the mechanical properties of the agglomerates. In this context, X-ray microtomography (micro-CT) stands out as a powerful tool for non-destructive evaluation of material structure. The technique enables high-resolution three-dimensional (3D) analysis from large volumes of data through the reconstruction of two-dimensional (2D) cross-sections and volumetric rendering, allowing the identification of distinct phases or components [30,31].

In recent years, the swelling and shrinkage behavior of agglomerates during reduction has attracted increasing attention, driven by the interest in applying cold-bonded briquettes in ironmaking. However, the understanding of these phenomena in self-reducing briquettes, particularly those incorporating different biomass sources as reducing agents, remains limited. Although the reduction behavior of these agglomerates has been extensively investigated under inert and reducing atmospheres [6,32–37], the influence of biomass pyrolysis temperature on the structural evolution of the briquettes has not been reported. Moreover, studies employing micro-CT as a characterization tool for self-reducing briquettes are notably scarce. Thus, the present study investigated the structural behavior of self-reducing briquettes produced from pellet feed and sugarcane bagasse pyrolyzed at different temperatures (250, 400, and 550 °C), providing a more detailed analysis of these agglomerates during reduction and a better understanding of their metallurgical and mechanical performance at different reduction stages.

3.2. Materials and methods

3.2.1. Raw materials

The raw materials employed in this study (Figure 3.1) were a hematitic-goethitic iron ore, identified by X-ray diffraction (XRD) using a Panalytical Empyrean diffractometer (Figure 3.2), and sugarcane bagasse biochar as the biomass-derived reducing agent. The pellet feed consisted predominantly of particles smaller than 212 μm, and its chemical composition, determined by an energy-dispersive X-ray fluorescence spectrometer ARL™ QUANT'X - Thermo Scientific™, is presented in Table 3.1. The sugarcane bagasse was pyrolyzed at different temperatures under controlled laboratory conditions, with a particle size ranging from 0.053 to 0.5 mm (85% by mass > 0.106 mm) in a vertical resistive furnace equipped with a stainless-steel reactor tube. Approximately 15 g of dried biomass were placed in a graphite crucible and heated under an inert N_2 atmosphere (1.5 L/min) at a heating rate of 10 °C/min, followed by a 2-hour isothermal plateau at 250, 400, or 550 °C. The resulting biochars were characterized by proximate analysis using a LECO TGA 701 thermogravimetric analyzer (ASTM D7582-15), and by BET surface area and pore volume measurements using a Quantachrome NOVA 2200 instrument, as shown in Table 3.2. For BET measurements, N_2 adsorption was performed at P/P_O below 0.3 (adsorption pressure to atmospheric pressure of this gas), and the samples were degassed at 120 °C under vacuum for 2 h.

Figure 3.1. Visual aspect of (a) pellet feed, (b) raw biomass and biochars obtained after pyrolysis at (c) 250 °C, (d) 400 °C, and (e) 550 °C.

Table 3.1. Chemical composition in mass percentage (%) of pellet feed.

Fe	SiO_2	Al_2O_3	MgO	MnO	Co	P_2O_5	Cl	LOI
63.23	5.19	2.59	0.63	0.55	0.44	0.27	0.23	2.47

LOI: loss on ignition

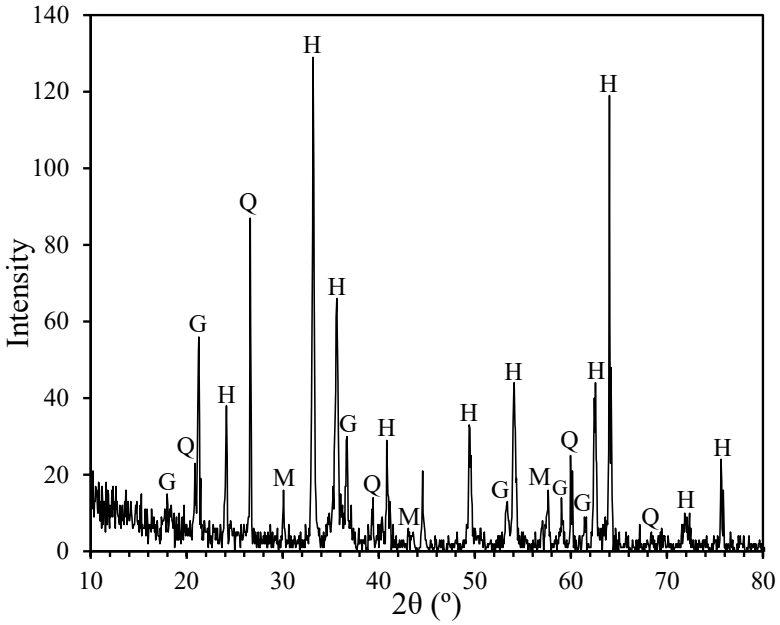

Figure 3.2. XRD pattern of pellet feed. H: hematite; M: magnetite; G: goethite; and Q: quartz.

Table 3.2. Proximate analysis (in dry basis) and physical characteristics of biochars obtained from sugarcane bagasse pyrolyzed at different temperatures.

Pyrolysis temperature (°C)	Volatile matter (%)	Fixed carbon (%)	Ash (%)	Specific surface area (m^2/g)	Total pore volume (mm^3/g)	Average pore diameter (Å)
Raw biomass	81.25	16.89	1.92	N/A	N/A	N/A
250	74.31	22.96	2.72	0.58	1.90	130.52
400	26.39	65.69	7.93	2.44	4.04	66.35
550	15.18	76.21	8.60	114.58	75.86	26.48

N/A: not measured

3.2.2. Production of self-reducing briquettes

The self-reducing briquettes were prepared from a mixture consisting of 75% pellet feed, 15% sugarcane bagasse-derived biochar, and 10% aqueous sodium silicate solution (52.86% of moisture content) with a SiO_2/Na_2O ratio of 2.17, with a total moisture content of 12% by mass. After manually homogenizing the mixture for 15 min, the briquettes were individually produced in a cylindrical steel die with an internal diameter of 10 mm, using a Bovenau hydraulic press (maximum load of 15 tons) under an applied load of 2 tons for 3 min, followed by curing in a muffle furnace at 200 °C for 2 h. Briquettes were identified according to the pyrolysis temperature of the biochar: B250, B400, and B550.

3.2.3. High-temperature interrupted tests

Interrupted tests at different temperatures were performed to evaluate the structural and reduction behavior of the self-reducing briquettes after heating. The experimental setup, shown in Figure 3.3, consisted of a high-temperature resistive furnace (maximum temperature of 1600 °C), an alumina reaction tube (70 mm diameter), a sample holder (stainless-steel basket with a diameter of 40 mm) suspended by a Kanthal DS wire (FeCrAl alloy with a diameter of 0.404 mm), and a K-type thermocouple for monitoring the sample temperature. Continuous monitoring of the outlet gas composition was carried out using a Gasboard 3100 gas analyzer (Cubic-Ruiyi) connected to the furnace exhaust line. This setup allowed real-time detection and quantification of CO and CO_2 concentrations throughout the tests, providing insights into the reaction progress.

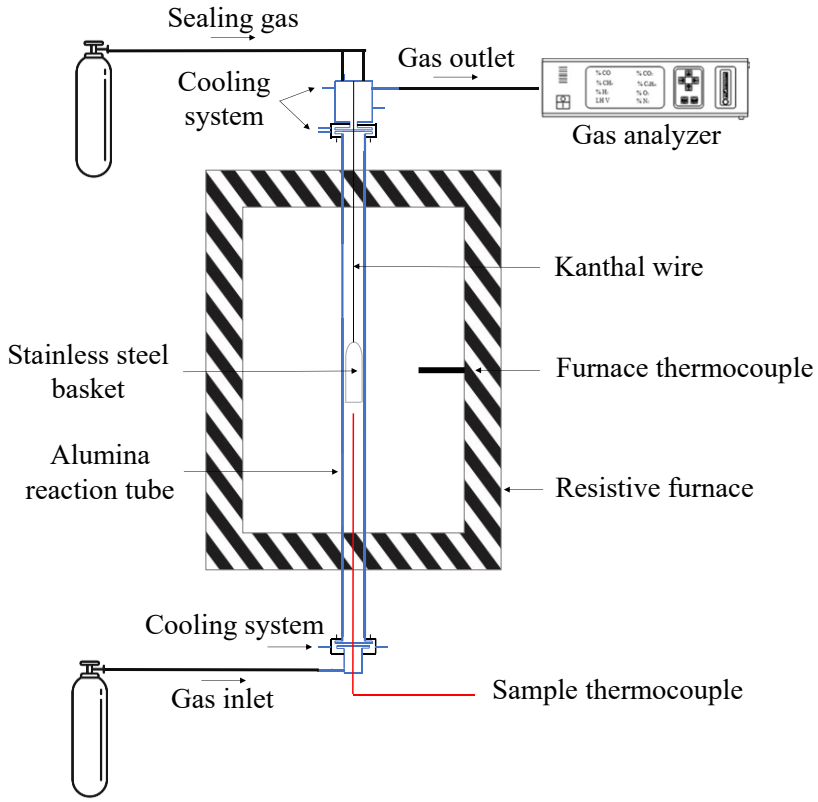

Figure 3.3. Resistive furnace setup used for high-temperature interrupted tests.

In each interrupted test, six briquettes were heated under an N_2 atmosphere at a constant flow rate of 3 L/min, with a heating rate of 5 °C/min up to 1250 °C. An isothermal 30-min plateau was maintained at 950 °C to simulate the thermal reserve zone of the blast furnace. The tests were interrupted at 950 °C after the plateau temperature and 1250 °C by a rapid cooling in a

pure N_2 atmosphere, achieved by suspending the wire basket with the samples to the upper region of the alumina tube, to interrupt the self-reduction reactions.

3.2.4. Characterization of self-reducing briquettes

X-ray diffraction (XRD) analysis was performed to identify the main phases present in the briquettes, providing insight into the mineralogical changes occurring during the reduction. A Panalytical Empyrean diffractometer was employed, using Cu (Kα) radiation and operating under scanning conditions of 3-80° (2θ), scan step size of 0.06°, acquisition time of 2 s, tube voltage of 35 kV, and current of 35 mA. Semi-quantitative phase analysis was conducted using the Rietveld refinement method with HighScore Plus software (version 4.9, Malvern Panalytical). Briquette samples were ground and sieved to a particle size smaller than 75 μm.

Swelling and shrinkage of the briquettes were quantified through dimensional analysis before and after tests, enabling the determination of relative expansion and contraction during heating. The average diameter and height measurements were used to calculate the volume, as shown in Equations 3.1 and 3.2, where V_i and V_f correspond to the volumes of the briquettes (mm^3) before and after heating, respectively.

$$\text{Swelling index (\%)} = \frac{V_f - V_i}{V_i} \cdot 100 \tag{3.1}$$

$$\text{Shrinkage index (\%)} = \frac{V_i - V_f}{V_i} \cdot 100 \tag{3.2}$$

The microstructural characterization of the briquettes was first assessed by scanning electron microscopy (SEM), where samples were sectioned perpendicular to the diameter, embedded in polymeric resin, and prepared through sequential steps of grinding (120, 240, 320, 400, 600, and 1000 grit) and polishing with diamond pastes of 9, 3, and 1 μm. SEM images were acquired using an FEI Inspect S50 microscope, operated with an acceleration voltage of 20 kV. Chemical contrast images of the polished samples were obtained using backscattered electrons (EBSD) and energy-dispersive X-ray spectroscopy (EDS). Morphological analysis using secondary electrons (ETD) was performed in a FEI Quanta 200 FEG scanning electron microscope operating with an acceleration voltage of 15 kV and magnifications of up to 2500x. The analysis

was conducted on sectioned samples mounted on metallic stubs with double-sided carbon adhesive tape and coated with a thin gold layer (without conventional metallographic preparation, metallized only).

X-ray micro-computed tomography (micro-CT) was employed to obtain a three-dimensional view of the internal structure of the briquettes, enabling analysis of the spatial distribution of phases and semi-quantitative assessment of the constituents before and after the high-temperature tests. The image contrast—reflected in variations in grayscale levels—is determined by differences in the X-ray attenuation coefficients of the phases present in the samples. The attenuation is governed by the probability of photon interactions per unit distance traveled through a material, which depends on the effective atomic number, density, and photon energy [38]. The measurements were performed using a ZEISS Xradia 610 Versa 3D X-ray microscope with an optical magnification of 0.4x and 4x, with an image pixel size ranging from 3.78 to 11.26 µm. The applied voltage and power were 140 kV and 21 W, respectively. The projections were obtained over a 360° rotation of the samples, with exposure time per projection ranging from 0.3 to 3.5 s. Image processing was carried out using FIJI/ImageJ and the commercial Avizo software (Thermo Scientific).

The mechanical strength of the briquettes was evaluated before and after the interrupted tests. The measurements were performed via radial compressive strength testing, in which five briquettes were individually tested using a Shimadzu AGS-X 300 kN universal machine with a constant cross-head speed of 0.01 mm/s until fracture.

3.3. Results and discussion

3.3.1. Analysis of mineralogical phases of self-reducing briquettes

Figure 3.4 shows the XRD patterns and phases detected in the briquettes before and after the high-temperature interrupted tests, while the results obtained from the Rietveld method are presented in Figure 3.5. These analyses allowed the assessment of reduction progress as a function of biomass pyrolysis temperature across different heating stages, based on the transformations of the crystalline phases.

Before testing, hematite was identified as the major phase in all briquettes, accompanied by goethite, quartz, and magnetite, consistent with the iron-bearing raw material used in these agglomerates. The absence of carbon-related peaks can be attributed to the limitations of the technique, which has no sensitivity for detecting amorphous phases, a characteristic commonly associated with pyrolysis-derived carbon.

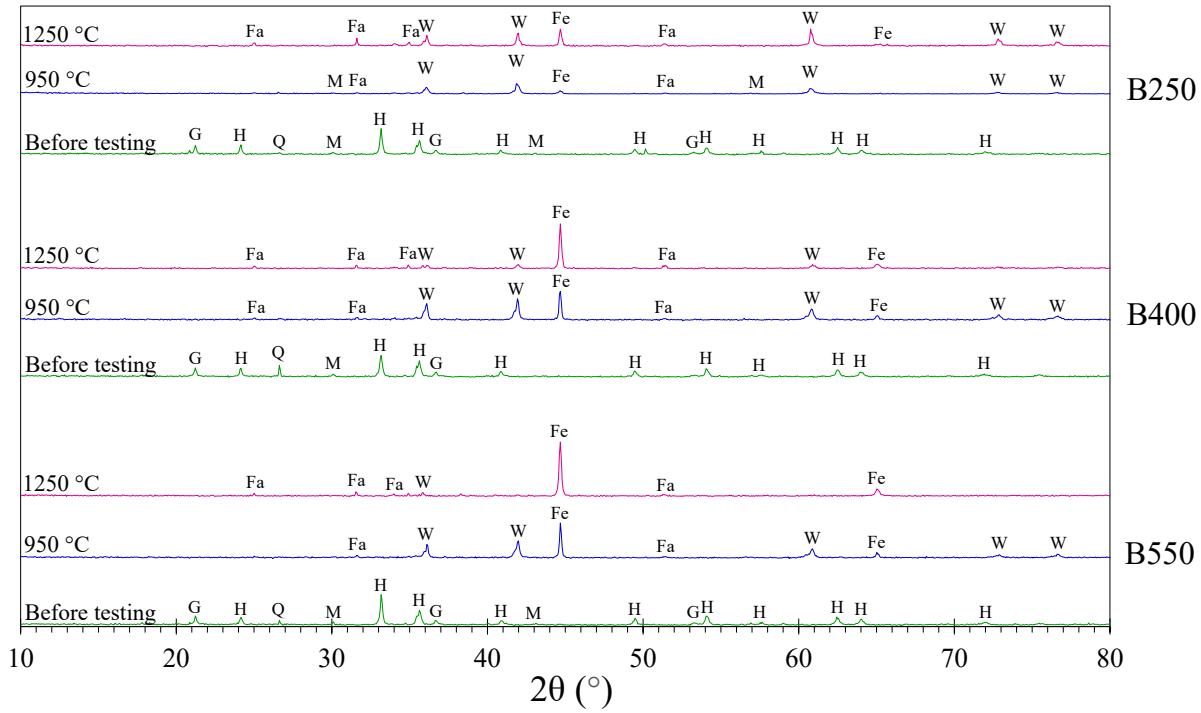

Figure 3.4. DRX patterns of the briquettes before and after high-temperature interrupted tests. H: hematite; M: magnetite; G: goethite; Q: quartz; W: wustite; Fa: fayalite; and Fe: metallic iron.

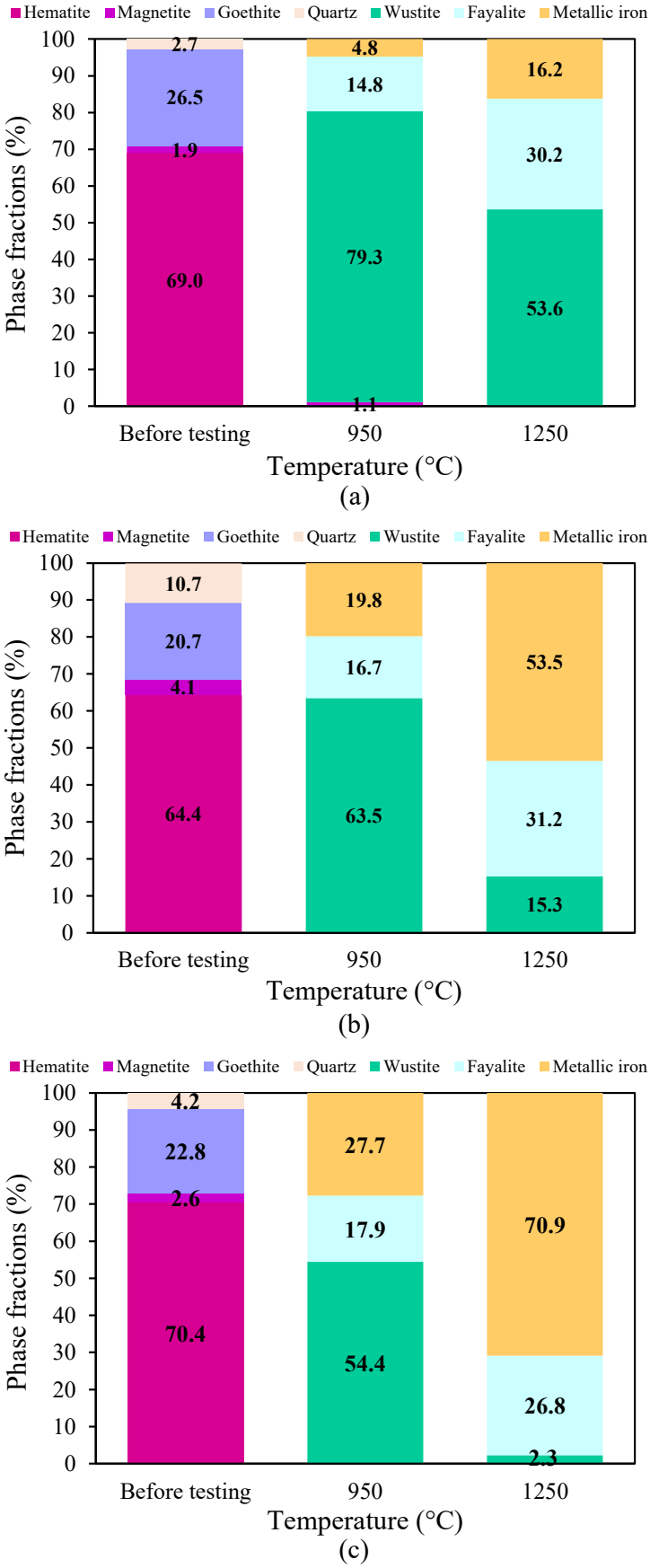

Figure 3.5. Phase fractions determined by the Rietveld analysis for (a) B250, (b) B400, and (c) B550.

At 950 °C, the hydrated goethite and hematite phases were no longer detected in any samples, indicating their complete decomposition [39] and reduction, respectively. In B250, magnetite peaks were still observed, reflecting the lower reduction efficiency of these briquettes. At this temperature, wustite was the predominant phase, and metallic iron was identified in all samples, confirming the effectiveness of the self-reduction reactions. At high temperatures (> 800 °C), carbon gasification via the Boudouard reaction (Equation 3.3) is thermodynamically favored, promoting CO formation within the briquettes and the reduction of iron oxides (Equation 3.4), leading to the formation of metallic iron [40]. Fayalite (Fe_2SiO_4) was also detected at this temperature, which is formed from the reaction between wustite and silica; its presence is undesirable, as it negatively affects the reducibility of the agglomerates [41].

$$C_{(s)} + CO_{2(g)} = 2CO_{(g)} \quad (3.3)$$

$$Fe_xO_{y(s)} + CO_{(g)} = Fe_xO_{y-1(s)} + CO_{2(g)} \quad (3.4)$$

As the temperature increased to 1250 °C, more intense metallic iron peaks were observed, reflecting the progressive reduction of wustite. B550 exhibited the most pronounced formation of metallic iron, likely due to the greater carbon available (Table 3.2) for the gasification and the consequent reduction of iron oxides. For B250, in contrast, the iron remained predominantly in the form of wustite and fayalite. These results clearly show that the biomass pyrolysis temperature has a significant influence on the reduction performance of the briquettes. The higher the pyrolysis temperature, the higher the reduction degree due to the increased availability of fixed carbon for self-reduction reactions.

3.3.2. Gas analysis of self-reducing briquettes

The continuous flow rates of CO and CO_2 during sample heating are presented in Figure 3.6. Both gases were detected in B250 starting at 280 °C, likely due to the release of residual volatile matter from the biochar content in these briquettes. According to the literature [42,43], the release of these gases is primarily caused by the decomposition of hemicellulose and cellulose. Between 200 and 450 °C, the degradation of these components intensifies, resulting in significant emission of volatile compounds. On the other hand, minimal gas generation at low

temperatures for B400 and B550 is attributed to the prior pyrolysis process, where the biomass underwent more extensive devolatilization.

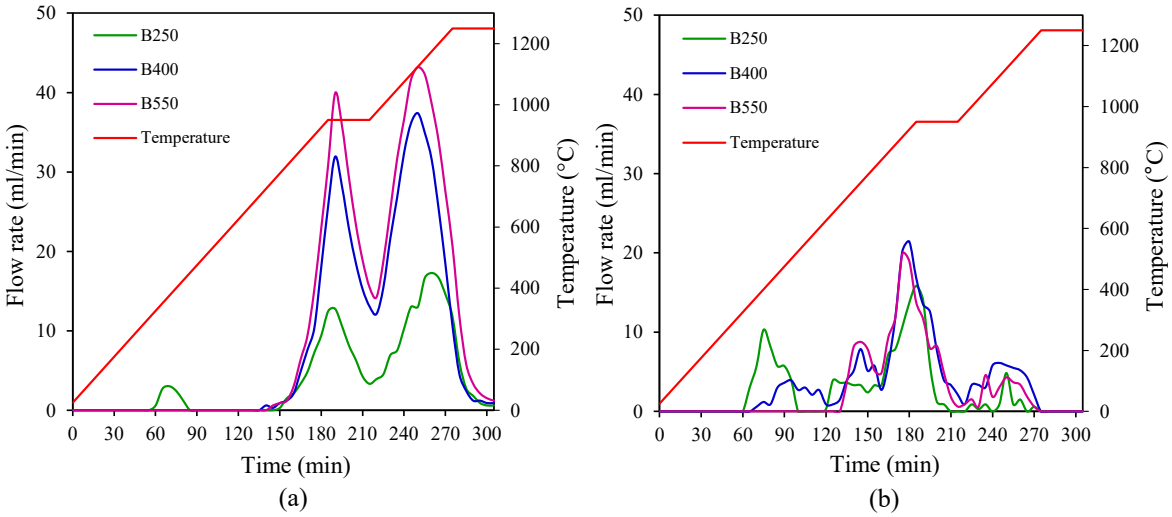

Figure 3.6. Variation in the flow rate of (a) CO and (b) CO_2 generated during heating of the briquettes up to 1250 °C.

With increasing temperature, a significant rise in gas generation was observed, particularly in briquettes containing biochar produced at higher pyrolysis temperatures. Overall, B550 exhibited more pronounced CO peaks compared to the other briquettes, likely due to the greater carbon availability in these briquettes, which promoted more intense self-reduction reactions. These results indicate that the CO_2 produced by the reduction of iron oxides is partially consumed by carbon gasification (Equation 3.3), thereby favoring CO formation. Moreover, as the temperature increases, the CO generation increases and CO_2 decreases, which is consistent with the shift in the Boudouard reaction equilibrium at high temperatures.

In general, a better understanding of the self-reduction potential of the briquettes can be achieved by their gaseous products. The higher the CO partial pressure, the greater the reduction potential of the briquette. Then, it can be observed that higher biomass pyrolysis temperatures result in a greater reducing gas potential and, therefore, a more intense reduction degree.

3.3.3. Swelling and shrinkage behavior of self-reducing briquettes

Figure 3.7a presents a macroscopic view of the briquettes containing biochar pyrolyzed at different temperatures, both before and after the high-temperature interrupted tests. Before

testing, horizontal cracks were observed on the surface of the samples, resulting from the uniaxial compaction applied during their preparation. After heating to 950 °C, B400 and B550 exhibited noticeable swelling, with volumetric expansions of 31% and 75%, respectively, as shown in Figure 3.7b. This swelling generated internal stresses, leading to crack propagation and greater deformation of the briquettes. In contrast, B250 maintained its physical and geometric integrity, with minimal volume increase upon heating and swelling indices below 2%. This behavior indicates a swelling trend in self-reducing briquettes as the biomass pyrolysis temperature increases, although the biochar pyrolyzed at higher temperatures presents lower volatile matter content. A volume variation of up to 20% is considered normal, whereas higher values are classified as abnormal or catastrophic [16,19,44]. Excessive swelling may result in loss of mechanical strength and disintegration during reduction, which can negatively affect blast furnace operation [24,28,45].

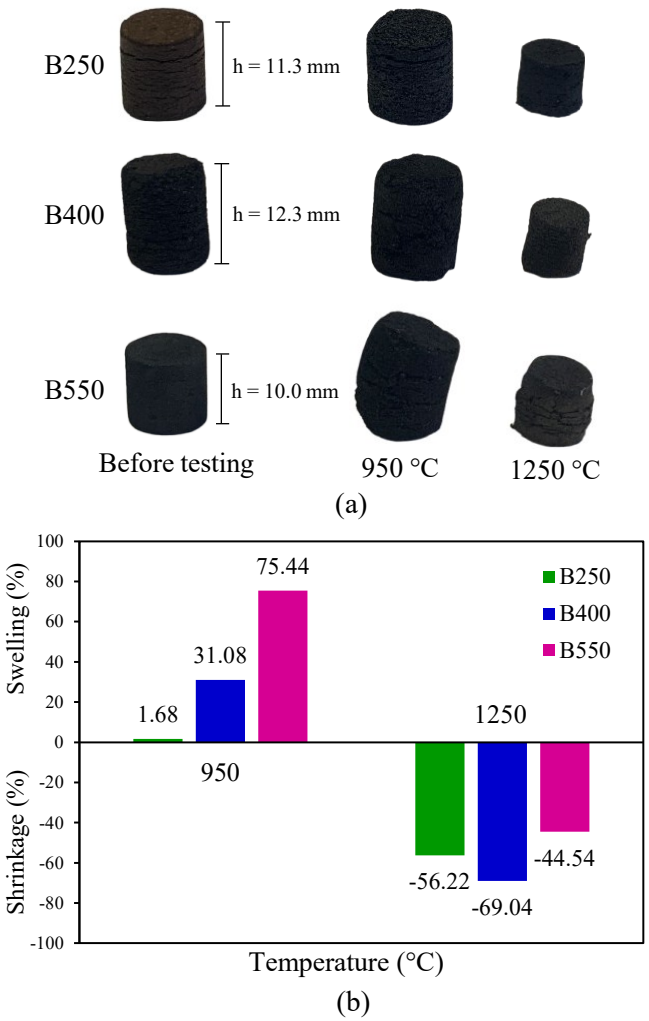

Figure 3.7. (a) Macroscopic views and (b) swelling and shrinkage indices of the briquettes before and after high-temperature interrupted tests. h: briquette height.

Previous studies have indicated that the magnitude of swelling is related to the nature and composition of the raw materials, the properties of the agglomerates (e.g., porosity), and parameters associated with the reduction process, such as temperature, time, heating rate, reduction degree, and the reducing atmosphere, including the composition and flow rate of the reducing gas [12,13,15,17,28,44,46,47]. Thus, the parameters that affect the reduction rate also influence the swelling behavior of the agglomerates [48]. However, the precise determination of the main causes of swelling is complex, as it involves the interaction of multiple, often overlapping factors [13,19]. In this context, several subsequent factors may have contributed to the different behaviors observed in the briquettes under study.

The occurrence of catastrophic swelling in agglomerates is closely linked to high-temperature reduction processes and is influenced by the total iron and carbon content of the samples, as also discussed by Vitikka et al. [49]. Tang et al. [50] suggested that phase transitions accompanied by volume changes may be one of the possible causes of this behavior, resulting from the transformations of the crystalline structure of iron oxides during reduction [25]. Normal swelling of up to 20% is characteristic of the conversion of hematite to magnetite, involving a change from a hexagonal to a cubic crystalline structure, and partially as magnetite is reduced to wustite. Catastrophic swelling, however, occurs during the transformation of wustite into metallic iron in the final reduction stages [19,21,23]. In this work, expressive volume expansion of the briquettes at 950 °C was observed during the reduction to wustite and metallic iron, consistent with previous reports [40,44,49,51] for the same temperature range (900–1100 °C). Differences in swelling magnitude can be related to variations in the extent of reduction. Among the samples analyzed, B550 showed the highest reduction to metallic iron, indicating more intense reactions in these briquettes. XRD analysis (Figures 3.4 and 3.5) confirmed that increasing the biomass pyrolysis temperature promoted greater conversion of oxides to metallic iron.

The intensification of self-reduction reactions may be directly associated with the significant volumetric expansion observed in the briquettes. The inner generation of reducing gases during the reduction process strongly affects their swelling behavior. The increase in internal pressure resulting from gas generation and release at the reaction interface, combined with the reduction of iron oxides at high temperatures, can induce structural stresses that lead to the pronounced swelling observed in B550. As evidenced by the analysis of evolved gases (Figure 3.6), these

briquettes exhibited higher CO and CO_2 generation at elevated temperatures, which is directly related to more intense self-reduction reactions, promoted by the high carbon content in the matrix of these agglomerates and enhanced carbon gasification. Thus, catastrophic swelling in self-reducing agglomerates occurs under conditions where the internal gas composition is dominated by products of the Boudouard reaction. Similarly, El-Geassy et al. [17] associated the marked volumetric expansion of pellets with increased internal gas pressure due to the rapid formation of CO/CO_2 and H_2/H_2O at the reaction interface.

In contrast, the high volatile matter content of biochar treated at 250 °C (74.31%) promotes the formation of a more porous structure in B250 during the initial heating stages, facilitating the subsequent release of gases generated internally by self-reduction reactions at elevated temperatures. In these briquettes, devolatilization occurs at lower temperatures and more gradually compared to the other studied agglomerates, resulting in lower internal pressure and reduced swelling. Kang et al. [52] associated high porosity with lower swelling indices, as it allows better accommodation of stresses induced during reduction. A similar behavior was observed by Han et al. [11] in agglomerates composed of iron ore and different biomass sources at high temperatures. The authors reported lower swelling in pellets produced with biochar containing higher volatile matter (straw fiber), in which the volume was less affected by the crystalline transformations of iron oxides.

In a previous work [53], the higher magnetite formation in B250 at 600 °C was attributed to reduction by volatiles. Briquettes produced with biochar pyrolyzed at lower temperatures release a larger volume of gases (CO and H_2) during devolatilization, promoting more intense internal reduction at early stages, which can lead to the formation of porous magnetite and, subsequently, porous wustite. On the other hand, higher pyrolysis temperatures tend to produce denser wustite, which, in turn, contributes to greater swelling [28]. Gonçalves et al. [54] compared the morphology of wustite formed after the reduction of hematitic iron ore at 980 °C using different reducing agents. Their results showed that a denser structure was obtained when charcoal was employed, whereas reduction by volatiles from raw biomass produced a less compact microstructure, resulting in a more porous wustite. The high porosity and surface area of this wustite tend to hinder whisker growth, as the discontinuous matrix and dispersed metallic cores limit the formation of long, cohesive filaments. Consequently, fewer whiskers are observed, accompanied by more uniform reduction behavior and reduced agglomerate swelling.

Therefore, the wustite structure largely controls the surface area and the potential number of nuclei available for the FeO-Fe reduction step [55].

Swelling behavior may also be influenced by the compositional characteristics of the agglomerates and their individual components. Thus, the higher ash content of biochar pyrolyzed at 550 °C (Table 3.2) may have contributed to the greater volume expansion observed in B550 by increasing the concentration of basic oxides in the briquettes. Furthermore, it should be noted that no peaks corresponding to iron carbide (Fe_3C) were identified in the XRD analysis, although this phase has been suggested as a potential contributor to swelling in the literature [17,56].

After testing to 1250 °C, all briquettes exhibited volumetric shrinkage of varying magnitudes, as shown in Figure 3.7. This phenomenon can be attributed to the coalescence and sintering of metallic iron particles, as well as the formation of a liquid slag phase at high temperatures, resulting from the combined presence of binder, ore gangue, and biochar ash. The liquid phase facilitates the sintering process by promoting particle coalescence and reducing porosity, leading to greater volumetric contraction of the agglomerates [29]. In this study, B400 exhibited the highest shrinkage, corresponding to approximately 69% of the initial volume, whereas B550 showed the lowest shrinkage index (45%).

Similar behaviors associated with the sintering of iron particles have also been reported in the literature for self-reducing agglomerates during the final reduction stages [11,28,29]. These studies also indicated that the extent of swelling decreases with increasing temperature until shrinkage becomes dominant. According to Takano and Mourão [16], exposure of agglomerates to temperatures above 1200 °C promotes iron nucleation and sintering. These processes involve particle rearrangement and densification, leading to volumetric contraction. Halder and Fruehan [29] also identified carbon and oxygen loss during reduction as a probable cause of this shrinkage. At high temperatures, shrinkage progresses more rapidly due to accelerated reaction kinetics, resulting in enhanced carbon loss and intensified iron sintering.

3.3.4. SEM microstructural analysis of self-reducing briquettes

SEM-EDS was employed to investigate changes in the microstructure of the briquettes before and after heating to 1250 °C (Figure 3.8). Chemical analysis was performed on representative regions of the samples, as detailed in Table 3.3. At the initial stage, the briquettes exhibited a structure consisting of particles with different sizes and shapes, distributed among iron oxides such as hematite, magnetite, and goethite (different shades of light gray/A-B), and quartz (dark gray/C), indicating that the individual characteristics and original morphologies of the iron ore were preserved after briquetting. These particles were dispersed in a carbon-rich matrix composed of embedding resin and biochar, along with internal pores (black/D). Under these conditions, the briquettes showed relatively similar microstructures, with biochar particles easily identified, appearing as dark, fibrous regions.

After heating to 1250 °C, the microstructure of the briquettes was completely changed, with the formation of new phases resulting from reduction reactions and the components' assimilation. Chemical analysis identified the presence of metallic iron (white/E), wustite (light gray/F), fayalite (intermediate gray/G), and a molten slag phase (dark gray/H). This slag phase, composed mainly of iron, oxygen, silicon, and sodium, with minor amounts of other elements, can be associated with liquid formation at high temperatures. The slag originates from the partial melting of chemical constituents contained in the briquettes, including iron ore gangue, biochar ash, and binder, and acts as a matrix that assimilates other phases, promoting the coalescence. The presence of this liquid phase, combined with the coalescence and sintering phenomena, promotes microstructural densification and directly contributes to the volumetric shrinkage observed in the briquettes at this temperature (Figure 3.7). The darkest regions (black/D) represent a porous matrix composed of resin and residual biochar. The microstructural observations are consistent with the XRD results, confirming the evolution of reduction products during heating.

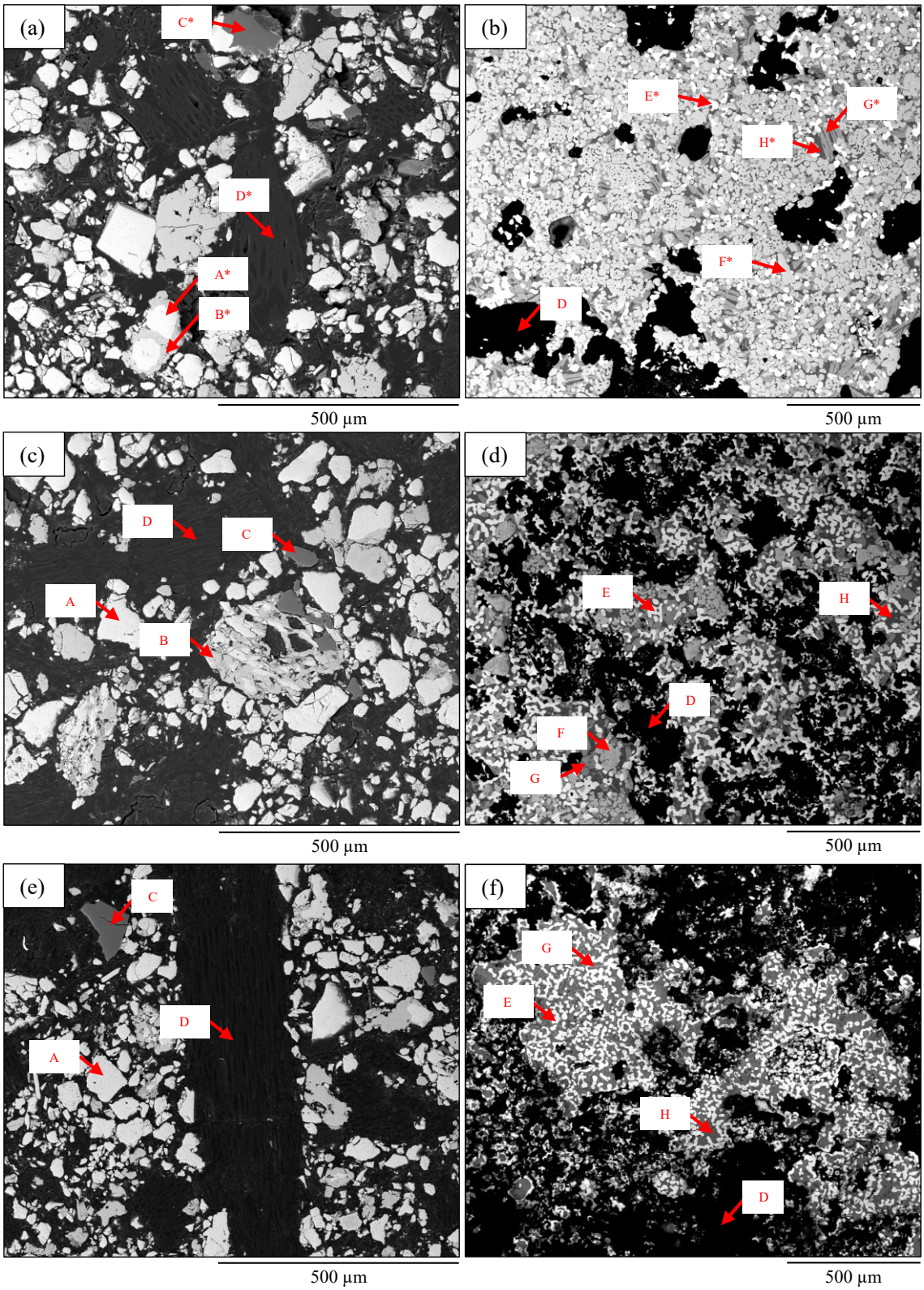

Figure 3.8. SEM microstructure of the briquettes before testing: (a) B250, (c) B400, and (e) B550, and after heating to 1250 °C: (b) B250, (d) B400, and (f) B550. A/B: iron oxides (hematite, magnetite, and goethite); C: quartz; D: resin, biochar, and pore; E: metallic iron; F: wustite; G: fayalite; and H: slag.

Table 3.3. EDS point analysis of B250 before and after heating to 1250 °C.

Point	Chemical composition (%)
A*	Fe:84.61; O:15.12; Si:0.27
B*	Fe:72.85; O:24.69; Si:2.45
C*	Si:64.17; O:35.83
D*	C:63.20; O:35.73; K:1.07
E*	Fe:98.9; O:0.90; Si:0.20
F*	Fe:88.86; O:13.51; Si:0.62
G*	Fe:59.67; O:20.86; Si:16.81; Mn:2.66
H*	Fe:29.40; Si:25.92; O:24.23; Na:12.65; Al:2.82; K:2.44; P:1.33; Mn:1.21

The B400 and B550 briquettes were also morphologically characterized after testing at 950 °C, and representative images are shown in Figure 3.9. Both samples presented a sparse microstructure, characterized by a dispersed and discontinuous distribution of particles, with relatively high porosity. The images revealed the presence of iron-bearing phases and partially reacted biochar residues that retained part of their original structure after heating. These particles exhibited lamellar and fibrous structures, along with a fragmented and porous morphology, indicating that the reducing agent was not completely consumed, even at the high temperature tested.

Regarding the iron-bearing phases, three distinct morphologies were identified: dense wustite, porous wustite, and metallic iron in filamentary form. Commonly referred to as whiskers, filamentary iron consists of fine, elongated, acicular structures formed when metallic iron begins to nucleate and grow preferentially along specific crystallographic directions on the surface of wustite. The morphologies of the iron-bearing phases observed in this study were similar to those reported in pioneering investigations on wustite reduction [45,57,58].

Several studies have reported that the formation of iron whiskers during the reduction of wustite to metallic iron is one of the main causes of large-scale swelling [28,46,59,60]. Whisker growth leads to significant volume expansion as the filaments press against adjacent grains [28], generating internal stresses that may result in microcracks or structural distortion [13]. Moreover, the filamentous morphology itself intensifies this effect, as the whiskers grow outward from the particle surface, occupying additional space within the agglomerates. In this study, the presence of iron whiskers observed in B400 and B550 at 950 °C can be directly associated with the greater swelling magnitude of these briquettes during reduction. According to Iljana et al. [60], whisker formation not only contributes to swelling but also promotes crack

development, as the bonding strength of the briquettes is assumed to be lower than the mechanical stresses generated by the growing filaments pushing against adjacent iron grains.

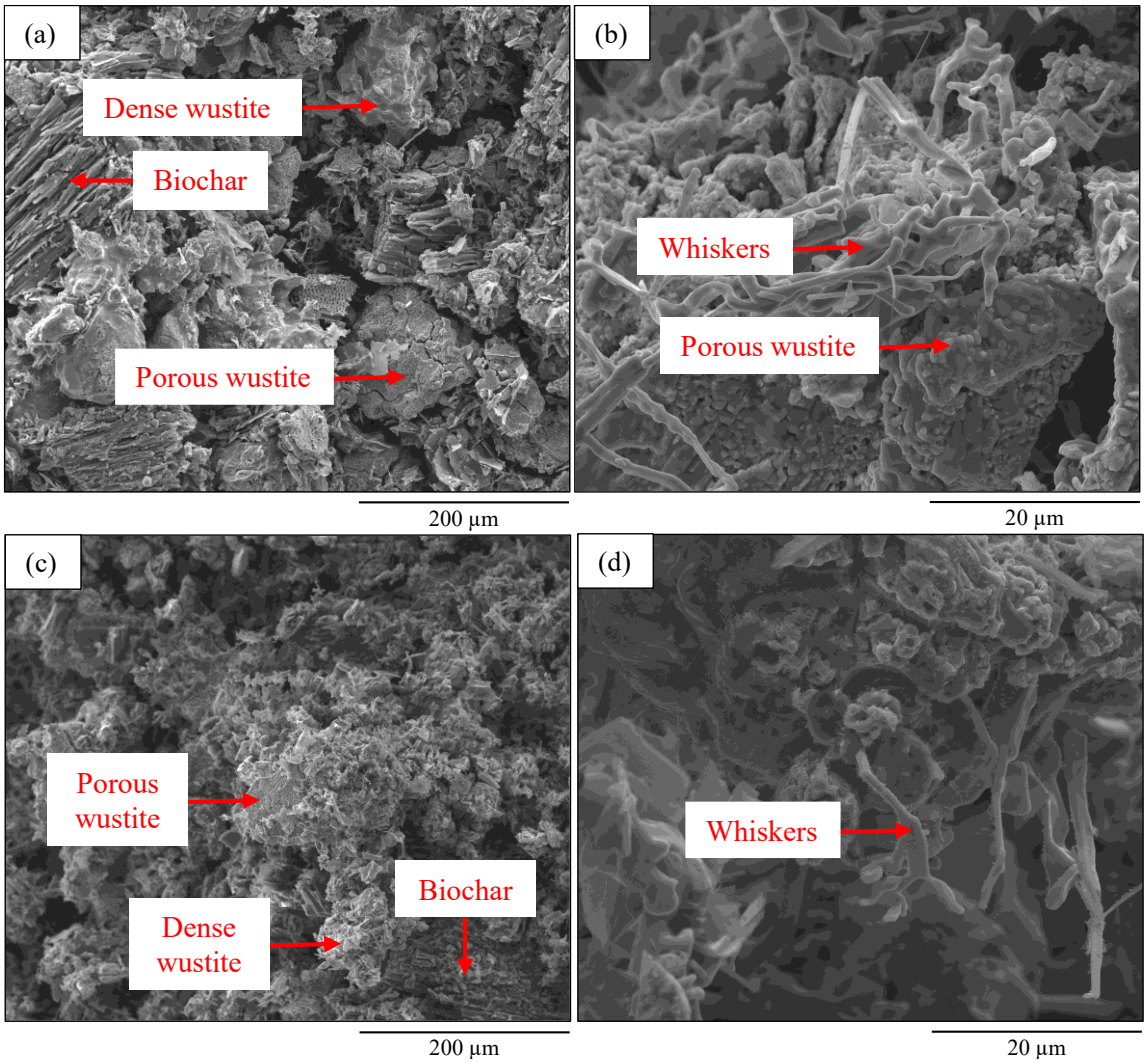

Figure 3.9. SEM microstructure of the briquettes after heating to 950 °C: (a/b) B400 and (c/d) B550.

3.3.5. Micro-CT analysis of self-reducing briquettes

Micro-CT enabled a comprehensive assessment of the internal structure of the briquettes, providing insights into the reduction process based on the spatial distribution of the main constituents and the phases formed, as well as their mechanical behavior. In the as-prepared briquettes (before testing), a homogeneous distribution of the raw materials was observed. Grayscale intensity profiles allowed the segmentation of two main domains: high-attenuation regions associated with iron oxides and low-attenuation regions corresponding to the combined

presence of pores and biochar. Due to the subtle differences in attenuation coefficients, it was not possible to distinguish individual iron oxides (hematite, magnetite, and goethite) or to differentiate pores from biochar particles. Nevertheless, the clear contrast between these broader domains enabled a meaningful structural analysis of the briquettes. Upon heating, a third phase, corresponding to metallic iron clusters, became clearly distinguishable as a result of the progression of self-reduction reactions. This behavior demonstrates the technique's sensitivity to both structural and compositional evolution during the reduction process.

Figure 3.10 presents cross-sectional views of the tomographic volumes of the briquettes before and after each interrupted test. Before heating, intermediate gray regions were observed and attributed to iron oxides, based on their expected X-ray attenuation properties. In contrast, darker regions detected—ranging from dark gray to black—corresponded to the combined domain of pores and biochar, both characterized by low attenuation due to their lower density and effective atomic number. After heating, bright regions became prominent, indicating the formation and growth of metallic iron, which exhibits the highest X-ray attenuation among the phases present.

Overall, at 1250 °C, B250 and B400 exhibited a more uniform and homogeneous reduction, with metallic iron distributed throughout their cross-sections. Among them, B400 showed a higher volume of the bright region, indicating more extensive sintering and a higher density of nucleation and coalescence sites, which may explain the greater shrinkage observed among the briquettes studied (Figure 3.7). On the other hand, despite the larger amount of metallic iron formed in B550 (Figure 3.5), the reduction progressed preferentially from the external surface toward the core. This resulted in a more heterogeneous structure, with metallic iron predominantly concentrated near the surface and sparsely distributed in the interior. This behavior must be related to the lower volatile matter and higher carbon content of B550. The greater carbon content promotes a greater Boudouard reaction rate and a greater heat consumption, which decreases the heat transfer into the briquette. Consequently, reduction was more effective at the surface exposed to the heat source, while the inner regions remained less reduced. This reduction pattern is consistent with the lower shrinkage index observed for B550. Conversely, the higher volatile content in B250 and B400 promoted a uniform reduction in the briquettes during the biomass devolatilization.

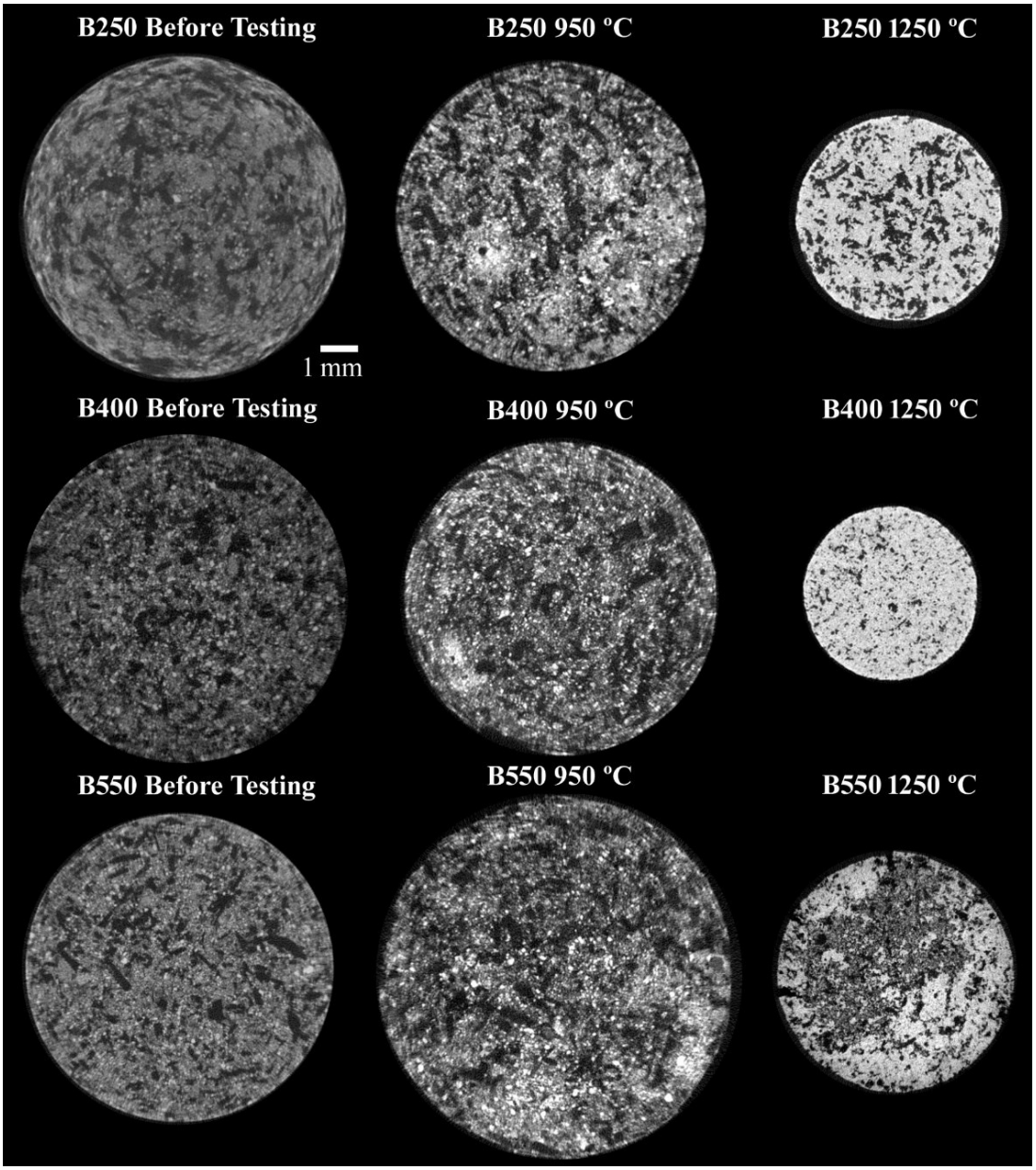

Figure 3.10. Representative cross-sectional views extracted from tomography volumes of the briquettes before and after heating.

Micro-CT also allowed a semi-quantitative assessment of the volume fractions of the identified phases, as summarized in Table 3.4. Segmentation of the reconstructed volumes was carried out using a fixed threshold applied to the 2D layers of the model, enabling the estimation of the relative volume fraction occupied by each domain in relation to the total volume of the briquettes. The analysis focused on two main domains: the combined pores and biochar region and the metallic iron phase formed during the reduction process. A separate analysis of porosity was not performed, as it is intrinsically associated with the biochar particles, as evidenced by the SEM micrographs (Figure 3.8).

Table 3.4. Volume fractions of the phases as determined by micro-CT.

	Phase/domain	Briquette		
		B250	B400	B550
Before testing	Metallic iron	N/D	N/D	N/D
	Pores and biochar	20.34	25.46	26.46
950 °C	Metallic iron	4.57	14.14	20.01
	Pores and biochar	33.03	27.21	31.37
1250 °C	Metallic iron	15.86	30.84	53.10
	Pores and biochar	29.26	19.29	21.09

N/D: not detected

According to Table 3.4, before testing, the volume fraction of the pores and biochar domain increased slightly with the biomass pyrolysis temperature, ranging from 20.34% in B250 to 26.46% in B550. This behavior is attributed to the intrinsic porosity of the biochar itself (Table 3.2), as the mass fraction added to the briquettes was the same for all samples. During heating, the temperature played an important role in the evolution of porosity. At 950 °C, the pores and biochar domain increased in all briquettes relative to their initial state. This effect can be associated with gas release during biochar devolatilization and carbon gasification, both of which contribute to pore development. After heating to 1250 °C, its fraction decreased due to the consumption of biochar (carbon) during self-reduction, concomitant with the formation of metallic iron and slag. This process results in the filling of internal voids and pores, reducing the overall porosity [38]. The decrease in porosity was more pronounced in briquettes with higher metallization, as a result of sintering of the formed iron and the presence of a liquid slag phase within the briquettes.

On the other hand, the formation of metallic iron showed a positive correlation with increasing heating temperature, since the iron oxide reduction reactions are favored at high temperatures. Furthermore, the strong relationship between biomass pyrolysis temperature and the extent of iron oxide reduction highlights the critical role of carbon availability on the metallization. Notably, B550 briquettes, which combine high fixed carbon content and low volatile matter, exhibited the highest metallic iron fraction. Overall, the micro-CT segmentation results quantitatively corroborate the trends observed in XRD and SEM analyses, confirming the progressive transformation of iron oxides into metallic iron as a function of both heating temperature and biochar characteristics. The differences between micro-CT and XRD results are considered acceptable, given the complex, multiphase nature of the samples and the inherent limitations of each technique.

To achieve a more detailed characterization of the metallic iron network, a 3D analysis of the briquettes was performed, focusing exclusively on metallic iron clusters and complemented by individual statistical analyses. This approach enabled a comprehensive evaluation of briquette reduction at high temperatures by considering the entire reduced structure, unlike other methods that focus only on specific regions of the samples. Furthermore, it provided deeper insights into the connectivity, coalescence, and volumetric evolution of the metallic phase within the briquette matrix.

Figures 3.11–3.13 show the 3D distribution and quantitative analysis of metallic iron clusters in B250, B400, and B550 after heating. For each briquette, the left-side images display the total matrix volume, followed by the representation of metallic iron clusters rendered in distinct colors. Each color corresponds to an individual metallic iron particle or cluster, representing a region of voxels (3D pixels) exhibiting the grayscale intensity of the phase and connected through a point, edge, or face. In this way, interconnected metallic iron clusters are rendered in the same color, enabling visual assessment of particle coalescence and sintering. To facilitate 3D visualization, at least one dimension of the briquettes is indicated in the images as a scale reference. The graphs on the right display histograms of metallic iron cluster size distribution, expressed as the number of clusters (count) versus their volume (μm^3) on a logarithmic scale.

In Figure 3.11, B250 exhibited small, dispersed metallic iron clusters at 950 °C, with limited coalescence and a maximum cluster volume of 1.6×10^9 μm^3. After heating to 1250 °C, the clusters became larger and more interconnected, with the maximum volume increasing to 2.7×10^{10} μm^3, indicating progressive sintering. In Figure 3.12, B400 showed a more advanced reduction already at 950 °C, with greater cluster coalescence compared to B250, reaching a maximum volume of 1.8×10^{10} μm^3. At 1250 °C, a denser and more uniform metallic network was formed, with metallic iron clusters reaching volumes up to 3.1×10^{10} μm^3. B550, in Figure 3.13, displayed the most advanced reduction behavior, with a high density of metallic iron and large, interconnected clusters with a maximum volume of 1.2×10^{11} μm^3 at 950 °C. After heating to 1250 °C, the metallic phase became further consolidated, maintaining the maximum cluster volume while exhibiting enhanced structural connectivity.

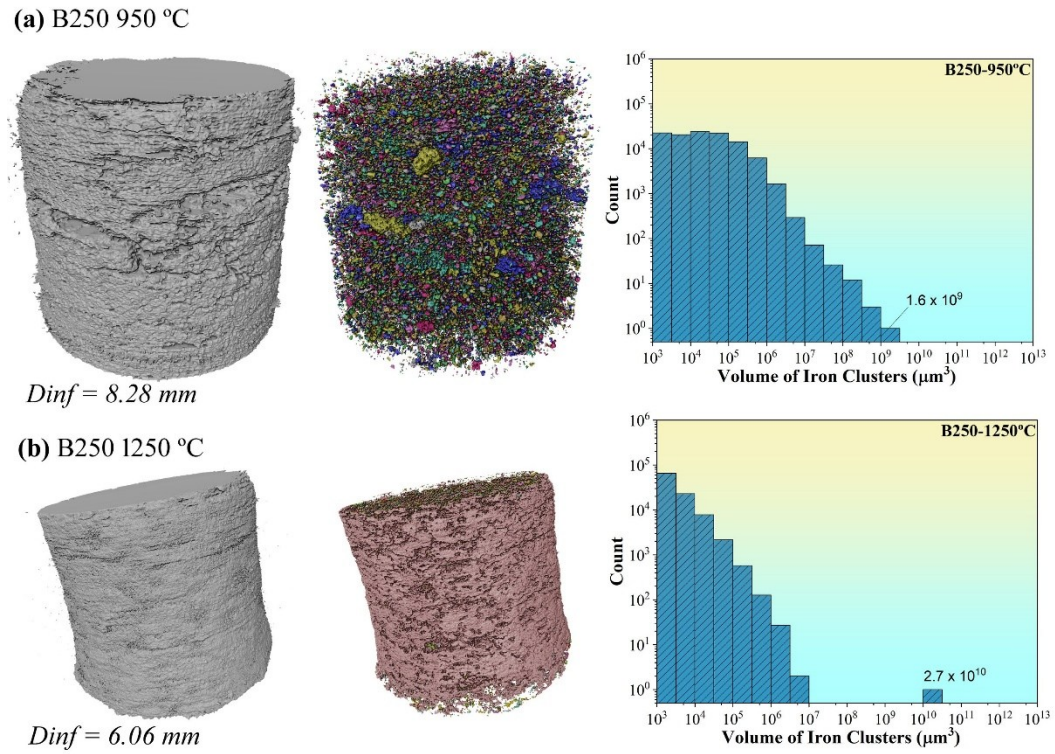

Figure 3.11. 3D distribution and volume analysis of metallic iron clusters in B250 after heating to (a) 950 °C and (b) 1250 °C.

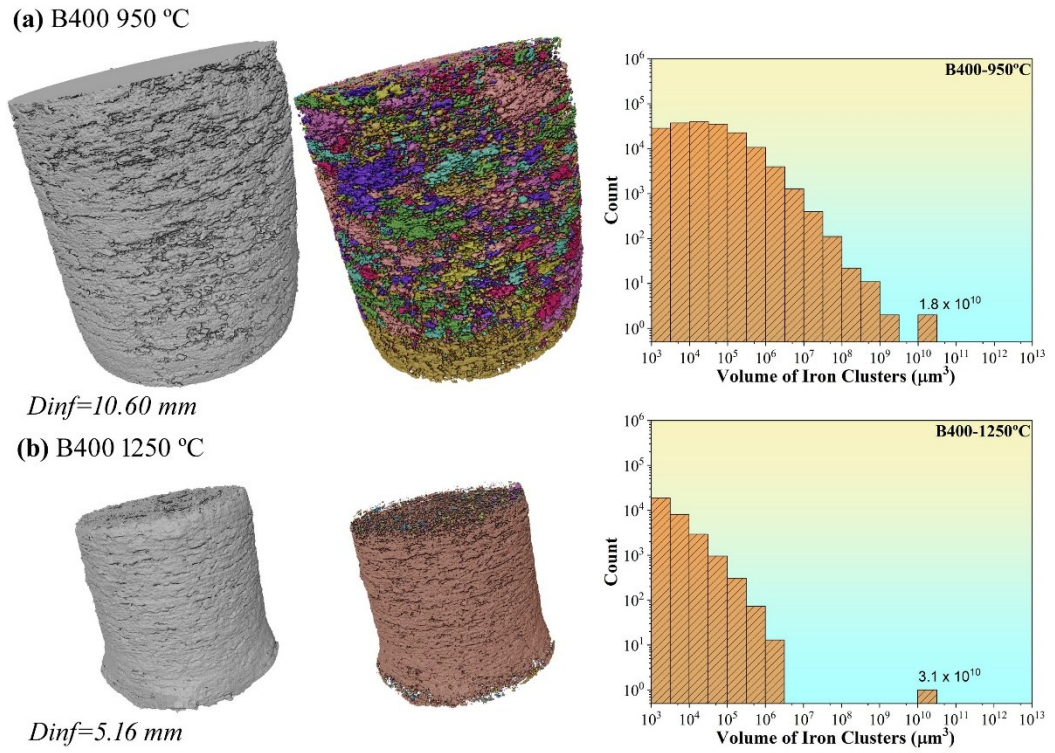

Figure 3.12. 3D distribution and volume analysis of metallic iron clusters in B400 after heating to (a) 950 °C and (b) 1250 °C.

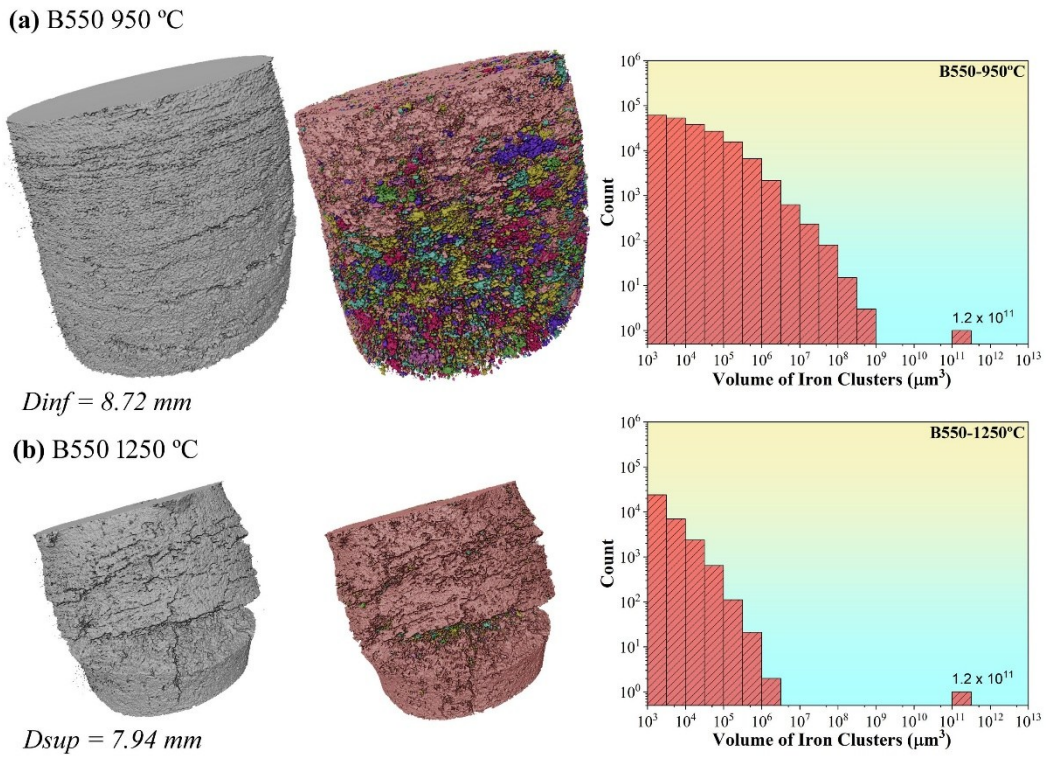

Figure 3.13. 3D distribution and volume analysis of metallic iron clusters in B550 after heating to (a) 950 °C and (b) 1250 °C.

Overall, increasing the heating temperature enhanced both the presence and spatial distribution of metallic iron. At 1250 °C, the clusters formed a highly interconnected structure, indicative of intense sintering and characterized by the coalescence or partial melting of solid iron particles. In each 3D reconstruction, the same color (pink) represents a metallic iron cluster whose particles are physically connected, whereas different colors indicate smaller, isolated iron particles that remain unconnected to others. This behavior reflects the increased connectivity and interaction within the metallic structure. Moreover, the formation of these metallic networks from the surface toward the core of the briquettes results in the development of a metallic shell, likely contributing to the observed increase in mechanical strength after high-temperature treatment.

It is important to note that the total volume of the briquettes decreased as the temperature increased up to 1250 °C. Consequently, the absolute sizes of metallic iron clusters may not be directly comparable across temperature stages, as the analyzed volume itself was reduced. Therefore, the observed trends in cluster growth and connectivity are more appropriately

interpreted in relative terms, reflecting the extent of reduction and the structural evolution of each briquette under the specific thermal conditions.

In summary, this 3D perspective provides a more representative understanding of material structures, particularly in heterogeneous systems where features such as pore networks and particle interconnectivity critically influence material behavior. In contrast, 2D techniques are inherently limited to specific planes and cannot capture the full spatial arrangement or connectivity of internal features, potentially leading to incomplete or misleading interpretations. In this context, micro-CT stands out as a powerful, non-destructive tool for advanced materials characterization, bridging the gap between surface-level observations and full-volume structural analysis. This technique proved particularly valuable in the present study, especially for evaluating the reduction behavior of self-reducing briquettes at high temperatures as a function of the biomass treatment temperature used in their composition.

3.3.6. Mechanical strength of self-reducing briquettes

The results of the compressive strength tests, along with the corresponding standard deviations (values in parentheses), are presented in Figure 3.14. Initially, B400 exhibited the lowest mechanical strength, which can be attributed to thermal decomposition of biomass constituents during the pyrolysis process. At this temperature (400 °C), the cellulose fraction becomes predominant, resulting in a higher concentration of fibrous material in the briquettes and, consequently, lower structural strength.

At 950 °C, all briquettes exhibited low mechanical strength due to cumulative phenomena occurring during heating, including binder dehydration, biomass devolatilization (primarily below 600 °C), and the progression of self-reduction reactions accompanied by volumetric swelling within this temperature range. These reactions generate gaseous intermediates whose continuous release increases the internal pressure within the briquettes, inducing mechanical stresses that result in structural weakening [10,38]. Significant volume expansion, particularly beyond the 20% typically considered normal, is well known to cause a marked decrease in agglomerate strength [44]. According to Takano and Mourão [16], the lowest strength values for cold-bonded agglomerates are generally observed at temperatures between 900 and 1000 °C.

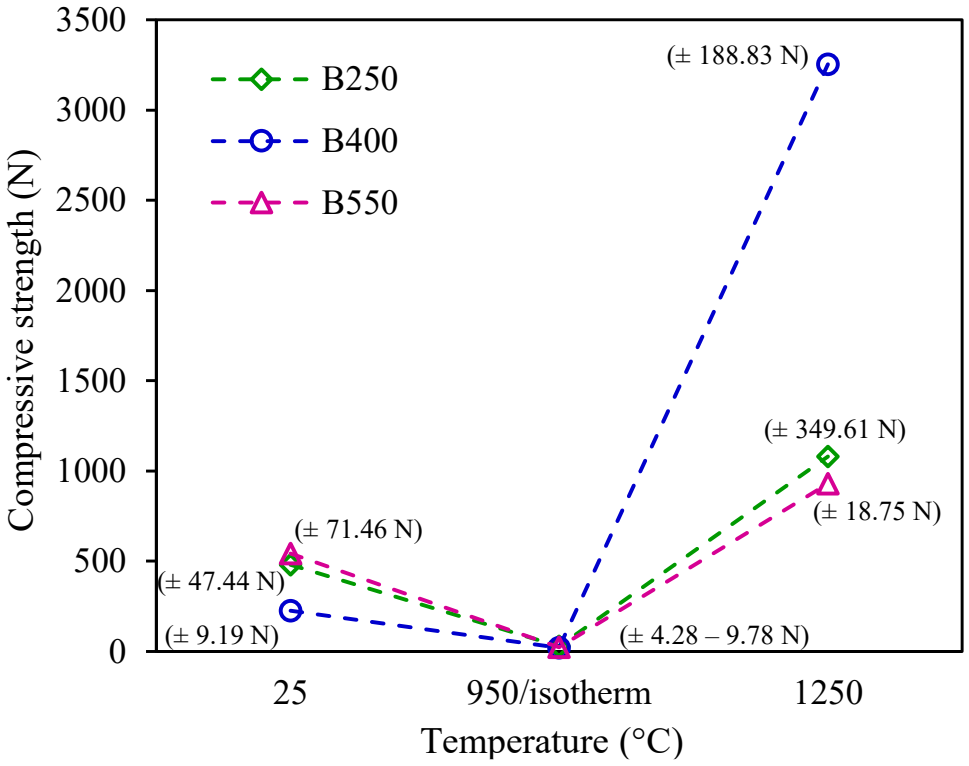

Figure 3.14. Compressive strength of the briquettes before and after high-temperature interrupted tests.

After heating to 1250 °C, an increase in briquette strength was observed, attributed to the enhanced formation of metallic iron and sintering of reduced iron particles [55,61]. At this temperature, B400 showed the highest strength among the evaluated briquettes, approximately three times greater than that of the other samples. This superior performance likely results from the combined effects of metallic iron formation and the swelling phenomenon, which occur differently depending on the biomass pyrolysis temperature. As shown in Figure 3.10, a more uniform reduction was observed in B400 at 1250 °C, evidenced by the uniform formation and distribution of metallic iron throughout the sample. Thus, this promoted a more homogeneous and consolidated structure, enhancing the mechanical strength of the briquettes. In contrast, the catastrophic swelling of B550 at 950 °C, associated with the formation and coalescence of the metallic phase concentrated near the surface of these briquettes (non-uniform reduction), likely compromised structural cohesion and high-temperature strength. These findings highlight micro-CT as a valuable tool for identifying and correlating microstructural changes with the mechanical behavior of briquettes under different thermal conditions.

Table 3.5 summarizes the main phenomena observed in self-reducing briquettes after high-temperature heating, highlighting the effects of biochar pyrolysis temperature and enabling a clear comparison of the intensity and nature of these phenomena across the different samples.

Table 3.5. Main phenomena observed in self-reducing briquettes with biochar pyrolyzed at different temperatures.

Briquette	Reduction	Cracking	Swelling	Shrinkage	Strength
B250	Low, uniform	Moderate	Low (porous structure, lower internal pressure)	Intermediate	Intermediate
B400	Intermediate, uniform	Moderate	High, catastrophic (whiskers, intermediate gas generation)	Highest	Highest
B550	High, superficial	High	Highest, catastrophic (whiskers, intense gas generation, higher ash content)	Lowest	Lowest

3.4. Conclusions

This study investigated the structural evolution of self-reducing briquettes produced from pellet feed and sugarcane bagasse pyrolyzed at 250, 400, and 550 °C at different reduction stages. Non-isothermal interrupted tests, combined with complementary characterization techniques, enabled a comprehensive analysis of the reduction process, correlating the swelling and shrinkage behavior of the briquettes with structural transformations and their impact on metallurgical and mechanical performance.

XRD analysis revealed the presence of metallic iron in all briquettes from 950 °C onward, with B550 presenting a higher reduction degree, which can be attributed to the greater carbon availability. This behavior is corroborated by the gas analysis, which indicated more intense CO peaks for these briquettes, confirming the higher intensity of the self-reduction reactions.

After heating to 950 °C, B400 and B550 exhibited considerable swelling, intensified with increasing biomass pyrolysis temperature, resulting in volumetric expansions of 31% and 75%, respectively. The presence of metallic iron whiskers, identified by SEM analysis, was

associated with the catastrophic swelling of these briquettes during reduction. Furthermore, the greater swelling magnitude observed in B550 may be attributed to the increased internal pressure resulting from the greater generation and release of gases at the reaction interface, which induces structural stresses within the agglomerates, as well as to the higher ash content of the biochar produced at 550 °C. In contrast, B250 maintained its physical and geometrical integrity. At 950 °C, all briquettes showed low mechanical strength, primarily due to the combined effects of binder dehydration, intensified self-reduction reactions, and swelling behavior observed at this temperature range.

At 1250 °C, all briquettes exhibited volumetric shrinkage, attributed to the coalescence and sintering of metallic iron particles, as well as to the formation of a liquid slag phase, as evidenced by micro-CT and SEM analyses. In B250 and B400, the reduction occurred more uniformly and homogeneously, with metallic iron distributed throughout the cross-section, with more intense sintering in B400, which may explain the greater shrinkage observed. In contrast, B550 displayed a more heterogeneous structure, with metallic iron predominantly concentrated near the surface, reflecting a lower shrinkage index. At this temperature, an increase in mechanical strength was observed, resulting from extensive metallic iron formation and sintering of the iron particles. The uniform internal reduction and greater sintering in B400 promoted a more consolidated structure, favoring the highest mechanical strength among the briquettes.

This study highlighted the potential of micro-CT as a characterization tool for self-reducing briquettes, which, when combined with complementary techniques such as XRD and SEM, enables a more comprehensive understanding of the structural evolution of these materials under different biochar treatment conditions. This integrated approach aligns with the use of biomass as a renewable carbon source and supports the development of more sustainable practices in the iron and steelmaking industry.

Acknowledgments

The authors express gratitude to CAPES-PROEX and CNPq for the accomplishment and support of this work, and the Center of Microscopy at the Federal University of Minas Gerais

(UFMG) for providing the equipment and technical support for the experiments involving electron microscopy.

3.5. References

[1] Jeon M, Jeon S, Yi J, Park M-J. Analysis of the techno-economics and CO_2 emissions of DME production using by-product gases in the steel industries. J Clean Prod 2025;492:144893. https://doi.org/10.1016/j.jclepro.2025.144893.

[2] Korobeinikov Y, Meshram A, Harris C, Kovtun O, Govro J, O'Malley RJ, et al. Reduction of iron-ore pellets using different gas mixtures and temperatures. Steel Res Int 2023;94:2300066. https://doi.org/10.1002/srin.202300066.

[3] World Steel Association. World Steel in Figures. 2025. Available in: https://worldsteel.org/data/world-steel%20in-Figures/world-steel-in-Figures-2025/. [Accessed 25 Sep 2025].

[4] Suopajärvi H, Pongrácz E, Fabritius T. The potential of using biomass-based reducing agents in the blast furnace: A review of thermochemical conversion technologies and assessments related to sustainability. Renew Sustain Energy Rev 2013;25:511–28. https://doi.org/10.1016/j.rser.2013.05.005.

[5] Mandova H, Leduc S, Wang C, Wetterlund E, Patrizio P, Gale W, et al. Possibilities for CO_2 emission reduction using biomass in European integrated steel plants. Biomass Bioenergy 2018;115:231–43. https://doi.org/10.1016/j.biombioe.2018.04.021.

[6] El-Tawil AA, Ahmed HM, Ökvist LS, Björkman B. Self-reduction behavior of bio-coal containing iron ore composites. Metals 2020;10:133. https://doi.org/10.3390/met10010133.

[7] Mousa E, Wang C, Riesbeck J, Larsson M. Biomass applications in iron and steel industry: An overview of challenges and opportunities. Renew Sustain Energy Rev 2016;65:1247–66. https://doi.org/10.1016/j.rser.2016.07.061.

[8] Suopajärvi H, Kemppainen A, Haapakangas J, Fabritius T. Extensive review of the opportunities to use biomass-based fuels in iron and steelmaking processes. J Clean Prod 2017;148:709–34. https://doi.org/10.1016/j.jclepro.2017.02.029.

[9] Khasraw D, Martin C, Herbert J, Li Z. A comprehensive literature review of biomass characterisation and application for iron and steelmaking processes. Fuel 2024;368:131459. https://doi.org/10.1016/j.fuel.2024.131459.

[10] Bagatini MC, Fernandes T, Silva R, Galvão DF, Flores IV. Mill scale and flue dust briquettes as alternative burden to low height blast furnaces. J Clean Prod 2020;276:124332. https://doi.org/10.1016/j.jclepro.2020.124332.

[11] Han H, Duan D, Yuan P, Li D. Biomass reducing agent utilisation in rotary hearth furnace process for DRI production. Ironmak Steelmak 2015;42:579–84. https://doi.org/10.1179/1743281215Y.0000000001.

[12] Purohit S, Pownceby MI, Guiraud A. Sticking and swelling of iron ore pellets: Mechanisms and controlling factors. J Sustain Metall 2025;11:67–87. https://doi.org/10.1007/s40831-024-01000-3.

[13] Elsherbiny AA, Omran M, Qiu D, Xiong Y, Galal AM, Saxén H, et al. Swelling behavior and stress analysis of hematite pellets: Predicting failure through distortion energy criteria. Powder Technol 2025;457:120893. https://doi.org/10.1016/j.powtec.2025.120893.

[14] Kowitwarangkul P, Babich A, Senk D. Reduction behavior of self-reducing pellet (SRP) for low height blast furnace. Steel Res Int 2014;85:1501–9. https://doi.org/10.1002/srin.201300399.

[15] Kovtun O, Levchenko M, Oldinski E, Gräbner M, Volkova O. Swelling behavior of iron ore pellets during reduction in H_2 and N_2/H_2 atmospheres at different temperatures. Steel Res Int 2023;94:2300140. https://doi.org/10.1002/srin.202300140.

[16] Takano C, Mourão MB. Self-reducing pellets for ironmaking: Mechanical behavior. Miner Process Extr Metall Rev 2003;24:233–52. https://doi.org/10.1080/714856823.

[17] El-Geassy AA, Nasr MI, Hessien MM. Effect of reducing gas on the volume change during reduction of iron oxide compacts. ISIJ Int 1996;36:640–9. https://doi.org/10.2355/isijinternational.36.640.

[18] Lei J, Zhang C, An J, Kong Y-Q, He S, Long H, et al. Mechanism study on gas-based reduction swelling behavior of ultra-high grade pellets. J Mater Res Technol 2023;26:823–36. https://doi.org/10.1016/j.jmrt.2023.07.183.

[19] Yang J, Li L, Liang Z, Peng X, Deng X, Li J, et al. Direct reduction of iron ore pellets by H_2-CO mixture: An in-situ investigation of the evolution and dynamics of swelling. Mater Today Commun 2023;36:106940. https://doi.org/10.1016/j.mtcomm.2023.106940.

[20] Sharma T, Gupta RC, Prakash B. Effect of gangue content on the swelling behaviour of iron ore pellets. Miner Eng 1990;3:509–16. https://doi.org/10.1016/0892-6875(90)90043-B.

[21] Li GH, Tang ZK, Zhang YB, Cui ZX, Jiang T. Reduction swelling behaviour of haematite/magnetite agglomerates with addition of MgO and CaO. Ironmak Steelmak 2010;37:393–7. https://doi.org/10.1179/030192310X12690127076352.

[22] Wang HT, Sohn HY. Effect of CaO and SiO_2 on swelling and iron whisker formation during reduction of iron oxide compact. Ironmak Steelmak 2011;38:447–52. https://doi.org/10.1179/1743281211Y.0000000022.

[23] Song W, Luo G-P, Sun C-C, Zhang J, Zhu J-G. Effect of K and Na on reduction swelling performance of oxidized roasted briquettes. High Temp Mater Process 2021;40:241–52. https://doi.org/10.1515/htmp-2020-0091.

[24] Umadevi T, Kumar A, Karthik P, Srinidhi R, Manjini S. Characterisation studies on swelling behaviour of iron ore pellets. Ironmak Steelmak 2016;45:157–65. https://doi.org/10.1080/03019233.2016.1250043.

[25] Guo Y, Liu K, Chen F, Wang S, Zheng F, Yang L, et al. Effect of basicity on the reduction swelling behavior and mechanism of limestone fluxed iron ore pellets. Powder Technol 2021;393:291–300. https://doi.org/10.1016/j.powtec.2021.07.057.

[26] Wang P, Wang C, Wang H, Long H, Zhou T. Effects of SiO_2, CaO and basicity on reduction behaviors and swelling properties of fluxed pellet at different stages. Powder Technol 2022;396:477–89. https://doi.org/10.1016/j.powtec.2021.09.080.

[27] Xu R-S, Zhang J-L, Zuo H-B, Jiao K-X, Hu Z-W, Xing X-D. Mechanisms of swelling of iron ore oxidized pellets in high reduction potential atmosphere. J Iron Steel Res Int 2015;22:1–8. https://doi.org/10.1016/s1006-706x(15)60001-2.

[28] Yi L, Huang Z, Jiang T, Wang L, Qi T. Swelling behavior of iron ore pellet reduced by H_2-CO mixtures. Powder Technol 2015;269:290–95. https://doi.org/10.1016/j.powtec.2014.09.018.

[29] Halder S, Fruehan RJ. Reduction of iron-oxide-carbon composites: Part III. Shrinkage of composite pellets during reduction. Metall Mater Trans B 2008;39:809–17. https://doi.org/10.1007/s11663-008-9201-3.

[30] Zhang H, Zhong W, Qiu R, Han L. Kinetics and modeling of Pb (II) adsorption in pellet biochar based on micro-computed tomography characterization. Bioresour Technol 2023;387:129645. https://doi.org/10.1016/j.biortech.2023.129645.

[31] Cavaliere P, Sadeghi B, Dijon L, Laska A, Koszelow D. Three-dimensional characterization of porosity in iron ore pellets: A comprehensive study. Miner Eng 2024;213:108746. https://doi.org/10.1016/j.mineng.2024.108746.

[32] Bagatini MC, Zymla V, Osório E, Vilela ACF. Scale recycling through self-reducing briquettes to use in EAF. ISIJ Int 2017;57:2081–90. https://doi.org/10.2355/isijinternational.ISIJINT-2017-242.

[33] Coleti JL, Manfredi GVP, Vinhal JT, Junca E, Espinosa DCR, Tenório JAS. Kinetic investigation of self-reduction basic oxygen furnace dust briquettes using charcoals from different biomass. J Mater Res Technol 2020;9:13282–93. https://doi.org/10.1016/j.jmrt.2020.09.061.

[34] Hammam A, Nasr MI, El-Sadek MH, Omran M, Ahmed A, Li Y, et al. Comparative study on the isothermal reduction kinetics of iron oxide pellet fines with carbon-bearing materials. Sustainability 2022;14:8647. https://doi.org/10.3390/su14148647.

[35] Gandra BF, Oliveira AFL, Bagatini MC, Osório E. Iron ore-petcoke briquettes as complementary burden for blast furnaces. J Mater Res Technol 2025;35:1556–64. https://doi.org/10.1016/j.jmrt.2025.01.123.

[36] Zulkania A, Rochmadi R, Hidayat M, Cahyono RB. Reduction reactivity of low-grade iron ore-biomass pellets for a sustainable ironmaking process. Energies 2022;15:137. https://doi.org/10.3390/en15010137.

[37] Rosso Neto L, Borgert CH, Grillo FF, Oliveira JR, Coleti JL, Frizon TEA, et al. Sustainable steel production: Evaluating the reduction kinetics of iron ore self-reducing briquettes with eucalyptus charcoal. J Clean Prod 2024;457:142426. https://doi.org/10.1016/j.jclepro.2024.142426.

[38] Ye L, Zhang J, Yu J, Xu R, Dang H. Evolution behavior and kinetic analysis of vacuum-extruded iron-rich dust briquette in blast furnace. J Clean Prod 2023;433:139753. https://doi.org/10.1016/j.jclepro.2023.139753.

[39] Strezov V, Ziolkowski A, Evans TJ, Nelson PF. Assessment of evolution of loss on ignition matter during heating of iron ores. J Therm Anal Calorim 2010;100:901–7. https://doi.org/10.1007/s10973-009-0398-4.

[40] Kemppainen A, Iljana M, Heikkinen E-P, Paananen T, Mattila O, Fabritius T. Reduction behavior of cold-bonded briquettes under simulated blast furnace conditions. ISIJ Int 2014;54:1539–45. https://doi.org/10.2355/isijinternational.54.1539.

[41] Nguyen C-S, Nguyen T-H, Nguyen S-L, Bui A-H. Study on the reducibility of iron ore pellets at high temperature. Vietnam J Sci Technol Eng 2021;63:3–7. https://doi.org/10.31276/VJSTE.63(4).03-07.

[42] Yang H, Yan R, Chen H, Lee DH, Zheng C. Characteristics of hemicellulose, cellulose, and lignin pyrolysis. Fuel 2007;86:1781–8. https://doi.org/10.1016/j.fuel.2006.12.013.

[43] Safdari M-S, Amini E, Weise DR, Fletcher TH. Heating rate and temperature effects on pyrolysis products from live wildland fuels. Fuel 2019;242:295–304. https://doi.org/10.1016/j.fuel.2019.01.040.

[44] Singh M, Björkman B. Effect of reduction conditions on the swelling behaviour of cement-bonded briquettes. ISIJ Int 2004;44:294–303. https://doi.org/10.2355/isijinternational.44.294.

[45] Halim KSA, Bahgat M, El-Kelesh HA, Nasr MI. Metallic iron whisker formation and growth during iron oxide reduction: Basicity effect. Ironmak Steelmak 2009;36:631–40. https://doi.org/10.1179/174328109X463020.

[46] Nascimento RC, Mourão MB, Capocchi JDT. Kinetics and catastrophic swelling during reduction of iron ore in carbon bearing pellets. Ironmak Steelmak 1999;26:182–6. https://doi.org/10.1179/030192399677040.

[47] Mishra S. Review on reduction kinetics of iron ore-coal composite pellet in alternative and sustainable ironmaking. J Sustain Metall 2020;6:541–56. https://doi.org/10.1007/s40831-020-00299-y.

[48] Sharma T, Gupta RC, Prakash B. Effect of reduction rate on the swelling behaviour of iron ore pellets. ISIJ Int 1992;32:812–8. https://doi.org/10.2355/isijinternational.32.812.

[49] Vitikka O, Iljana M, Heikkilä A, Tkalenko I, Kovtun O, Koriuchev N, et al. Effect of biocarbon addition on metallurgical properties of mill scale-based auger pressing briquettes. ISIJ Int 2024;64:964–77. https://doi.org/10.2355/isijinternational.ISIJINT-2023-417.

[50] Tang K, Wang YD, Niu Y, Honeyands TA, O'Dea D, Mostaghimi P, et al. Particle classification of iron ore sinter green bed mixtures by 3D X-ray microcomputed tomography and machine learning. Powder Technol 2023;415:118151. https://doi.org/10.1016/j.powtec.2022.118151.

[51] Ahmed HM, Persson A, Ökvist LS, Björkman B. Reduction behaviour of self-reducing blends of in-plant fines in inert atmosphere. ISIJ Int 2015;55:2082–9. https://doi.org/10.2355/isijinternational.isijint-2015-182.

[52] Kang T, Gupta S, Sahajwalla V. Characterizing swelling behaviour of iron oxides during solid state reduction for COREX application and their implications on fines generation. ISIJ Int 2007;47:1590–8. https://doi.org/10.2355/isijinternational.47.1590.

[53] Leão PMGC, Zicker TB, Ferreira NHA, Ardisson JD, Bagatini MC. Influence of biomass pyrolysis temperature on the performance of self-reducing briquettes for use in blast furnaces. Biomass Bioenergy 2026;206:108691. https://doi.org/10.1016/j.biombioe.2025.108691.

[54] Gonçalves MVB, Mendonça LM, Flores IV, Bagatini MC. Investigation of the phenomena associated with iron ore reduction by raw biomass and charcoal volatiles. J Sustain Metall 2024;10:1094–1111. https://doi.org/10.1007/s40831-024-00851-0.

[55] Mantovani MC, Takano C. The strength and the high temperature behaviors of self-reducing pellets containing EAF dust. ISIJ Int 2000;40:224–30. https://doi.org/10.2355/isijinternational.40.224.

[56] Singh M, Björkman B. Testing of cement bonded briquettes under laboratory and blast furnace conditions Part 2 - Swelling of briquettes. Ironmak Steelmak 2007;34:41–53. https://doi.org/10.1179/174328106X118080.

[57] Moujahid SE, Rist A. The nucleation of iron on dense wustite: A morphological study. Metall Trans B 1988;19:787–802. https://doi.org/10.1007/BF02650198.

[58] Iguchi Y, Uyeda Y-I, Goto K, Hayashi S. In situ observation of nucleation and growth of iron whiskers from supersaturated wüstite. Oxid Met 1994;42:103–8. https://doi.org/10.1007/BF01061926.

[59] Singh M, Björkman B. Effect of processing parameters on the swelling behaviour of cement-bonded briquettes. ISIJ Int 2004;44:59–68. https://doi.org/10.2355/isijinternational.44.59.

[60] Iljana M, Mattila O, Alatarvas T, Visuri V-V, Kurikkala J, Paananen T, et al. Dynamic and isothermal reduction swelling behaviour of olivine and acid iron ore pellets under simulated blast furnace shaft conditions. ISIJ Int 2012;52:1257–65. https://doi.org/10.2355/isijinternational.52.1257.

[61] Chai Y, Wang S, Zhang J, Shi Y, Liu P, An S, et al. Study on strength and reduction characteristics of iron ore powder-green carbon composite briquettes. Fuel 2024;377:132741. https://doi.org/10.1016/j.fuel.2024.132741.

4. ARTIGO 3: REDUCTION AND MECHANICAL STRENGTH PERFORMANCE OF SELF-REDUCING BRIQUETTES WITH DIFFERENT BIOCHAR CONTENTS

Paula Maria Gomes Cunha Leão*, Maurício Covcevich Bagatini

Laboratory of Ironmaking Processes (LPS), Department of Metallurgical and Materials Engineering, Federal University of Minas Gerais (UFMG), Av. Antônio Carlos, 6627, Escola de Engenharia, 31270-901, Belo Horizonte, MG, Brazil

* Corresponding author

Abstract

For blast furnace applications, self-reducing briquettes must meet specific quality requirements related to their metallurgical and mechanical properties, which are influenced by both the carbon source and its proportion in the mixture. This study investigated the effect of biochar content on the reduction behavior and mechanical strength of self-reducing briquettes produced with pellet feed and sugarcane bagasse biochar pyrolyzed at 400 °C. Briquettes containing 5–15% by mass of biochar were subjected to high-temperature tests under a reducing atmosphere representative of a blast furnace, while additional tests were conducted under an inert atmosphere to assess the relative contributions of external reducing gases and solid carbon from the biochar. Increasing temperature and biochar content enhanced mass loss and metallization, with briquettes containing 15% biochar achieving the highest values, confirming the critical role of solid carbon as a reducing agent. Although the reducing atmosphere intensified mass loss and metallic iron formation, high metallization was also observed in briquettes with 10% and 15% biochar under inert conditions, suggesting that reduction was predominantly driven by biochar-derived carbon in intimate contact with iron oxides. The briquettes presented superior reduction performance compared with conventional blast furnace burdens (sinter and pellets), particularly at higher biochar contents. The composition containing 10% biochar exhibited the highest mechanical strength at elevated temperatures, accompanied by substantial metallic iron formation without generating excessive internal pressure due to gas evolution, as observed in B15. The results indicate the existence of an optimal biochar content of 10%, providing the best balance between self-reduction efficiency and briquette integrity.

Keywords: biochar content; self-reducing briquette; reduction; mechanical strength; blast furnace.

Graphical Abstract

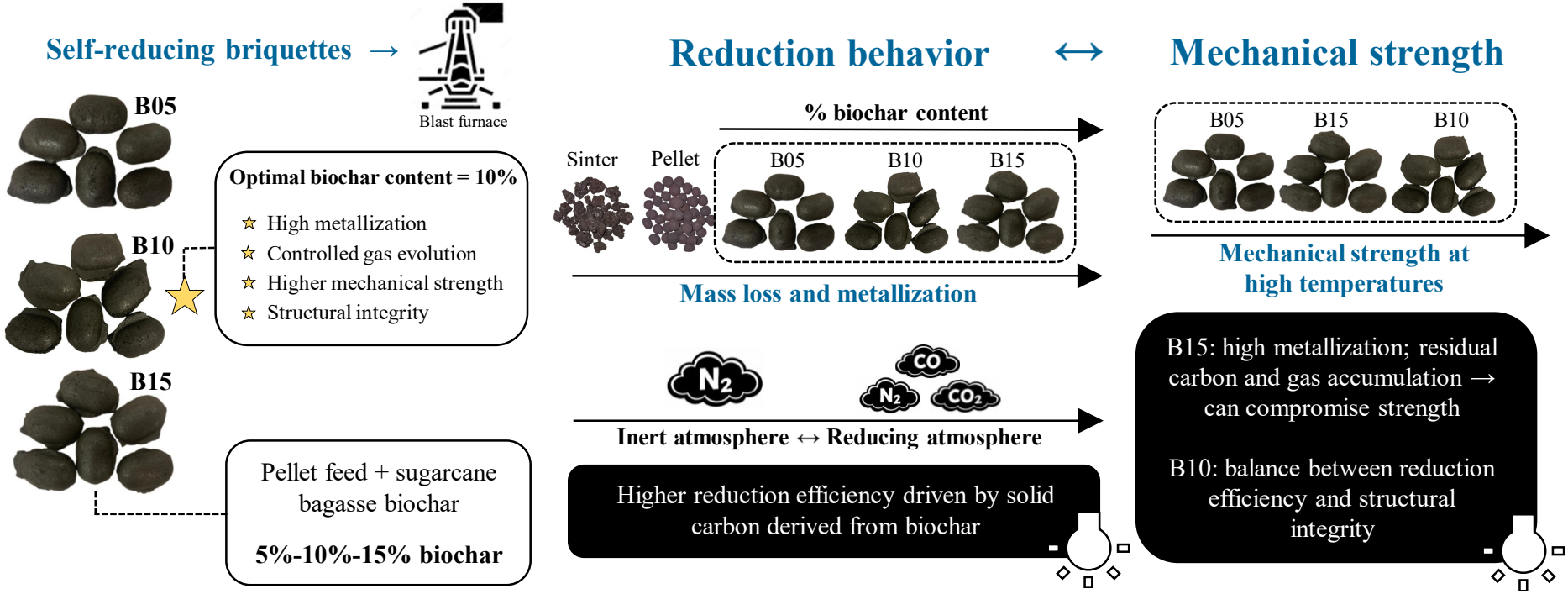

4.1. Introduction

As an energy-intensive sector with high greenhouse gas emissions (GHG), particularly CO_2, the iron and steelmaking industry demands sustainable transformations in its production processes, both to meet global emission-reduction targets and to ensure long-term competitiveness (Fan and Friedmann 2021; Liang et al., 2023). In this context, biomass and its derivatives (biochar), considered renewable and carbon-neutral energy sources (Li S et al., 2022; Wang et al., 2026), can be employed as alternative fuels in steelmaking, enabling the partial substitution of fossil inputs and thereby decreasing carbon emissions (Cao et al., 2023; Chen et al., 2025; Wei et al., 2025). According to Sah and Dutta (2010) and Chai et al. (2024), self-reducing agglomerates enhance the reaction interface between iron oxides and carbon, providing more favorable kinetic conditions for reduction, decreasing energy consumption and emissions in blast furnaces, especially when biomass-based sources are employed.

However, for application in blast furnaces, self-reducing briquettes must meet specific quality requirements related to reduction performance and mechanical strength (Bizhanov and Zagainov 2022; Gandra et al., 2023). In such agglomerates, both the carbon source and its proportion employed in the self-reducing mixture significantly influence their overall performance. As indicated by Chuanchai et al. (2024), the carbon-oxygen (C/O) ratio directly affects the extent of reduction, while excessive use of reducing agents can increase raw material costs. Therefore, the amount of reducing agent added must be sufficient to ensure a high reduction degree of iron oxides (Bagatini et al., 2014) without compromising the physical integrity of the agglomerates.

Several studies have evaluated alternative carbonaceous materials in varying proportions as potential reducing agents in self-reducing briquettes. According to Gandra et al. (2025b), briquettes containing up to 10% petcoke exhibited sufficient mechanical strength for use in small blast furnaces and achieved a higher metallization degree under a reducing atmosphere compared to an inert atmosphere, highlighting the limited participation of petcoke in the reduction reactions. In self-reducing briquettes containing electric arc furnace dust and anthracite, an increased C/O ratio caused a progressive decrease in mechanical strength, with the optimal molar ratio ranging between 1.0 and 1.1 (Wu et al., 2017). Chai et al. (2024) examined the high-temperature behavior of briquettes with treated biomass (waste wood) and

observed that, for high C/O ratios, the briquettes contained excess carbon that was not fully consumed, resulting in low compressive strength at 1200 °C. In a previous study, Leão et al. (2026) investigated the influence of biochar pyrolysis temperature on the performance of self-reducing briquettes produced at a laboratory scale. Although the use of biochar pyrolyzed at 550 °C resulted in a higher metallization degree, briquettes containing biomass treated at 400 °C exhibited greater high-temperature strength, indicating more favorable conditions for blast furnace applications.

However, the development of technologically viable self-reducing briquettes for use in blast furnaces, as well as the identification of the impact of biochar content and the external atmosphere in contact with the briquettes, are critical parameters that must affect both the efficiency of self-reduction and the mechanical strength during heating. In this context, the present study aimed to evaluate the effect of biochar content on the reduction and mechanical strength performance of pilot-scale self-reducing briquettes, subjected to a reducing atmosphere representative of the blast furnace granular zone. The behavior of the briquettes was also investigated under an inert atmosphere to determine the relative contribution of external reducing gases and self-reduction reactions promoted by solid carbon from the biochar, reflecting the reactivity of the reducing agent employed. The tests conducted enabled a comprehensive evaluation of the reduction mechanisms, phase transformations, gas evolution, microstructural features, and mechanical behavior of the briquettes under various heating conditions. A better understanding of the influence of variables related to the addition of reducing agents in these agglomerates allows process optimization in terms of metallurgical and mechanical properties, which can contribute to reducing fuel consumption in blast furnaces and mitigating the environmental impact associated with CO_2 emissions from the steelmaking industry.

4.2. Materials and methods

4.2.1. Raw materials

The briquettes were produced using different proportions of pellet feed and biochar. An ultrafine hematitic ore was employed, with particles predominantly below 75 μm (93%). The corresponding chemical composition, determined using an ARL™ QUANT'X energy-dispersive X-ray fluorescence (EDXRF) spectrometer (Thermo Scientific™), is presented in

Table 4.1. Sugarcane bagasse pyrolyzed at 400 °C was used as the biomass source, with particle sizes ranging from 0.075 to 3.36 mm, of which 92% were within the intermediate range of 0.15 to 2.0 mm. The pyrolysis temperature was defined based on preliminary studies (Leão et al., 2026), and the briquettes that exhibited the best performance were then selected for pilot-scale production. The proximate analysis of the biochar, performed using a LECO TGA 701 thermogravimetric analyzer, is shown in Table 4.2.

Table 4.1. Chemical composition of pellet feed (% by mass).

$Fe_{(T)}$	Fe_2O_3	SiO_2	Al_2O_3	Mn	CaO	TiO_2	P	O_{red}
68.92	94.64	0.93	1.32	0.07	0.06	0.05	0.01	29.62

O_{red}: reducible oxygen

Table 4.2. Proximate analysis of biochar on a dry basis (% by mass).

	Fixed carbon	Volatile matter	Ash
Biochar component content	62.59	28.82	8.59

Mixtures containing 5%, 10%, and 15% by mass of biochar, 10% binders, and pellet feed in complementary proportions were homogenized in an Eirich R08W intensive mixer for 1 min, with the moisture content adjusted to achieve briquetability above 80%. The binder composition included a combination of an organic starch-based and an inorganic aqueous sodium silicate binder in a 1:1 mass ratio. Briquettes were produced using a pilot-scale JReal briquetting press equipped with pillow-shaped cavities and supplied by an ironmaking company. Drying and curing were performed at 95 °C for 45 min. The resulting agglomerates exhibited average dimensions of 31 × 22 × 16 mm and an average mass ranging from 15.8 to 11.9 g per briquette, which decreased with increasing biochar content. Based on the proportions of the raw materials and their chemical compositions, the calculated C/O molar ratios were 0.17, 0.35, and 0.56 for B05, B10, and B15, respectively. Briquettes were identified according to the biochar content of each mixture.

Table 4.3 presents the chemical composition of the as-received briquettes, including the reducible oxygen content calculated from the chemical analysis. Total iron content was determined by wet chemical analysis, while the remaining components were quantified by XRF. Carbon and sulfur contents were measured using a LECO CS230 elemental analyzer. For comparison, conventional iron-bearing materials used in blast furnaces (sinter and iron ore

pellets) were also evaluated. These materials were supplied by an ironmaking company, and their chemical compositions are included in Table 4.3. Figure 4.1 shows a macroscopic view of these agglomerates.

Table 4.3. Chemical composition of the agglomerates evaluated in this study (% by mass).

	$Fe_{(T)}$	SiO_2	Al_2O_3	CaO	MnO	C	S	O_{red}
B05	60.28	11.26	0.73	0.14	0.04	6.09	0.05	25.90
B10	53.30	14.19	0.45	0.19	0.03	11.08	0.07	22.90
B15	50.70	17.10	0,76	0.26	0.04	15.91	0.08	21.79
Sinter	51.21	8.78	2.01	11.46	0.64	N/A	N/A	22.01
Pellets	59.88	8.94	1.52	1.60	0.25	N/A	N/A	25.73

O_{red}: reducible oxygen; N/A: not measured

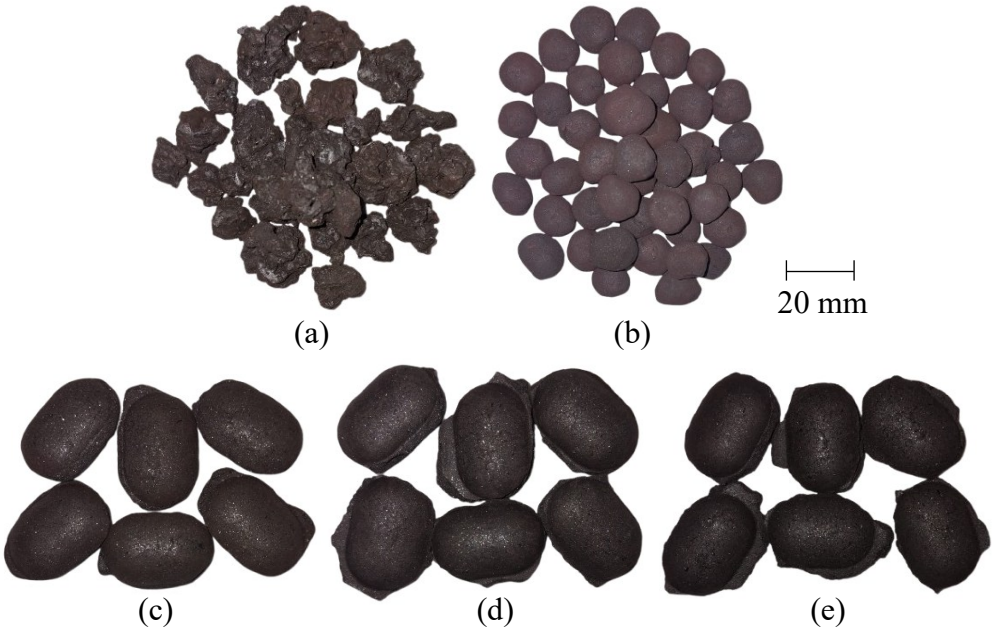

Figure 4.1. Macroscopic view of the agglomerates evaluated in the study: (a) sinter, (b) iron ore pellets, and self-reducing briquettes containing (c) 5% (B05), (d) 10% (B10), and (e) 15% biochar (B15).

4.2.2. Interrupted heating tests

The briquettes were subjected to interrupted tests at different temperatures to evaluate their reduction performance and mechanical strength under conditions representative of a blast furnace shaft. The experimental apparatus (macro-thermobalance) is illustrated in Figure 4.2a and consists of a resistive electric furnace (with molybdenum disilicide ($MoSi_2$) heating elements and a maximum temperature of 1600 °C), an alumina reaction tube with an internal

diameter of 70 mm, and a stainless-steel basket sample holder with a diameter of 40 mm suspended by a Kanthal DS wire (FeCrAl alloy with a diameter of 0.404 mm). Coupled to the furnace, an electronic Shimadzu balance (model UW620H) equipped with an RS232C output enabled real-time acquisition of sample mass, while continuous measurements of CO and CO_2 generation were obtained using a Gasboard 3100 gas analyzer (Cubic-Ruiyi). A type-K thermocouple was used to measure the sample temperature, and digital mass flowmeters were employed to control individual gas flows.

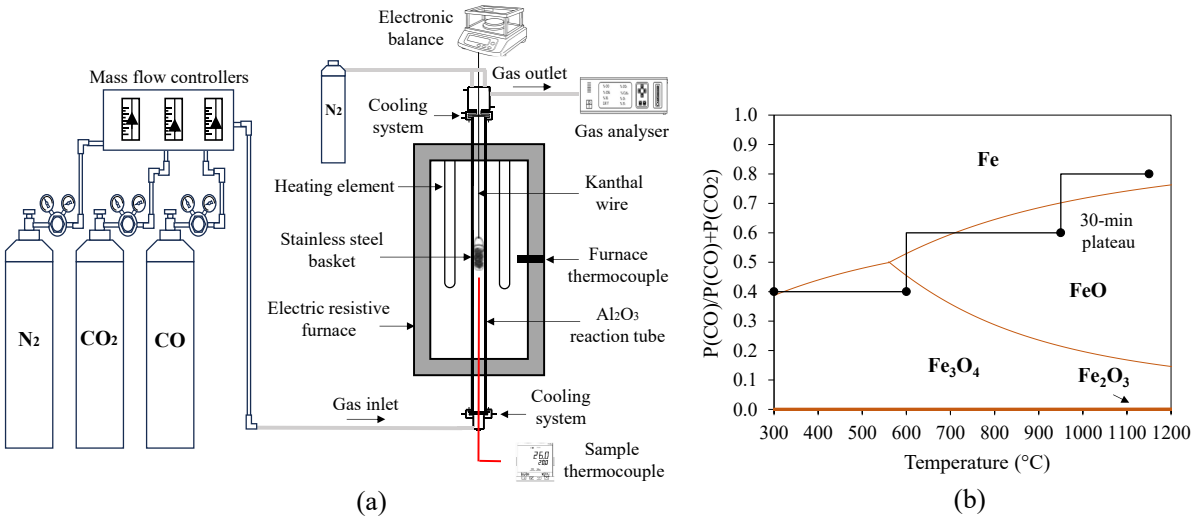

Figure 4.2. (a) Schematic representation of the experimental apparatus used in interrupted heating tests, and (b) temperature and atmosphere conditions of the tests carried out under a reducing atmosphere, projected on the Baur-Glaessner diagram, indicating the reaction path during the experiments.

Batches of six briquettes per test were heated at a rate of 5 °C/min from room temperature up to 600, 950 (after a 30-min isothermal plateau representing the blast furnace thermal reserve zone), and 1150 °C. At each temperature, the tests were interrupted, and the briquettes were rapidly cooled under a N_2 atmosphere (flow rate of 3 L/min) by lifting the sample holder to the upper region of the alumina tube to interrupt the self-reduction reactions. In the reducing atmosphere tests, a gas mixture composed of 60% N_2 and 40% of varying proportions of CO and CO_2 was used, with a total flow rate of 5 L/min. The atmosphere was controlled by mass flow controllers to achieve partial pressure ratios $PCO/(PCO+PCO_2)$ of 0.4, 0.6, and 0.8 in the temperature ranges of 25–600 °C, 600–950 °C, and 950–1150 °C, respectively. Figure 4.2b shows the experimental atmosphere composition and temperature plotted on the Baur-Glaessner

diagram. Similar heating conditions were applied in tests conducted under an inert (N_2) atmosphere; however, a lower gas flow rate of 1.5 L/min was used.

Sinter and pellets were tested under a reducing atmosphere, using the same conditions previously described for the briquettes. The samples were heated to a temperature of 1150 °C at a heating rate of 5 °C/min.

4.2.3. Characterization of self-reducing briquettes

The samples were characterized in terms of chemical composition, mechanical strength, and microstructural analysis in the different stages of heating. X-ray diffraction (XRD) analysis was employed to identify the main phases present in the briquettes after the interrupted tests, providing insights into the reduction behavior of the iron oxides. Measurements were performed on a Philips-PANalytical Empyrean diffractometer, with a scan range of 3–90° (2θ), a step size of 0.06°, and an acquisition time of 2 s per step. The X-ray tube was operated at a tube voltage and current of 35 kV and 35 mA, respectively. Semi-quantitative phase analysis was conducted using the Rietveld refinement method with HighScore Plus software (Malvern Panalytical 4.9).

Chemical analysis was also performed to determine the carbon content using a LECO CS230 carbon and sulfur elemental analyzer, as well as the total iron (Fe_T) and metallic iron (Fe^0) contents by wet chemical analysis. These results were used to calculate the metallization degree of the briquettes at different heating stages, expressed as a mass percentage, according to Equation 4.1.

$$\text{Metallization degree (\%)} = \frac{Fe^0}{Fe_T} \cdot 100 \quad (4.1)$$

For the evaluation of mechanical strength, five briquettes were tested individually under each condition using an IMPAC compression machine (model IP-90ME-5000 N) at a constant cross-head speed of 15 mm/min. Radial tests along the thickness direction were conducted, and the final value was calculated as the average of the results.

Microstructural analysis was performed by scanning electron microscopy (SEM) using a Thermo Fisher APREO 2C microscope, operating with an acceleration voltage of 15 kV and

equipped with secondary electron (ETD) and energy-dispersive X-ray spectroscopy (EDS) detectors. For this characterization, the briquettes were sectioned perpendicular to their longest axis and coated with a thin layer of gold, without any additional surface preparation steps.

4.3. Results and discussion

Figures 4.3 and 4.4 show the visual appearance of the briquettes before and after the interrupted tests conducted under various heating and atmospheric conditions.

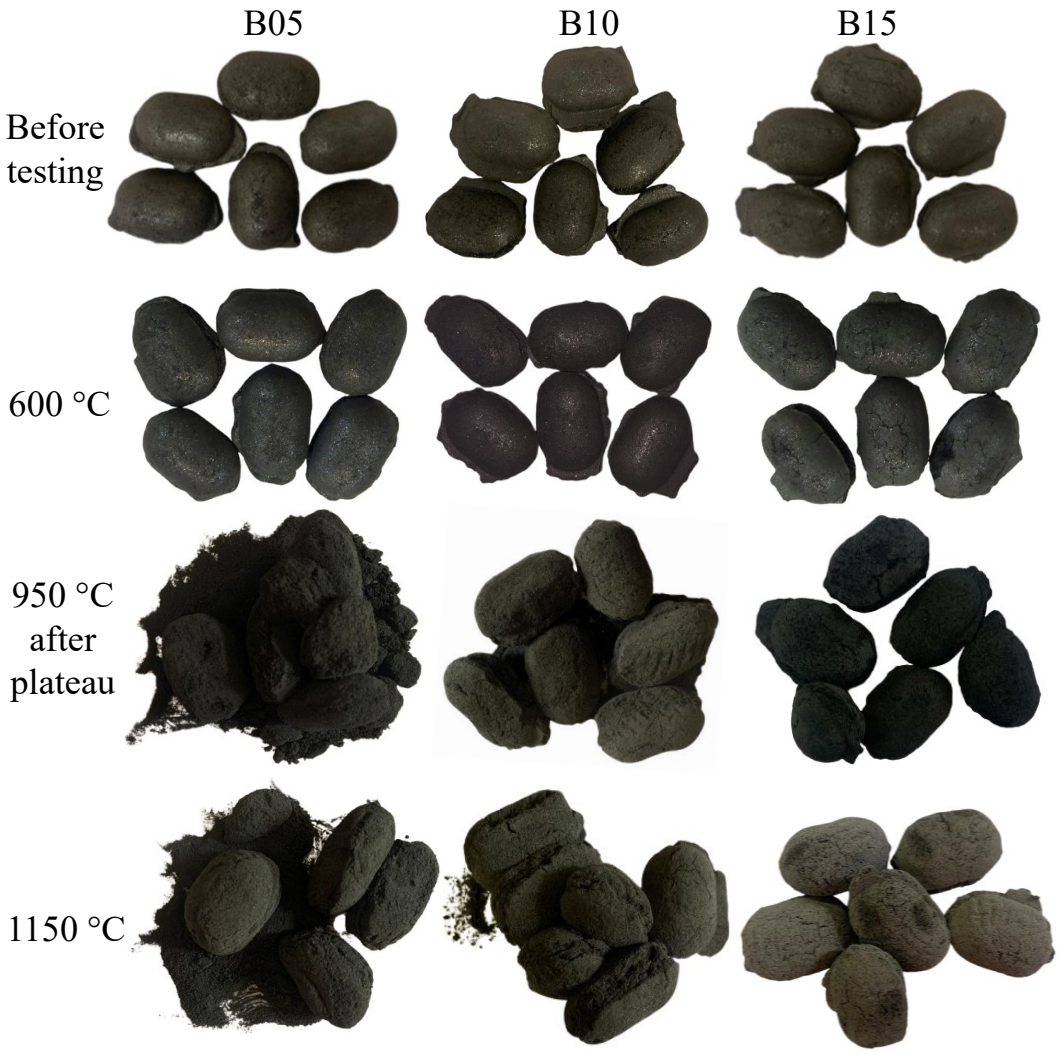

Figure 4.3. External appearance of briquettes with different biochar contents before and after interrupted heating tests conducted under an inert atmosphere at different temperatures.

Figure 4.4. External appearance of briquettes with different biochar contents before and after interrupted heating tests conducted under a reducing atmosphere at different temperatures.

Macroscopic analysis revealed differences in the behavior of briquettes produced with varying proportions of biochar. Briquettes B05 exhibited greater disintegration at high temperatures, particularly at 950 °C after a 30-min isothermal plateau, whereas B10 and B15 maintained higher structural integrity, although crack formation was more pronounced in B15. Furthermore, the atmosphere also influenced the structural behavior of the briquettes. Under an inert atmosphere, increased generation of fines was observed after tests at elevated temperatures, with this effect being more pronounced in samples containing 5% and 10% biochar. In contrast, under a reducing atmosphere, B05 exhibited more intense fragmentation, indicating that, in addition to temperature and composition, the reaction environment can directly affect the structural integrity and macroscopic stability of the briquettes following heating.

4.3.1. Mass loss of self-reducing briquettes

The mass-loss curves of the briquettes under different atmospheric conditions are presented in Figure 4.5. Up to 350 °C, the mass loss can be attributed to dehydration (moisture loss) and the decomposition and volatilization of the organic binder. According to Pigłowska et al. (2020), the thermal decomposition of starch typically occurs between 280 and 350 °C, resulting in molecular breakdown and the release of gases and volatile by-products. In this temperature range, residual volatile matter from biomass pyrolysis may also be released. Overall, a similar behavior was observed among all samples, even under different atmospheres, as this mass loss is not dependent on the external atmosphere.

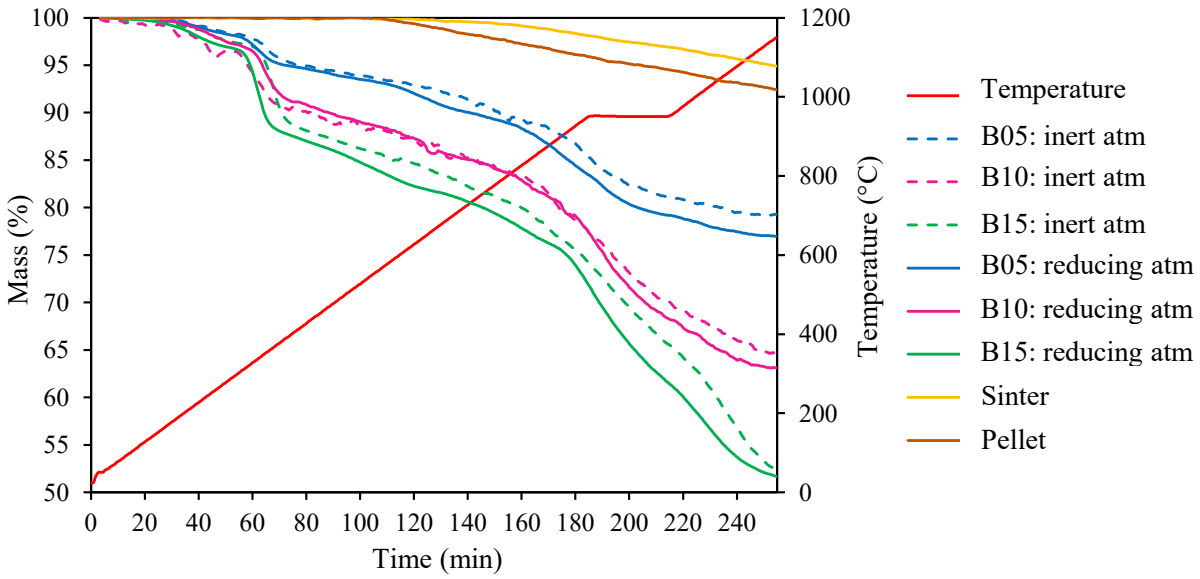

Figure 4.5. Mass loss during heating of briquettes with different biochar contents under inert and reducing atmospheres, together with the mass loss of sinter and pellets under a reducing atmosphere, indicating the influence of the atmosphere on the reduction behavior of the agglomerates.

From 350 °C up to 400 °C, the mass loss of the briquettes increased according to the biochar content, indicating that this step was majorly dominated by the decomposition of volatiles retained in the biochar. From 400 °C onwards, the mass loss progressed at a constant reaction rate with temperature, probably due to the continuous biochar devolatilization, the initial iron oxide reduction due to the volatiles released (Wei et al., 2016), the external gas when reducing atmosphere was applied, and even to the beginning of internal self-reduction reactions.

At high temperatures, particularly above 950 °C, the reaction rate increased considerably, and differences between the briquettes became more pronounced. This behavior may be attributed to the intensified self-reduction reactions occurring within the briquettes, which are favored at high temperatures (Gandra et al., 2023), combined with the effect of an external atmosphere with higher CO partial pressure (Figure 4.2b). At 1150 °C, the results indicated that the higher the biochar content in the briquettes, the greater the final mass loss. This behavior is associated with the higher carbon availability in B15, which promotes CO generation and intensifies the self-reduction reactions, consequently resulting in higher reaction rates within this temperature range. These findings demonstrate that, in addition to the thermal effect, the amount of reducing agent available plays a decisive role in the overall kinetics of the process.

In general, the total mass loss tends to be higher under an atmosphere with CO and CO_2, indicating that the external reducing gases contributed, even if subtly, to the reduction of iron oxides. However, this small difference reflects the dominant influence of self-reduction reactions driven by solid carbon from the biochar. According to Bagatini et al. (2020), both external (gas-phase) and internal (solid-phase) diffusion of the inlet gas can be hindered by the movement of gases generated from internal reactions and by the compact structure of the briquettes.

The burdens traditionally used in the blast furnace were tested under a reducing atmosphere and compared with the briquettes containing different proportions of biochar (Figure 4.5). Pellets and sinter exhibited negligible mass loss at low temperatures due to their essentially inorganic nature and the absence of volatile phases. The iron oxide reduction (gas-solid reactions) becomes kinetically favorable mainly above approximately 600 °C. Nevertheless, even at high temperatures, the mass loss of these agglomerates remained relatively low, indicating that the reduction conditions were insufficient to promote significant oxygen removal from their structures.

4.3.2. Gas analysis of self-reducing briquettes

The data on CO and CO_2 generated during the heating of briquettes in an inert atmosphere are presented in Figure 4.6. From 280 °C onward, gas evolution was associated with the decomposition of the organic binder and the release of residual volatile matter from the biochar

contained in the briquettes. Up to 400 °C, greater devolatilization was observed with increasing biochar proportion, in agreement with the mass loss results (Figure 4.5).

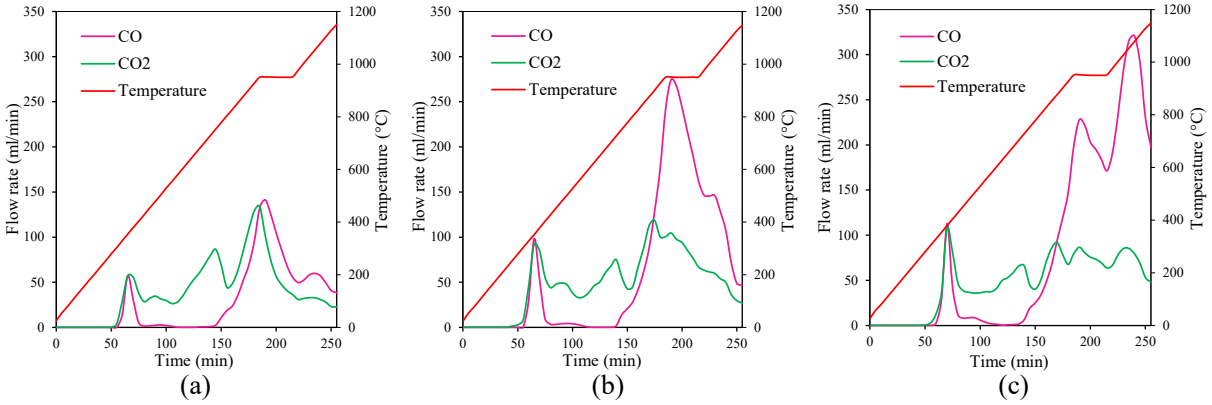

Figure 4.6. CO and CO_2 evolution during heating of self-reducing briquettes under an inert atmosphere: (a) 5% (B05), (b) 10% (B10), and (c) 15% biochar (B15).

From 700 °C onward, the increase in gas generation was mainly associated with carbon gasification (Boudouard) and iron oxide reduction. For all evaluated samples, the flow rate and, consequently, the partial pressure of CO progressively increased up to the isothermal temperature (950 °C), followed by a decrease in CO formation, reflecting the strong temperature dependence of the Boudouard reaction. At the end of the isothermal period and during the subsequent temperature increase, CO formation resumed, especially in briquettes with higher biochar content (B15). In these agglomerates, the CO peaks were more pronounced, likely due to the greater amount of carbon available for regenerative reactions via the Boudouard reaction, thereby intensifying self-reduction. The decrease in CO observed in the curves at higher temperatures can be attributed to the lower availability of carbon, especially in B05 and B10, which have insufficient carbon for self-reduction reactions. Regarding CO_2, its generation follows the CO trend, highlighting the interdependence of self-reduction reactions. For example, in B15, CO_2 continues to be produced due to the intensified self-reduction.

4.3.3. Evolution of mineralogical phases of self-reducing briquettes

Figures 4.7 and 4.8 show the XRD patterns and the phases identified in the briquettes before and after the interrupted tests carried out under inert and reducing atmospheres, respectively, providing a deeper insight into the evolution of iron oxide reduction at different heating stages. Qualitative and semi-quantitative analyses revealed hematite as the only phase detected in all

briquettes in the as-received condition, consistent with the nature of the iron-bearing raw material used in their production. The absence of carbon-related peaks is attributed to the limitations of the XRD technique in detecting amorphous phases, which is characteristic of carbon obtained from low-temperature pyrolysis.

After heating to 600 °C, magnetite peaks were detected, indicating partial reduction of hematite. In both atmospheres evaluated, this reduction may be partially promoted by reactions with volatiles generated during heating, which are released in greater quantities as the biochar proportion increases. Under a reducing atmosphere, the presence of magnetite is consistent with the temperature and gas composition employed up to 600 °C, as projected by the Baur-Glaessner diagram (Figure 4.2b). Under these conditions, a significant increase in the proportion of magnetite was observed, particularly with higher biochar content, likely associated with the higher porosity resulting from the release of volatiles, which enhances the diffusion of the external gas. The reducing potential of these volatile species was confirmed by Bagatini et al. (2021) and Gonçalves et al. (2024), who showed that the gases released during biomass pyrolysis contribute to the reduction of iron oxides (hematite and magnetite) at temperatures below 800 °C.

With increasing temperature, magnetite was gradually reduced, leading to the subsequent formation of wustite and metallic iron. All briquettes exhibited metallic iron at 950 °C (after an isothermal plateau), with its fraction progressively increasing both temperature and biochar content, although B05 showed a predominance of wustite at 1150 °C. This observation is consistent with the mass-loss data, which indicated that briquettes with lower biochar content exhibited slower reaction rates, likely due to the insufficient reducing carbon, thereby limiting self-reduction. In contrast, only metallic iron was detected in B15 at 1150 °C, indicating higher reduction rates and consequently a more advanced reduction process.

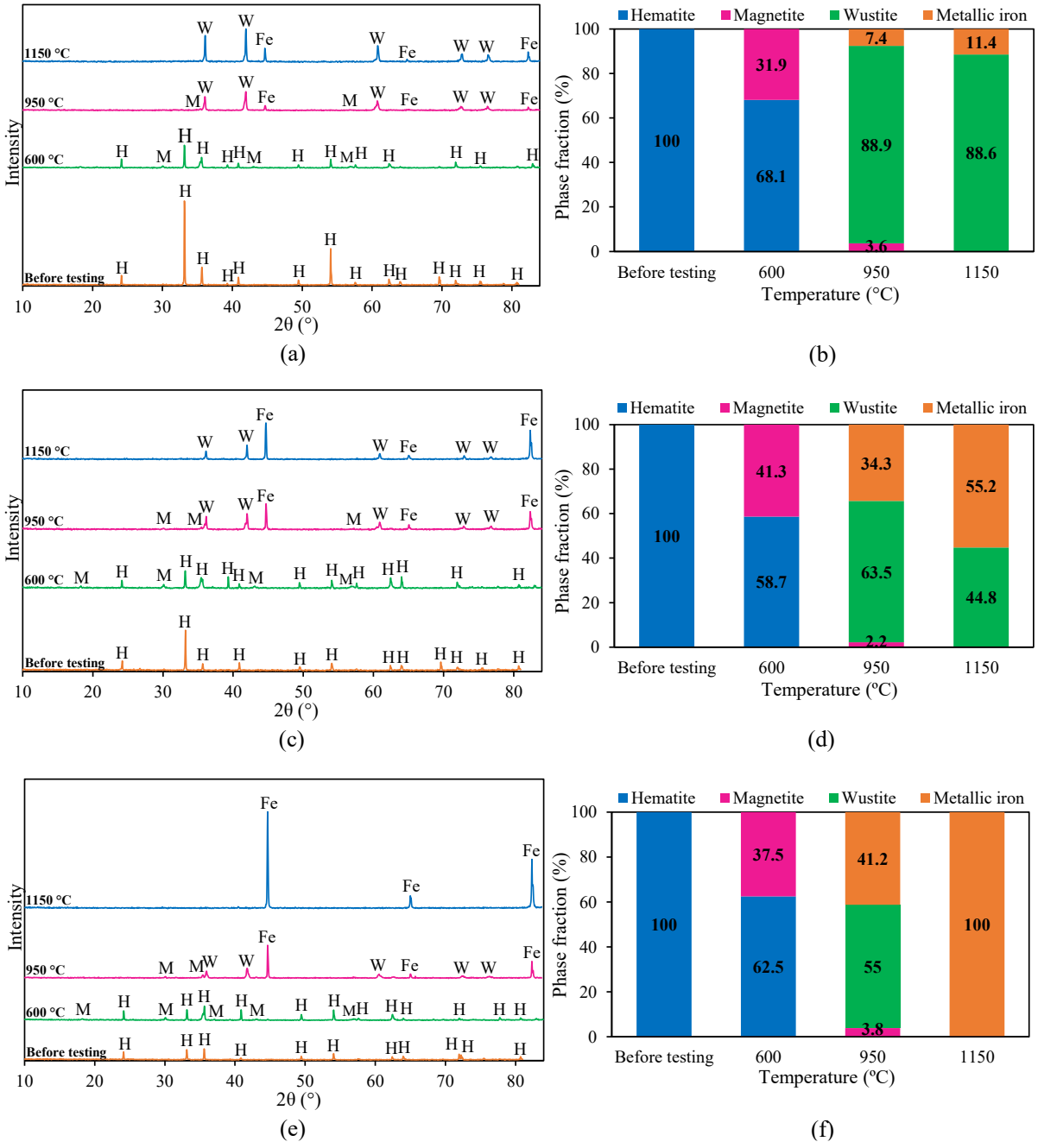

Figure 4.7. X-ray diffraction patterns and phase fractions determined by Rietveld analysis of briquettes containing 5% (B05), 10% (B10), and 15% biochar (B15), shown before and after interrupted heating tests under an inert atmosphere: (a/b) B05, (c/d) B10, and (e/f) B15. H: hematite; M: magnetite; W: wustite; and Fe: metallic iron.

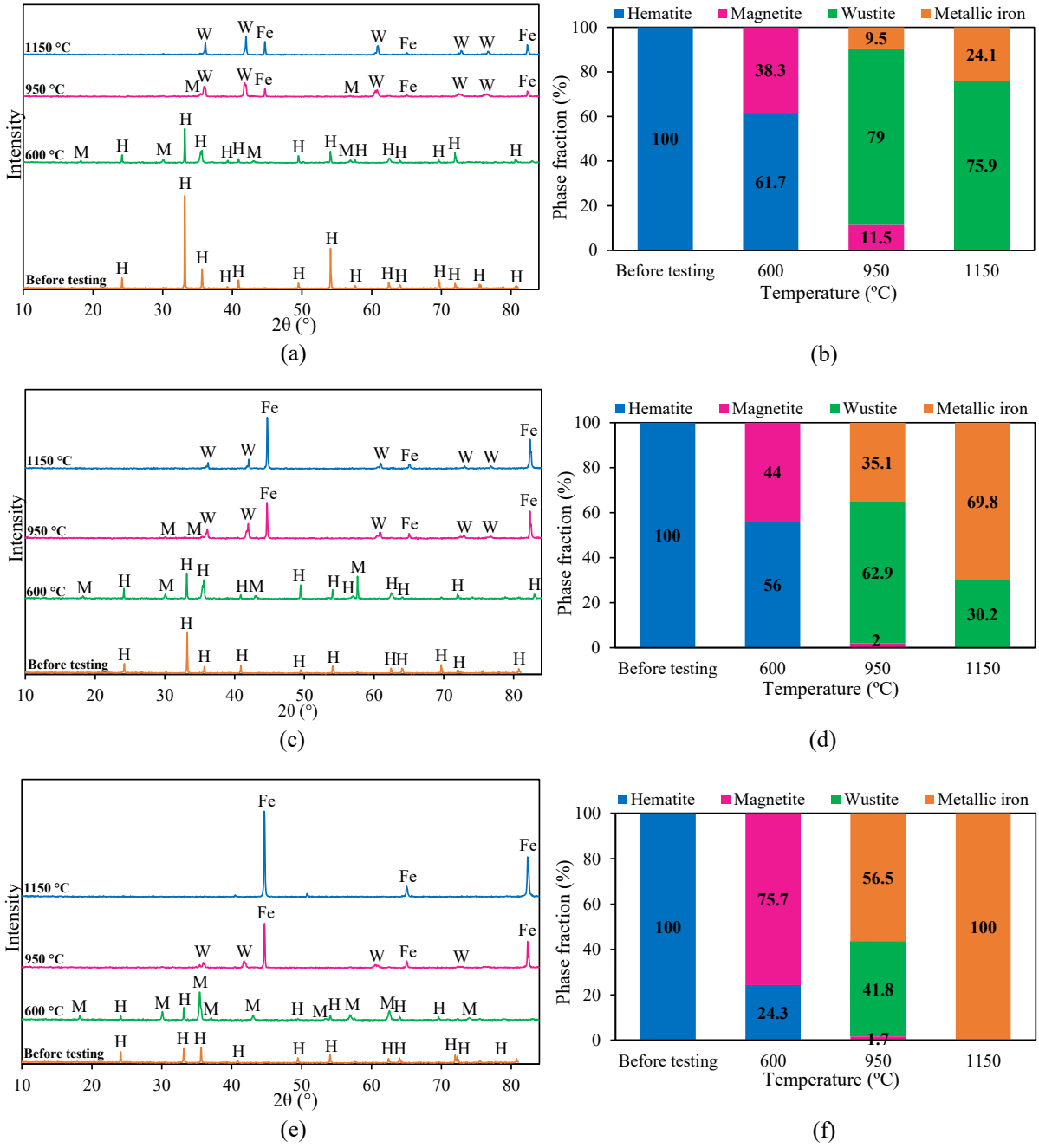

Figure 4.8. X-ray diffraction patterns and phase fractions determined by Rietveld analysis of briquettes containing 5% (B05), 10% (B10), and 15% biochar (B15), shown before and after interrupted heating tests under a reducing atmosphere: (a/b) B05, (c/d) B10, and (e/f) B15. H: hematite; M: magnetite; W: wustite; and Fe: metallic iron.

Under a reducing atmosphere, a more intense reduction was observed under all evaluated conditions. However, at 950 °C, the presence of metallic iron reinforces the role of self-reduction reactions driven by solid carbon from the biochar in enhancing the reduction performance of the iron oxides, as metallic iron is not in equilibrium with the temperature and

atmospheric composition adopted in the experiments (Figure 4.2b). According to Bagatini et al. (2020), the partial pressure of CO inside the briquettes can exceed the external pressure, intensifying the resulting reactions. Thus, the carbon contained in the briquettes contributed significantly to accelerating the reduction even under a reducing atmospheric condition, particularly at higher proportions of the reducing agent.

Figure 4.9 presents the XRD patterns of the sinter and pellets before and after heating at 1150 °C under a reducing atmosphere. Before testing, characteristic peaks of hematite and magnetite were identified in higher proportions in the sinter, along with phases associated with dicalcium silicate and SFCA (silico-ferrite of calcium and aluminum), formed from high-temperature reactions between the individual raw materials: iron ore, coke, and flux (Nicol et al., 2018). In the pellets, hematite was the predominant phase, followed by quartz and magnetite.

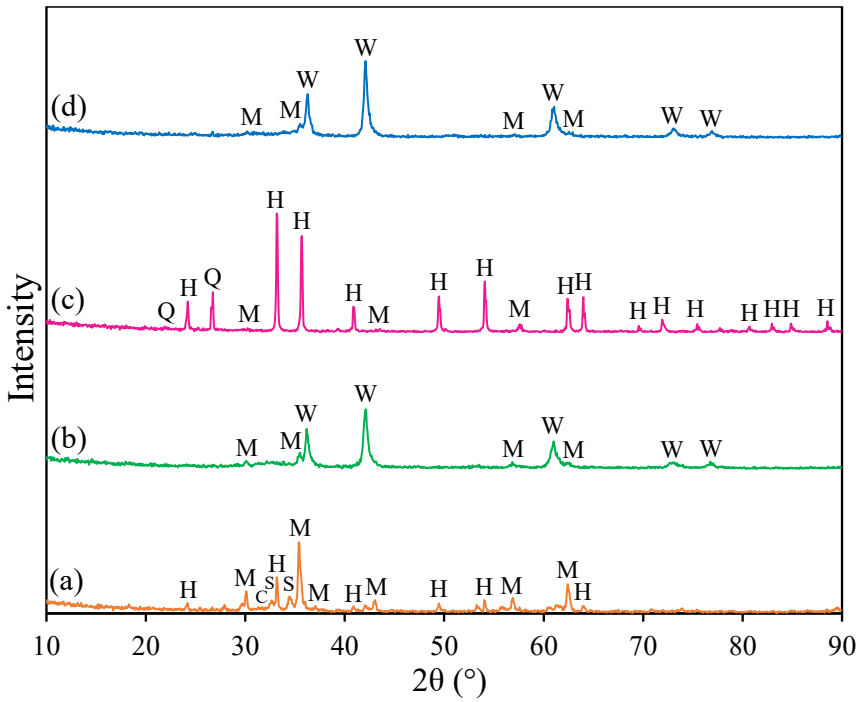

Figure 4.9. X-ray diffraction patterns of (a) sinter and (c) pellets before testing; and (b) sinter and (d) pellets after heating at 1150 °C under a reducing atmosphere. H: hematite; M: magnetite; W: wustite; Q: quartz; C: dicalcium silicate; and S: SFCA.

Under reducing conditions up to 1150 °C, peaks corresponding to magnetite and wustite were detected in both samples. Although the progress of reduction is evident, it remained limited, as

no metallic iron was detected. This behavior contrasts sharply with that observed in the self-reducing briquettes, which exhibited metallic iron formation in all compositions at 1150 °C, including those with the lowest biochar content. This result can be attributed to the reduction promoted by the fixed carbon in the biochar and the generation of pores during heating, which enhances the action of the external reducing agent and leads to more efficient utilization of the reducing gas in self-reducing briquettes. This difference underscores the more efficient reduction kinetics in these briquettes, due to intimate contact with the reducing agent and more favorable diffusion conditions provided by volatile release.

4.3.4. Metallization and carbon content of self-reducing briquettes

Figure 4.10 presents the total iron and carbon contents of the briquettes before and after the interrupted tests, as well as their metallization degrees. The total iron content before the tests was higher in briquettes B05, reflecting the greater proportion of pellet feed in their composition. Figures 4.10a and 4.10b show that this content increased progressively with temperature for all samples, due to the advancement of biochar devolatilization, carbon gasification, and iron oxide reduction reactions, leading to a relative increase in iron concentration. From 950 °C onward, briquettes with higher biochar content exhibited higher total iron values, indicating superior reduction performance at elevated temperatures.

The metallization degree calculated for the briquettes (Figure 4.10c) allowed to observe the fraction of iron converted into metallic iron under different temperature and atmospheric conditions. From 950 °C onward, regardless of the atmosphere used in the tests, both the increase of temperature and the biochar content in the briquettes directly enhanced the metallization, with B15 achieving the highest metallization degree (89.88% and 92.59% at 1150 °C in an inert and reducing atmosphere, respectively). Higher carbon content promotes continuous CO formation and maintains a more reducing atmosphere inside the briquettes, enhancing overall reduction efficiency and thereby increasing metallization. Consequently, improved reduction performance can result in higher operational efficiency and lower fuel consumption in blast furnaces (Gandra et al., 2025b).

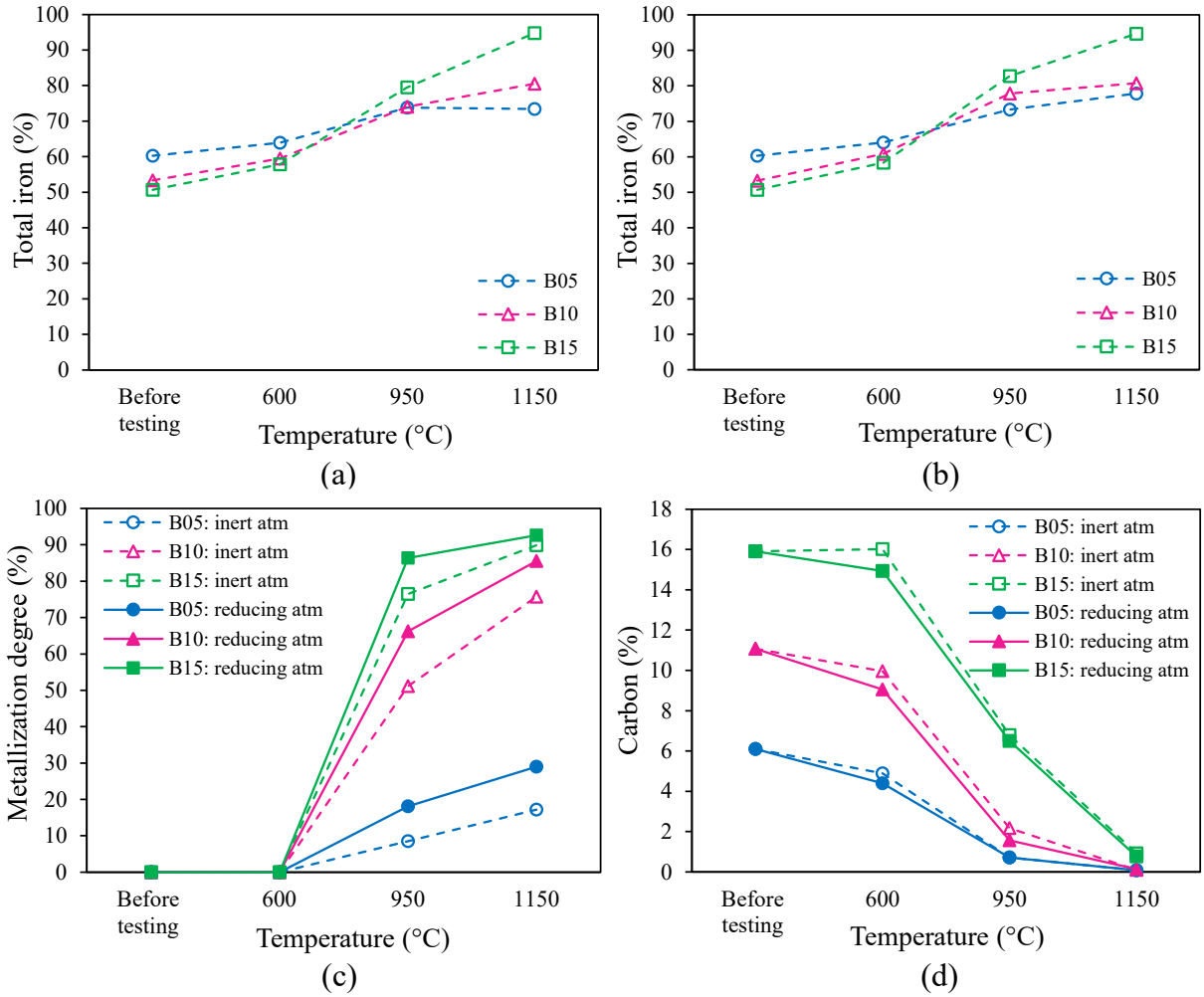

Figure 4.10. Total iron content in briquettes with different biochar contents before and after interrupted heating tests under (a) an inert atmosphere and (b) a reducing atmosphere; (c) metallization degree and (d) carbon content of the briquettes after testing under different atmospheres.

The reducing atmosphere was more effective in promoting metallization compared to the inert atmosphere. Thus, both reducing sources—the inlet gas and the solid carbon—contribute to achieving higher levels of reduction and metallization. This difference was less pronounced for B15 at 1150 °C, likely because the carbon content in the agglomerates was sufficient for advanced reduction at these conditions, regardless of the atmosphere employed. These findings highlight the interplay between the C/O molar ratio and the surrounding atmosphere, suggesting that even in systems with an additional supply of reducing gas, such as the blast furnace, a stoichiometric C/O molar ratio of 1, theoretically required for total reduction, may not be strictly necessary to achieve high metallization degrees.

The analysis of the carbon content in the briquettes (Figure 4.10d) showed that the initial carbon content was proportional to the amount of biochar added to the briquettes. As the temperature increased, carbon levels decreased, particularly above 600 °C, due to the progressive consumption of carbon during gasification. At 1150 °C, minimal carbon contents (< 0.1%) were identified in the briquettes containing 5% and 10% biochar, corroborating previous results that indicated complete reduction of these samples was limited by carbon availability. When the carbon content in the agglomerate is insufficient, self-reduction reactions cannot be sustained throughout the thermal process, reducing the conversion of iron oxides into metallic iron. Moreover, lower residual carbon contents were observed under a reducing atmosphere, reflecting the greater carbon consumption due to CO_2 generated from internal self-reduction reactions and from CO_2 from the external atmosphere, both through the Boudouard reaction.

In summary, the combined results enabled a detailed evaluation of the reducing performance of the briquettes with varying biochar contents under different atmospheric conditions, highlighting the superior reduction efficiency of briquettes with higher biochar content (B15). Compared to self-reducing agglomerates reported in the literature, this study demonstrated the high reactivity of the carbon source used, which significantly influenced the reduction of the briquettes due to the greater efficiency of carbon from the biochar in intimate contact with the iron oxides, even compared to the external reducing atmosphere. Self-reducing briquettes composed of iron ore and 10% petcoke, evaluated by Gandra et al. (2025a), achieved a metallization degree of 22.7% after heating to 900 °C under a reducing atmosphere, in contrast to 4.1% under an inert atmosphere. These results indicate that petcoke does not directly participate in reduction and that the atmosphere had a greater impact on reduction performance than the solid carbon content in the briquettes. Under temperature and atmospheric conditions similar to those of the present work, Bagatini et al. (2020) observed that briquettes produced with mill scale and blast furnace dust with a C/O mass ratio of 0.5 reached approximately 75% metallization at 1100 °C, resulting from the simultaneous action of reducing gas and solid carbon. In another study, Kowitwarangkul et al. (2014) evaluated self-reducing pellets containing different carbonaceous materials through non-isothermal tests at 1200°C under a reducing atmosphere, reporting metallization degrees of 79%, 80%, and 89% for agglomerates with 18% by mass of coal, charcoal, and coke, respectively, compared to 10% in conventional pellets. Collectively, these studies highlight the intensification of reduction reactions provided by the incorporated carbon.

4.3.5. Mechanical strength of self-reducing briquettes

The compressive strength of the briquettes after heating at different temperatures and atmospheres is presented in Figure 4.11, along with the corresponding standard deviations. In the as-received condition, increasing the biochar content led to a decrease in briquettes' strength, consistent with previous studies (Yokoyama et al., 2012; Wu et al., 2017; Gandra et al., 2025b), reaching values of 1321.8 N, 1006.2 N, and 854.6 N for B05, B10, and B15, respectively. This behavior can be attributed to structural, cohesive, and interparticle interaction factors within the briquette matrix. Higher biochar content results in a more porous and less dense structure due to the intrinsic characteristics of this material, which can reduce the mechanical strength of the agglomerates (Pascoal et al., 2022).

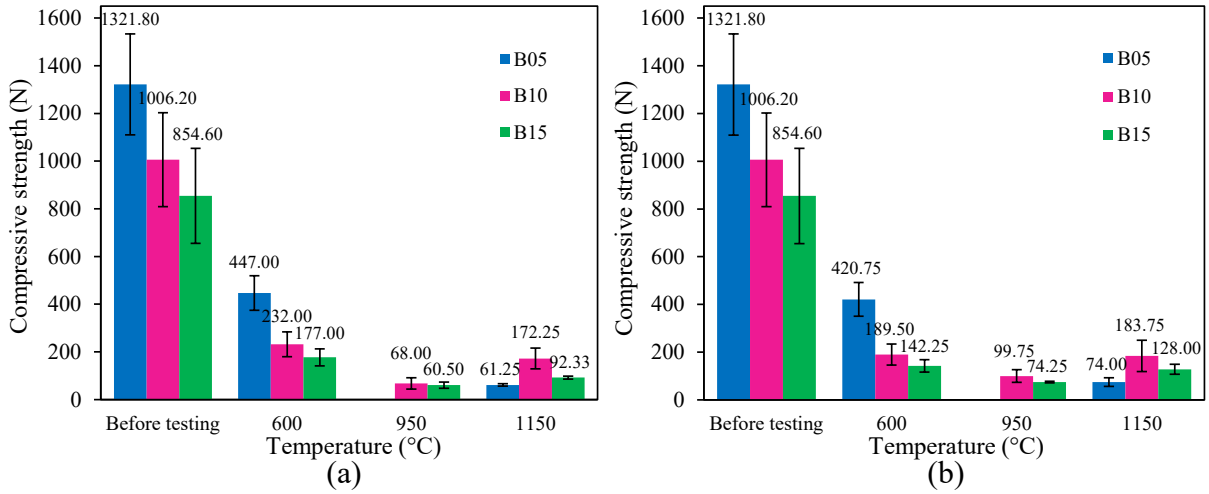

Figure 4.11. Compressive strength of briquettes with different biochar contents before and after interrupted heating tests under (a) an inert atmosphere and (b) a reducing atmosphere. Standard deviations are presented numerically above each bar and were calculated from the results obtained for multiple briquettes tested.

Although there is no established standard for the minimum required strength of briquettes in industrial applications, the literature provides reference values considered adequate to ensure physical integrity during handling, transportation, charging, and operation stages (Flores et al., 2025). According to Li et al. (2022b), cold-bonded briquettes with compressive strength above 2000 N are suitable for blast furnace use. Gandra et al. (2025b), in turn, adopted a reference value of 1600 N—originally established for iron ore pellets transported over long distances—when evaluating self-reducing briquettes containing petroleum coke. However, depending on

the fraction of briquettes used in the burden and for an on-site application in small blast furnaces (internal volume < 1000 m^3), the minimum compressive strength value may be reassessed according to the specific operational constraints of each reactor. The briquettes analyzed by these authors exhibited compressive strengths ranging from 210 N to 750 N for compositions containing 5–15% petcoke. In small blast furnaces, lower mechanical requirements may be acceptable (Kowitwarangkul et al., 2014). Additionally, Yokoyama et al. (2012) indicate that, in blast furnaces operating at lower charging rates, strength values around 1000 N may be sufficient. In the present study, the briquettes exhibited average compressive strength between 854 N and 1322 N before heating, which, although lower than some literature limits, are close to ranges typically observed for similar feedstocks. For comparison, Kowitwarangkul et al. (2014) reported that pellets containing 10% by mass of coal, charcoal, and coke achieved strengths of 590 N, 520 N, and 970 N, respectively, after hydration and curing.

The compressive strength of the briquettes showed a strong correlation with the extent of mass loss. In both atmospheres, increasing the temperature up to 600 °C resulted in a pronounced decrease in strength, likely associated with binder decomposition and biochar devolatilization. For all briquette compositions and atmospheric conditions, the lowest strength was observed at 950 °C after an isothermal plateau, possibly due to intense carbon gasification and reduction reactions occurring in this temperature range, as proved by the chemical analysis of the briquettes. The release of volatiles and gaseous intermediates during self-reducing reactions increases internal pressure within the briquettes, enhancing crack formation and porosity, consequently decreasing the mechanical strength (Bagatini et al., 2020; Ye et al., 2023). However, at 1150 °C, the briquettes increased their strength, which must be associated with the increased formation of metallic iron and sintering (Takano and Mourão, 2003; Chai et al., 2024), which favors particle coalescence and results in a denser and more cohesive structure.

At high temperatures, B05 exhibited the lowest strength due to the limited formation of metallic iron, which restricts particle sintering. This effect was even more pronounced after heating to 950 °C, when the extremely fragile structure prevented compressive strength measurement. On the other hand, at 1150 °C, despite the higher metallization degree of B15 resulting from intensified reduction, the composition with 10% biochar achieved the highest mechanical strength among the agglomerates. This superior performance can be attributed to the combined influence of gas release during heating and metallic iron formation, processes that occur

differently among the briquettes depending on the biochar content. At high temperatures, the positive impact of the reducing atmosphere on the mechanical strength of the briquettes was also observed, as it promoted reduction progress and, consequently, enhanced metallic iron formation, resulting in higher mechanical strength. This effect was more pronounced in B15, likely due to the consumption of excess carbon by the CO_2 in the atmosphere.

In B10, a substantial reduction of oxides to metallic iron was observed, accompanied by a decrease in the gas flow generated during heating (Figure 4.6b). These agglomerates are capable of effectively reducing the oxides and forming metallic iron, which reinforces the briquette matrix, but without producing the excessive internal pressure observed in B15. In briquettes with higher biochar content, intense gas generation and its release, evidenced by the pronounced CO peaks in Figure 4.6c, can compromise structural integrity, as the accumulation of internal pressure and the resulting porosity tend to reduce strength. Birol and Saridede (2013) and Chai et al. (2024) also reported that unreacted carbon can hinder the interconnection between metallic iron particles, leading to a significant decrease in mechanical strength. In the latter study, briquettes with a higher C/O ratio contained residual carbon, resulting in the formation of a granular metallic iron phase with insufficient bonding, which remained surrounded by a large amount of residual carbon after reduction. Thus, the mechanical strength of the briquettes at high temperatures is strongly dependent on the balance between metallic iron formation, which promotes sintering, and controlled gas release. This behavior suggests the existence of an optimal biomass content, determined by the balance between reduction efficiency and structural integrity of the briquettes.

The literature also reports changes in mechanical strength after heating, characterized by an initial decline followed by recovery at higher temperatures. Man-sheng et al. (2011), when analyzing carbon composite iron ore hot briquettes under simulated blast furnace heating conditions, observed a reduction in strength up to 800 °C (around 500 N), followed by an increase at higher temperatures. Similarly, Leão et al. (2026) evaluated self-reducing briquettes containing biomass pyrolyzed at different temperatures and identified minimum strength values around 950 °C. According to Kowitwarangkul et al. (2014), the strength of self-reducing agglomerates depends not only on the heating temperature but also on the type and fraction of the incorporated carbonaceous material. The authors reported values of approximately 220 N, 190 N, and 390 N for pellets containing 18% by mass of coal, charcoal, and coke, respectively,

after reduction at 1000 °C. Chai et al. (2024) also observed a decrease in compressive strength after reduction between 900 and 1000 °C in briquettes containing residual wood. Agglomerates with a C/O molar ratio of 0.8 exhibited a minimum strength of 544 N (a reduction of 72.8% relative to their initial values), whereas a ratio of 0.5 resulted in a compressive strength of 437 N after heating at 900 °C, with a considerable increase at 1200 °C. In the present study, the low strength values obtained after high-temperature heating (60–184 N) are slightly lower than those reported in the literature.

4.3.6. Microstructural analysis of self-reducing briquettes

The briquettes containing 10% and 15% biochar, which maintained their physical integrity during heating, were subjected to microstructural investigation after reduction tests carried out at 950 and 1150 °C under a reducing atmosphere (Figure 4.12). This analysis aimed to identify the morphological evolution and microstructural transformations occurring in the agglomerates at high temperatures. Semi-quantitative analysis by SEM-EDS allowed the identification of three distinct phases: biochar (point A), composed predominantly of carbon and oxygen, and characterized by larger particles with mainly fibrous morphology; metallic iron (point B), exhibiting iron contents above 93%, indicating the progress of the reduction reactions; and wustite (point C), associated with a denser structure. As the temperature increased, the microstructure of the briquettes showed higher porosity, reflecting the advancement of the reduction reactions and the intensification of diffusion processes.

The micrographs of B10 and B15 at 950 °C revealed a heterogeneous microstructure composed of multiple phases and distinct morphologies. In both samples, but more pronounced in B15, elongated and fibrous biochar fragments that had not yet reacted during heating were observed, partially preserving the original morphology of the lignocellulosic material, suggesting incomplete consumption of the solid reducing agent at this temperature. Furthermore, wustite particles were distributed throughout the matrix, often in contact with metallic iron, indicating that part of the briquettes remained in an intermediate reduction state. Overall, the coexistence of these phases confirms the progressive nature of the reduction in self-reducing briquettes at 950 °C and highlights its influence on the microstructure of the agglomerates.

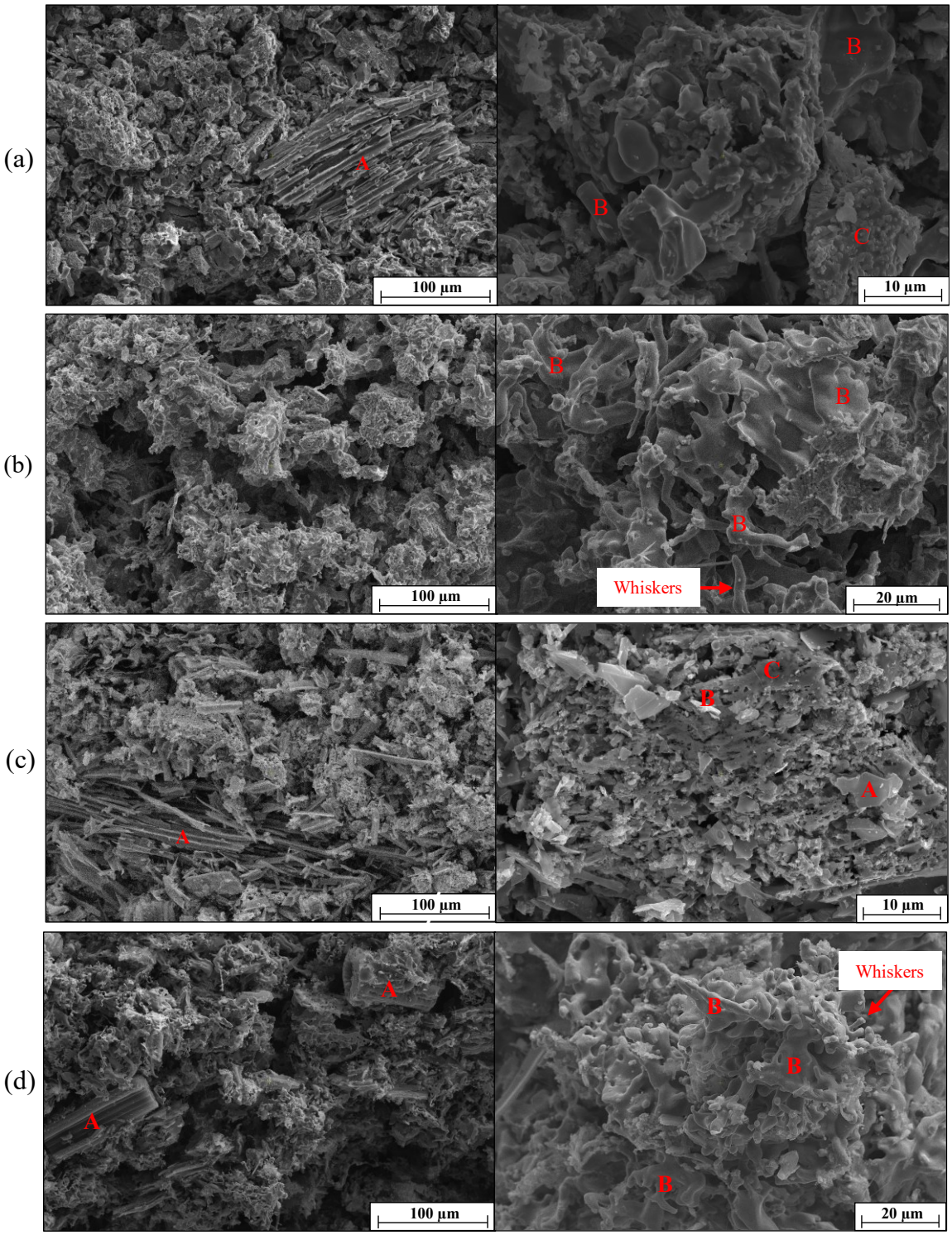

Figure 4.12. SEM microstructures of briquettes containing 10% (B10) and 15% biochar (B15) after heating under a reducing atmosphere to (a/c) 950 °C and (b/d) 1150 °C: (a/b) B10 and (c/d) B15. A: biochar; B: metallic iron; and C: wustite.

Comparison with briquettes tested at 1150 °C revealed a significant evolution of the microstructure relative to the samples treated at 950 °C, with notable differences in the ferrous

phase detected. In general, the briquettes exhibited a more homogeneous microstructure, characteristic of an advanced reduction stage, with fewer residual biochar particles, a higher fraction of regions corresponding to metallic iron, and an intensified sintering phenomenon. The metallic iron particles displayed more coalesced morphologies, forming larger continuous regions, in addition to the presence of filamentous structures typical of whisker formation, indicative of preferential growth under conditions of high reducing activity and enhanced surface mobility. These features further corroborate the progress of the reduction reactions and the microstructural evolution associated with higher temperatures. In B15 (Figure 4.12d), the persistence of biochar fragments indicates that part of the organic material was not fully consumed during heating at 1150 °C, although these briquettes achieved the highest reduction degree, reflecting the excess of the solid reducing agent, as evidenced by the carbon analysis. Additionally, the presence of residual biochar may have contributed to the higher porosity observed in B15 compared to B10.

The chemical map shown in Figure 4.13 illustrates the distribution of key elements in the briquette containing 15% biochar after reduction at 1150 °C in two distinct regions of the briquette (core and surface), corroborating the presence of biochar particles and iron-rich phases. The analysis was motivated by the observation of a radial color gradient at the macroscopic scale, suggesting different reduction degrees. The surface layer exhibited a lighter color compared to the inner regions, indicating higher metallization and mechanical strength, as evidenced by its lower friability during handling.

In the images, the central region of the briquette exhibited well-defined biochar particles characterized by high carbon contents, along with iron distributed throughout the analyzed area, predominantly in metallic form, and higher porosity. In contrast, the surface region showed a more homogeneous microstructure, with a higher fraction of identified iron and particle coalescence, as well as the absence of features associated with residual biochar, demonstrating that the briquette surface achieved a higher reduction degree than the core. Even though it is a self-reducing briquette, reduction tends to occur from the exterior toward the interior due to heat transfer, which is more intense at the surface. Since the Boudouard reaction is highly dependent on temperature, the briquette surface heats up more rapidly upon receiving heat from the external environment, allowing the available thermal energy to promote faster reduction reactions in this region. In contrast, heat transport toward the core of the particle is slower,

delaying carbon (biochar) consumption and resulting in thermal and reaction gradients across the briquette cross-section. These results corroborate the macroscopic observations and highlight significant differences in morphology and reduction behavior between the core and surface of the agglomerate.

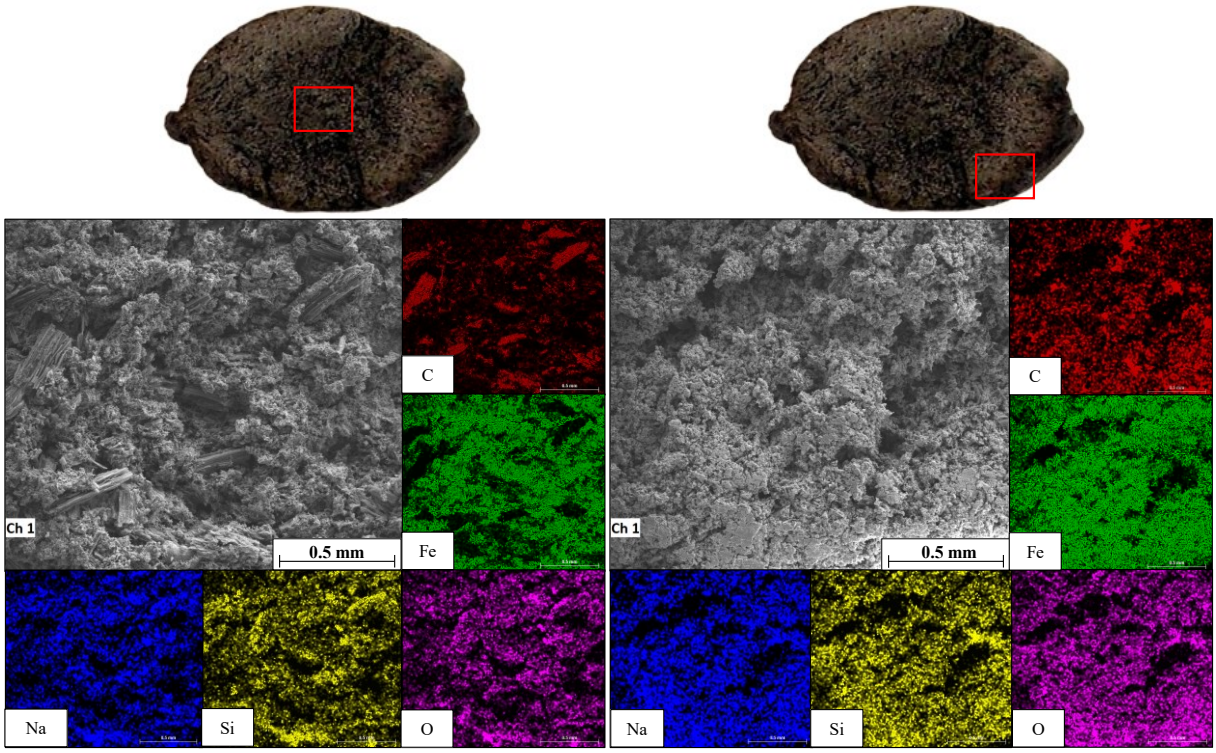

(a) (b)

Figure 4.13. EDS elemental mapping of a briquette containing 15% biochar (B15) after interrupted heating tests at 1150 °C under a reducing atmosphere: (a) core region and (b) surface region of the briquette.

4.4. Conclusions

In this study, self-reducing briquettes containing 5–15% biochar were evaluated for their reduction behavior and mechanical strength under different heating stages and atmospheres. The results indicated that the biochar content significantly influences briquette performance, affecting both self-reduction efficiency and physical integrity during heating.

A greater mass loss was observed in the briquettes with higher biochar content (B15). Although the presence of a reducing atmosphere caused a slight increase in mass loss, highlighting its contribution to the reduction of iron oxides and the consumption of reactants, this effect

remained minor, especially at low temperatures. The gas analysis corroborated the mass loss results and emphasized the interdependence of the self-reduction reactions. Gas evolution was associated with the decomposition of the organic binder and the biochar content in the briquettes, reflecting the influence of volatile matter and fixed carbon.

Under the evaluated conditions, all briquettes exhibited metallic iron at 950 °C, demonstrating high reduction efficiency in the blast furnace preparation zone, with the iron fraction progressively increasing with temperature and biochar content. XRD analysis identified only metallic iron in B15 at 1150 °C, reflecting a more advanced reduction process and greater carbon availability. These briquettes achieved the highest metallization degree, with values substantially higher than those of B05 (a difference of 63.63% at 1150 °C in a reducing atmosphere), confirming the essential role of solid carbon as a reducing agent. Carbon content decreased with increasing temperature, becoming practically negligible in B05 and B10 at 1150 °C, indicating that the reduction of these briquettes was limited by carbon availability. Compared with the conventional burdens used in blast furnaces (sinter and pellets), the briquettes exhibited greater mass loss and higher reduction performance.

The reducing atmosphere enhanced the reduction process, which can be attributed to the synergistic effect of the external gases and the internal self-reduction reactions, as well as to the increased porosity resulting from volatile release, which facilitates the diffusion of external gases. However, even under an inert atmosphere, high metallization was observed in B10 and B15, with differences of less than 10% and 3%, respectively, at 1150 °C. This behavior, associated with the mass loss of the briquettes, highlights the predominant action of self-reduction reactions promoted by the solid carbon derived from the biomass. Overall, the carbon incorporated into the briquettes is more effective than the external atmosphere due to its intimate contact with the iron oxides inside the briquettes, emphasizing the high reactivity of the biomass employed.

In the as-received condition, increasing the biochar content compromised the briquettes' strength. They exhibited average compressive strength values ranging from 854 N to 1322 N, which, although lower than some of the limits reported in the literature for blast furnace applications, fall within the typical ranges observed for similar agglomerates. After heating, the strength decreased up to 950 °C and subsequently increased at 1150 °C, a condition under which

the briquettes containing 10% biochar showed the best high-temperature mechanical performance. B10 experienced substantial formation of metallic iron, without generating excessive internal pressure resulting from gas generation, as observed in B15. The lower strength observed in B05 and B15 is linked, respectively, to low metallization and to both residual carbon and gas accumulation in the briquettes. SEM analysis revealed the progression of reduction in the briquettes at high temperatures, and also indicated the excess of reducing agent in B15, as further confirmed by carbon analysis. These results suggest the existence of an optimal biochar content of 10%, which maximizes mechanical performance, allowing reduction to proceed efficiently without compromising the structural integrity of the briquettes.

Acknowledgments

The authors acknowledge CAPES-PROEX and CNPq for their financial support of this work, as well as the Granioter/Nuclear Technology Development Center (CDTN/CNEN) for their assistance in conducting this study. The authors also thank the Center of Microscopy at the Federal University of Minas Gerais (UFMG) for providing the equipment and technical support for the experiments involving electron microscopy.

4.5. References

Bagatini MC, Fernandes T, Silva R, Galvão DF, Flores IV. 2020. Mill scale and flue dust briquettes as alternative burden to low height blast furnaces. J Clean Prod. 276:124332. https://doi.org/10.1016/j.jclepro.2020.124332.

Bagatini MC, Kan T, Evans TJ, Strezov V. 2021. Iron ore reduction by biomass volatiles. J Sustain Metall. 7:215–226. https://doi.org/10.1007/s40831-021-00337-3.

Bagatini MC, Zymla V, Osório E, Vilela ACF. 2014. Carbon gasification in self-reducing mixtures. ISIJ Int. 54(12):2687–2696. https://doi.org/10.2355/isijinternational.54.2687.

Birol B, Saridede MN. 2013. The effect of reduction parameters on iron nugget production from composite pellets. Miner Process Extr Metall Rev. 34(4):195–201. https://doi.org/10.1080/08827508.2012.695305.

Bizhanov AM, Zagainov SA. 2022. Use of ore-coal briquettes in blast furnaces. Metallurgist. 66(7–8):749–756. https://doi.org/10.1007/s11015-022-01385-0.

Cao Z et al. 2023. Insights into direct reduction iron using bamboo biomass as a green and renewable reducer: Reduction behavior study and kinetics analysis. Sci Total Environ. 880:163393. https://doi.org/10.1016/j.scitotenv.2023.163393.

Chai Y et al. 2024. Study on strength and reduction characteristics of iron ore powder-green carbon composite briquettes. Fuel. 377:132741. https://doi.org/10.1016/j.fuel.2024.132741.

Chen M et al. 2025. When crop straw meets CO_2-intensive process industries in China: The potential of CO_2 mitigation and techno-economic analysis. Biomass Bioenergy. 196:107755. https://doi.org/10.1016/j.biombioe.2025.107755.

Chuanchai A, Wu KT, Chen IG, Liu SH. 2024. Iron ore reduction using agricultural waste biochar with different carbon to oxygen ratios. J Taiwan Inst Chem Eng. 162:105573. https://doi.org/10.1016/j.jtice.2024.105573.

Fan Z, Friedmann SJ. 2021. Low-carbon production of iron and steel: Technology options, economic assessment, and policy. Joule. 5(4):829–862. https://doi.org/10.1016/j.joule.2021.02.018.

Flores IV, Leão PMGC, Alves JVS, Assis OHM, Bagatini MC. 2025. Reduction, softening, and melting characteristics of mill scale-based briquettes for blast furnace ironmaking. Steel Res Int. https://doi.org/10.1002/srin.202500921.

Gandra BF, Oliveira AFL, Bagatini MC, Osório E. 2025a. Atmosphere effect on the reducing behavior of iron ore-petcoke briquettes. J Sustain Metall. 11:2590–2605. https://doi.org/10.1007/s40831-025-01135-x.

Gandra BF, Oliveira AFL, Bagatini MC, Osório E. 2025b. Iron ore petcoke briquettes as complementary burden for blast furnaces. J Mater Res Technol. 35:1556–1564. https://doi.org/10.1016/j.jmrt.2025.01.123.

Gandra BF, Paula Junior GE, Bagatini MC, Osório E. 2023. Analysis of self-reducing composites with different iron ore-carbon ratio. J Mater Res Technol. 26:6433–6445. https://doi.org/10.1016/j.jmrt.2023.08.289.

Gonçalves MVB, Mendonça LM, Vemdrame Flores I. 2024. Investigation of the phenomena associated with iron ore reduction by raw biomass and charcoal volatiles. J Sustain Metall. 10:1094–1111. https://doi.org/10.1007/s40831-024-00851-0.

Kowitwarangkul P, Babich A, Senk D. 2014. Reduction behavior of self-reducing pellet (SRP) for low height blast furnace. Steel Res Int. 85(11):1501–1509. https://doi.org/10.1002/srin.201300399.

Leão PMGC, Ardisson JD, Zicker TB, Bagatini MC, Ferreira NHA. 2026. Influence of biomass pyrolysis temperature on the performance of self-reducing briquettes for use in blast furnaces. Biomass Bioenergy. 206:108691. https://doi.org/10.1016/j.biombioe.2025.108691.

Liang W et al. 2023. Life cycle assessment of blast furnace ironmaking processes: A comparison of fossil fuels and biomass hydrochar applications. Fuel. 345:128138. https://doi.org/10.1016/j.fuel.2023.128138.

Li S, Li J, Chen H, Xu J. 2022. Understanding the release behavior of biomass model components and coal in the co-pyrolysis process. J Energy Inst. 101:122–130. https://doi.org/10.1016/j.joei.2022.01.003.

Li Y et al. 2022. Study on properties of cold-bonded briquettes prepared from return fines of sinter. Steel Res Int. 93:2200304. https://doi.org/10.1002/srin.202200304.

Man-sheng C, Zheng-gen L, Zhao-cai W, Jun-ichiro Y. 2011. Fundamental study on carbon composite iron ore hot briquette used as blast furnace burden. Steel Res Int. 82:521–528. https://doi.org/10.1002/srin.201100044.

Nicol S, Chen J, Pownceby MI, Webster NAS. 2018. A review of the chemistry, structure and formation conditions of silico-ferrite of calcium and aluminum ('SFCA') phases. ISIJ Int. 58(12):2157–2172. https://doi.org/10.2355/isijinternational.ISIJINT-2018-203.

Pascoal AL, Rossoni HAV, Kaffash H, Tangstad M, Henriques AB. 2022. Study of the physical behaviour and the carbothermal reduction of self-reducing briquettes developed with iron ore fines, charcoal and silica fume residues. Sustainability. 14(17):10963. https://doi.org/10.3390/su141710963.

Pigołowska M, Kurc B, Rymaniak Ł, Lijewski P, Fuć P. 2020. Kinetics and thermodynamics of thermal degradation of different starches and estimation the OH group and H_2O content on the surface by TG/DTG-DTA. Polymers. 12(2):357. https://doi.org/10.3390/polym12020357.

Sah R, Dutta SK. 2010. Effects of binder on the properties of iron ore–coal composite pellets. Miner Process Extr Metall Rev. 31:73–85. https://doi.org/10.1080/08827500903404732.

Takano C, Mourão MB. 2003. Self-reducing pellets for ironmaking: Mechanical behavior. Miner Process Extr Metall Rev. 24:233–252. https://doi.org/10.1080/714856823.

Wang G et al. 2026. Application feasibility of corn cob hydrolyzed residues in blast furnace injection: Physicochemical, combustion behaviors and kinetics. Biomass Bioenergy. 205:108529. https://doi.org/10.1016/j.biombioe.2026.108529.

Wei R, Cang D, Bai Y, Huang D, Liu X. 2016. Reduction characteristics and kinetics of iron oxide by carbon in biomass. Ironmak Steelmak. 43(2):144–152. https://doi.org/10.1179/1743281215Y.0000000061.

Wei R, Peng Z, Wang J, Xue Q, Zuo H. 2025. Waste crayfish shell addition improves mechanical strength and reducibility of hematite briquettes. Biomass Bioenergy. 201:108107. https://doi.org/10.1016/j.biombioe.2025.108107.

Wu S, Chang F, Zhang J, Lu H, Kou M. 2017. Cold strength and high temperature behaviors of self-reducing briquette containing electric arc furnace dust and anthracite. ISIJ Int. 57(8):1364–1373. https://doi.org/10.2355/isijinternational.ISIJINT-2017-013.

Ye L, Zhang J, Yu J, Xu R, Dang H. 2023. Evolution behavior and kinetic analysis of vacuum extruded iron-rich dust briquette in blast furnace. J Clean Prod. 433:139753. https://doi.org/10.1016/j.jclepro.2023.139753.

Yokoyama H, Higuchi K, Ito T, Oshio A. 2012. Decrease in carbon consumption of a commercial blast furnace by using carbon composite iron ore. ISIJ Int. 52(11):2000–2006. https://doi.org/10.2355/isijinternational.52.2000.

5. CONSIDERAÇÕES FINAIS

No presente trabalho, foi avaliado o desempenho de redução e de resistência mecânica de briquetes autorredutores produzidos com *pellet feed* e biochar derivado do bagaço de cana-de-açúcar, visando sua aplicação como carga ferrosa complementar em altos-fornos.

A caracterização da biomassa bruta e dos biochars obtidos após pirólise em diferentes temperaturas evidenciou o aumento da área superficial e do volume de poros, especialmente a 550 °C, acompanhado da redução do diâmetro médio dos poros devido à formação de microporos e nanoporos. A análise termogravimétrica dos biochars permitiu correlacionar seus resultados com as respectivas composições, especialmente matéria volátil e carbono fixo, enquanto as análises de FTIR e microscopia revelaram a decomposição dos principais componentes da biomassa (hemicelulose e celulose) e a degradação progressiva da estrutura carbonizada em função da temperatura. Esses resultados demonstram que a temperatura de pirólise é um fator determinante no controle da composição, da morfologia e do comportamento térmico dos biochars, influenciando diretamente o desempenho de briquetes autorredutores.

A partir da caracterização dos briquetes contendo biochars pirolisados em diferentes temperaturas e produzidos em escala laboratorial, as análises de Mössbauer evidenciaram que os briquetes B250 apresentaram redução mais pronunciada até 600 °C, efeito atribuído ao mecanismo de redução por voláteis. Por outro lado, teores mais elevados de carbono fixo, como em B550, resultaram em maior perda de massa total e metalização. Considerando os parâmetros operacionais dos altos-fornos, nos quais a transformação da hematita em wustita na zona de preparação representa a condição ideal para o bom desempenho do processo, todos os briquetes avaliados demonstraram elevada eficiência de redução, com ferro metálico detectado a 950 °C, o que poderia resultar em menor consumo de combustível, especialmente no caso do B550. Nessa temperatura, B400 e B550 exibiram um comportamento de metalização similar (35% e 39%, respectivamente). Contudo, com o aumento da temperatura de aquecimento, B550 apresentou um grau de metalização superior, atingindo 86% a 1250 °C em comparação com o valor de 28% em B250, indicando maior desempenho de redução em temperaturas mais elevadas. A análise dos gases gerados revelou a alta reatividade dos biochars, resultando em elevada pressão parcial de CO a partir de 950 °C, condição termodinamicamente suficiente para reduzir wustita a ferro metálico.

Quanto ao desempenho mecânico, os briquetes apresentaram comportamentos distintos em função da temperatura de pirólise e de aquecimento. B550 apresentou a maior resistência inicial, enquanto os ensaios interrompidos indicaram uma resistência mínima de todos os briquetes em 950 °C. Durante o aquecimento, B400 e B550 exibiram um inchamento significativo, especialmente após o período de isoterma em 950 °C, atingindo níveis máximos em 1100 °C. Por outro lado, B250 manteve sua integridade física e geométrica, evidenciando uma tendência ao inchamento em função do aumento da temperatura de pirólise da biomassa. A maior magnitude desse fenômeno observada em B550 pode ser atribuída ao aumento da pressão interna decorrente da intensa geração de gases durante a autorredução, ao maior grau de redução com consequente formação de *whiskers* de ferro metálico e ao maior teor de cinzas no biochar pirolisado a 550 °C.

Após aquecimento a 1250 °C, os briquetes apresentaram contração volumétrica e aumento da resistência mecânica, associados à coalescência e sinterização das partículas de ferro metálico e à formação de uma fase de escória. B400 alcançou o maior índice de contração (69% do volume inicial) e uma resistência (3253 N) três vezes superior à dos demais briquetes, resultado da redução interna uniforme e de uma distribuição homogênea das partículas de ferro, o que promoveu uma estrutura mais sinterizada e coesa. Em contraste, a formação de ferro metálico preferencialmente na superfície externa de B550 foi associada a um menor índice de contração (45%), o que, combinado ao maior inchamento desses briquetes, resultou em uma menor coesão estrutural e menor resistência em altas temperaturas. Esses resultados evidenciam o potencial da micro-CT como uma ferramenta valiosa para identificar e correlacionar alterações microestruturais com o desempenho de briquetes sob diferentes condições térmicas.

O estudo ampliou a investigação sobre o uso de biomassa em briquetes autorredutores, ao avaliar a influência do teor de biochar sobre o desempenho desses aglomerados em escala piloto, contendo 5–15% em massa de bagaço de cana-de-açúcar pirolisado a 400 °C. A análise de gases corroborou os resultados de perda de massa e enfatizou a interdependência das reações de autorredução. Em ambas as atmosferas avaliadas (inerte e redutora), observaram-se maiores índices de perda de massa total e metalização nos briquetes com maior teor de biochar (B15), com valores substancialmente superiores aos do B05. Todos os briquetes apresentaram ferro metálico a 950 °C, com níveis de redução crescentes à medida que a temperatura e o teor de biochar aumentavam, reforçando a importância do carbono para a efetiva redução dos óxidos

de ferro. Teores desprezíveis de carbono (< 0,1%) foram identificados em B05 a 1150 °C, evidenciando a limitada redução desses briquetes, em razão da menor disponibilidade de carbono. A atmosfera redutora favoreceu o aumento da perda de massa e do grau de metalização dos briquetes. No entanto, B10 e B15 também apresentaram valores expressivos de metalização em atmosfera inerte (76% e 90%, respectivamente, a 1150 °C), comprovando a efetividade das reações de autorredução promovidas pelo carbono sólido proveniente do biochar na redução dos briquetes. Em comparação com sinter e pelota, os briquetes apresentaram eficiência de redução consideravelmente superior.

Na condição em que foram recebidos, os briquetes exibiram menor resistência com o aumento do teor de biochar, enquanto em altas temperaturas, B10 apresentou o melhor desempenho mecânico. Os resultados indicaram uma formação substancial de ferro metálico nesses aglomerados, sem gerar pressão interna excessiva resultante da geração de gás. A menor resistência observada nos demais briquetes está relacionada com a baixa metalização em B05 e com a presença de carbono residual e acumulação de gases em B15.

Esta Tese evidenciou a influência da temperatura de pirólise e do teor de biochar sobre o desempenho metalúrgico e a integridade mecânica de briquetes autorredutores. Ao considerar de forma conjunta os parâmetros fundamentais para aplicação em altos-fornos, briquetes com biochar pirolisado a 400 °C e teor de 10% mostraram-se mais favoráveis. Embora B550 tenha apresentado maiores índices de redução e metalização, especialmente em temperaturas elevadas, seu comportamento foi acompanhado por inchamento acentuado e menor resistência mecânica. Já B400 manteve um desempenho de redução comparável ao de B550 até 950 °C, exibindo, também, maior resistência em altas temperaturas, conferindo melhor estabilidade estrutural. Ademais, 10% de biochar proporcionou um equilíbrio quanto à eficiência de redução e integridade estrutural dos briquetes. Os resultados obtidos nesse estudo fornecem subsídios científicos e tecnológicos para a otimização do uso de biomassa tratada termicamente (biochar) como agente redutor em briquetes autorredutores, contribuindo para a substituição parcial de fontes fósseis de carbono na indústria siderúrgica e para o desenvolvimento de cargas complementares mais eficientes para altos-fornos.

6. CONTRIBUIÇÕES ORIGINAIS AO CONHECIMENTO

O estudo permitiu analisar, de forma inovadora, a influência da temperatura de pirólise da biomassa sobre o desempenho de redução, a resistência mecânica e o comportamento estrutural (inchamento e contração) dos briquetes em diferentes etapas de redução. Ademais, investigou briquetes autorredutores produzidos em escala piloto a partir de diferentes teores de biochar de bagaço de cana-de-açúcar, possibilitando a avaliação de sua resposta em condições mais representativas da aplicação industrial. A partir dessas abordagens, foram determinadas as condições de pirólise mais favoráveis que, em conjunto com teores adequados de incorporação de biochar na formulação dos briquetes, visam maximizar os índices de desempenho e requisitos operacionais dos altos-fornos. Nesse contexto, estabeleceram-se parâmetros consistentes capazes de atender às solicitações desses aglomerados, consolidando o uso do biochar como agente redutor e ampliando o aproveitamento da biomassa em processos siderúrgicos.

Outra contribuição relevante deste trabalho refere-se à indicação de que a composição e as propriedades do biochar podem influenciar significativamente os fenômenos envolvidos no processo de redução em sistemas autorredutores e na manutenção da integridade mecânica dos briquetes. Os resultados sugeriram a influência da desvolatilização sobre a geração de poros e consequente ganho de redutibilidade. A liberação de voláteis não apenas favorece a transformação dos óxidos de ferro, como também pode promover o incremento da porosidade interna dos briquetes, facilitando a difusão de gases externos e elevando a eficiência do processo. Esse comportamento foi principalmente evidenciado pela maior presença de magnetita nos briquetes com maior teor de biochar (maior teor de voláteis) nos ensaios realizados a 600 °C sob atmosfera redutora.

Ao comparar diferentes atmosferas nos ensaios, os dados de perda de massa e de metalização evidenciaram a predominância da redução pelo carbono sólido proveniente do biochar em relação à contribuição da atmosfera externa. Esses resultados destacam a elevada reatividade do biochar empregado nos briquetes produzidos em escala piloto (bagaço de cana-de-açúcar obtido após pirólise a 400 °C) e reforçam sua importância para a eficiência global do processo de redução em briquetes autorredutores.

Adicionalmente, esse estudo destacou a articulação entre a análise dos gases gerados e o comportamento dos briquetes durante a redução, enfatizando a interdependência das reações de autorredução e a reatividade dos biochars. A quantificação da geração de gases em função da temperatura de pirólise e do teor de biochar sugeriu variações na pressão interna desenvolvida durante a liberação de gases oriundos das reações de desvolatilização e autorredução, que podem influenciar diretamente a resistência mecânica dos briquetes e o comportamento de inchamento.

Observou-se, também, a formação de ferro metálico em temperaturas relativamente baixas (identificadas nos ensaios a 950 °C), inclusive em comparação com matérias-primas tradicionalmente empregadas em altos-fornos. Esse comportamento é decorrente da redução promovida pelo carbono derivado do biochar em contato íntimo com os óxidos de ferro, podendo contribuir para o aumento da eficiência na zona de preparação do alto-forno.

No âmbito tecnológico, esta Tese apresentou as vantagens e limitações da microtomografia de raios X como ferramenta para correlacionar a estrutura interna e o desempenho de redução e de resistência mecânica de briquetes autorredutores contendo biochar. Por ser uma técnica ainda pouco explorada na análise desses aglomerados, sua utilização revelou-se particularmente relevante ao aprofundar a compreensão do comportamento estrutural desses materiais ao longo do processo de redução. Dessa forma, este trabalho contribui não apenas para o entendimento fenomenológico do comportamento dos briquetes autorredutores, mas também estabelece uma base metodológica consistente para investigações futuras e para a otimização do desempenho desses aglomerados em altos-fornos.

7. CONTRIBUIÇÕES PARA A LITERATURA

7.1. Publicações geradas a partir da presente Tese

7.1.1. Artigos publicados em periódicos

Leão, P.M.G.C., Ardisson, J.D., Zicker, T.B., Ferreira, N.H.A., Bagatini, M.C., 2026. Influence of biomass pyrolysis temperature on the performance of self-reducing briquettes for use in blast furnaces. Biomass and Bioenergy 206, 108691. https://doi.org/10.1016/j.biombioe.2025.108691.

7.1.2. Artigos submetidos a periódicos

Leão, P.M.G.C., Oliveira, I.G., Issac, A., Bagatini, M.C., 2026. Structural behavior of self-reducing briquettes containing biochar pyrolyzed at different temperatures. Journal of Materials Research and Technology.

Leão, P.M.G.C., Bagatini, M.C. Reduction and mechanical strength performance of self-reducing briquettes with different biochar contents. Mineral Processing and Extractive Metallurgy Review.

7.1.3. Artigos publicados em anais de congressos

Leão, P.M.G.C., Zicker, T.B., Ferreira, N.H.A., Neta, A.C.I., Ardisson, J.D., Bagatini, M.C. Mechanical properties and reduction behavior of self-reducing briquettes with biomass treated in different temperatures. In: 10th International Congress on the Science and Technology of Ironmaking Conference (ICSTI 2025), 2025. Beijing, China. p. 482–489.

Leão, P.M.G.C., Zicker, T.B., Gonçalves, M.V.B., Parreira, F.V., Maranha, S.P.D., Bagatini, M.C. Influência da proporção de biochar no desempenho de redução e resistência mecânica de briquetes autorredutores. In: ABM Week, 2025, São Paulo, Brasil. Anais do 53º Seminário de Redução de Minérios e Matérias-Primas, 2025. v. 53. p. 632–644. 10.5151/2594-357X-42644.

Zicker, T.B., Leão, P.M.G.C., Bagatini, M.C. Investigação do fenômeno de inchamento em briquetes autorredutores com biomassa pirolisada a diferentes temperaturas. In: ABM Week, 2025, São Paulo, Brasil. Anais do 23º Enemet - Encontro Nacional de Estudantes de Engenharia Metalúrgica, de Materiais e de Minas, 2025. v. 23. p. 695–706. 10.5151/2594-4711-42760.

Ferreira, N.H.A., Leão, P.M.G.C., Bagatini, M.C. Análise termogravimétrica de misturas autorredutoras contendo biomassa tratada em diferentes temperaturas. In: ABM Week, 2024, São Paulo, Brasil. Anais do 52º Seminário de Redução de Minérios e Matérias-Primas, 2024. v. 52. p. 567–580. 10.5151/2594-357X-41531.

Leão, P.M.G.C., Neta, A.C.I., Bagatini, M.C. Utilização da técnica de microtomografia de raios X na caracterização de briquetes autorredutores. In: ABM Week, 2024, São Paulo, Brasil. Anais do 10º Seminário de Aglomeração de Minérios, 2024. v. 10. p. 345–357. 10.5151/2594-357X-41465.

Leão, P.M.G.C., Zicker, T.B., Ardisson, J.D., Bagatini, M.C. Influência da temperatura de pirólise da biomassa sobre o desempenho de briquetes autorredutores para uso em altos-fornos. In: ABM Week, 2024, São Paulo, Brasil. Anais do 52º Seminário de Redução de Minérios e Matérias-Primas, 2024. v. 52. p. 384–397. 10.5151/2594-357X-41176.

Pereira, L.M., Bagatini, M.C., Leão, P.M.G.C. Resistência mecânica de briquetes autorredutores com diferentes proporções de biomassa e temperatura de pirólise. In: ABM Week, 2024, São Paulo, Brasil. Anais do 22º Enemet - Encontro Nacional de Estudantes de Engenharia Metalúrgica, de Materiais e de Minas, 2024. v. 22. p. 768–777. 10.5151/2594-4711-41546.

7.2. Outras publicações no decorrer da formação acadêmica

7.2.1. Artigos publicados em periódicos

Flores, I.V., Leão, P.M.G.C., Alves, J.V.S., Assis, O.H.M., Bagatini, M.C., 2025. Reduction, softening, and melting characteristics of mill scale-based briquettes for blast furnace ironmaking. Steel Research International. https://doi.org/10.1002/srin.202500921.

Silva, A.M.B., Leão, P.M.G.C., Rodrigues, O.O., Lemos, L.R., Bagatini, M.C., 2025. Physical and numerical modelling permeability of blast furnace shaft zone with iron ore briquettes. Ironmaking & Steelmaking, 1–15. https://doi.org/10.1177/03019233251357178.

7.2.2. Artigos publicados em anais de congressos

Silva, A.M.B., Leão, P.M.G.C., Rodrigues, O.O., Lemos, L.R., Bagatini, M.C. Permeabilidade de leitos de cargas ferrosas com adição de briquetes. In: ABM Week, 2025, São Paulo, Brasil. Anais do 53º Seminário de Redução de Minérios e Matérias-Primas, 2025. v. 53. p. 312–324. 10.5151/2594-357X-42166.

Duarte, I.G., Santos, M.L.D., Leão, P.M.G.C., Ribeiro, M.A., Bagatini, M.C. Resistência mecânica de briquetes de pó e lama de aciaria para uso em conversor LD. In: ABM Week, 2023, São Paulo, Brasil. Anais do 76º Congresso Anual da ABM - Internacional, 2023. v. 76. p. 279–291. 10.5151/2594-5327-40253.

Leão, P.M.G.C., Ferreira, N.H.A., Brandão, P.R.G. Estudo do grau de dispersão do carvão vegetal com ensaios de sedimentação: influência do pH e da dosagem de reagente. In: ABM Week, 2023, São Paulo, Brasil. Anais do 76º Congresso Anual da ABM - Internacional, 2023. v. 76. p. 317–330. 10.5151/2594-5327-39497.

Ribeiro, M.A., Leão, P.M.G.C., Bagatini, M.C., Impacto do uso de briquetes de resíduos no LD sobre as emissões de gases de efeito estufa. In: ABM Week, 2023, São Paulo, Brasil. Anais do 76º Congresso Anual da ABM - Internacional, 2023. v. 76. p. 304–316. 10.5151/2594-5327-40303.

Santos, M.L.D., Duarte, I.G., Leão, P.M.G.C., Ribeiro, M.A., Bagatini, M.C. Análise termoquímica de briquetes de resíduos de aciaria para uso em conversor LD. In: ABM Week, 2023, São Paulo, Brasil. Anais do 76º Congresso Anual da ABM - Internacional, 2023. v. 76. p. 251–264. 10.5151/2594-5327-40241.

Leão, P.M.G.C., Parreira, F.V., Dutra, F.C., Maranha, S., Vieira, C.B., Silva, G.H.T.A. Uma revisão sobre a produção de aglomerados de rejeitos da mineração de minério de ferro e carvão

coqueificável para uso em reatores de redução. In: ABM Week, 2019, São Paulo, Brasil. Anais do 49º Seminário de Redução de Minério de Ferro e Matérias-Primas, 2019. v. 7. p. 126–137. 10.5151/2594-357X-33519.

Leão, P.M.G.C., Rodrigues, E.F., Silva, C.A., Silva, I.A., Seshadri, V. Influence of physical properties of slag and operational parameters on slag splashing process in an oxygen converter. In: Advances in Molten Slags, Fluxes, and Salts, 2016. Proceedings of the 10th International Conference on Molten Slags, Fluxes and Salts, 2016. Springer International Publishing, 2016. p. 1043–1051. http://dx.doi.org/10.1007/978-3-319-48769-4_111.

Leão, P.M.G.C., Rodrigues, E.F., Silva, C.A., Silva, I.A. Um estudo sobre a influência de propriedades físicas da escória e de parâmetros operacionais sobre o processo de slag splashing. In: ABM Week, 2015, Rio de Janeiro, Brasil. Anais do 46º Seminário de Aciaria - Internacional, 2015. v. 46. p. 583–592. 10.5151/1982-9345-26898.

8. SUGESTÕES PARA TRABALHOS FUTUROS

Entre os principais pontos recomendados para a realização de pesquisas futuras, seja em relação aos tópicos já abordados ou àqueles ainda não explorados, destacam-se:

- Reatividade do biochar: avaliar a reatividade dos diferentes biochars empregados na composição dos briquetes por meio de ensaios de gaseificação ao CO_2 e sua influência sobre a eficiência de redução e a cinética das reações de autorredução;

- Exploração de diferentes fontes de biomassa: avaliar o uso de outras fontes de biomassa e misturas de biochars, visando à identificação de combinações que possam otimizar a eficiência de redução e a resistência mecânica dos briquetes, considerando, adicionalmente, aspectos relacionados à disponibilidade regional e aos custos envolvidos;

- Efeito da atmosfera contendo H_2: avaliar a influência do H_2 como gás redutor no processo de redução dos briquetes, explorando seu potencial como rota siderúrgica de menor impacto ambiental e reduzido potencial de emissão de CO_2;

- Avaliação complementar do desempenho metalúrgico e mecânico dos briquetes: ampliar a caracterização do comportamento metalúrgico dos briquetes, incluindo a determinação do índice de degradação sob redução (RDI), redutibilidade (RI) e crepitação, além da realização de testes adicionais de resistência mecânica, como shatter test e tumbler test;

- Avaliação da porosidade dos briquetes: investigar a evolução da porosidade dos briquetes nos diferentes estágios de aquecimento, correlacionando a estrutura porosa e a distribuição do tamanho dos poros com a reatividade e o desempenho durante o processo de redução;

- Análise cinética: investigar os parâmetros cinéticos que influenciam a redução dos briquetes em sistemas autorredutores, correlacionando-os às condições de pirólise da biomassa e às variações no teor de biochar, com o objetivo de compreender sua influência sobre a eficiência de redução;

- Escala industrial: recomenda-se a validação dos resultados em escala industrial, incluindo testes em alto-forno, com o objetivo de avaliar o desempenho dos briquetes em condições operacionais realistas, complementando os dados obtidos em escala laboratorial e piloto;

- Impacto ambiental e ciclo de vida: avaliar o ciclo de vida e o impacto ambiental associados ao uso de biochar em briquetes autorredutores, considerando as emissões de gases de efeito estufa (CO_2), o carbono incorporado, o consumo e a eficiência energética, a utilização de recursos, a disponibilidade de matérias-primas e os benefícios ambientais, em comparação com processos e cargas tradicionalmente empregados em altos-fornos, contribuindo para a sustentabilidade do processo siderúrgico.

APÊNDICE A - Aspecto macroscópico da seção transversal dos briquetes produzidos em escala piloto

As Figuras A.1 e A.2 apresentam uma visão macroscópica dos briquetes seccionados na direção transversal, antes e após ensaios interrompidos conduzidos em atmosferas inerte e redutora, permitindo a observação, a olho nu, das regiões internas dos aglomerados estudados. Trata-se de uma análise dos briquetes produzidos em escala piloto com diferentes teores de biochar, conforme investigado no Capítulo 4 desta Tese.

A análise das superfícies seccionadas evidencia diferenças estruturais e variações de tonalidade ao longo da seção transversal dos briquetes, bem como a formação de trincas e de heterogeneidades internas. Tais características estão diretamente relacionadas aos teores de biochar e às diferentes temperaturas de aquecimento aplicadas, evidenciando como a composição e as condições térmicas influenciam o comportamento dos briquetes. Essas observações podem refletir em diferenças nos índices de resistência mecânica, no comportamento de redução (modelo reacional) e na expansão volumétrica, demonstrando que os briquetes apresentam respostas estruturais e reacionais específicas em função de sua formulação e do regime térmico adotado.

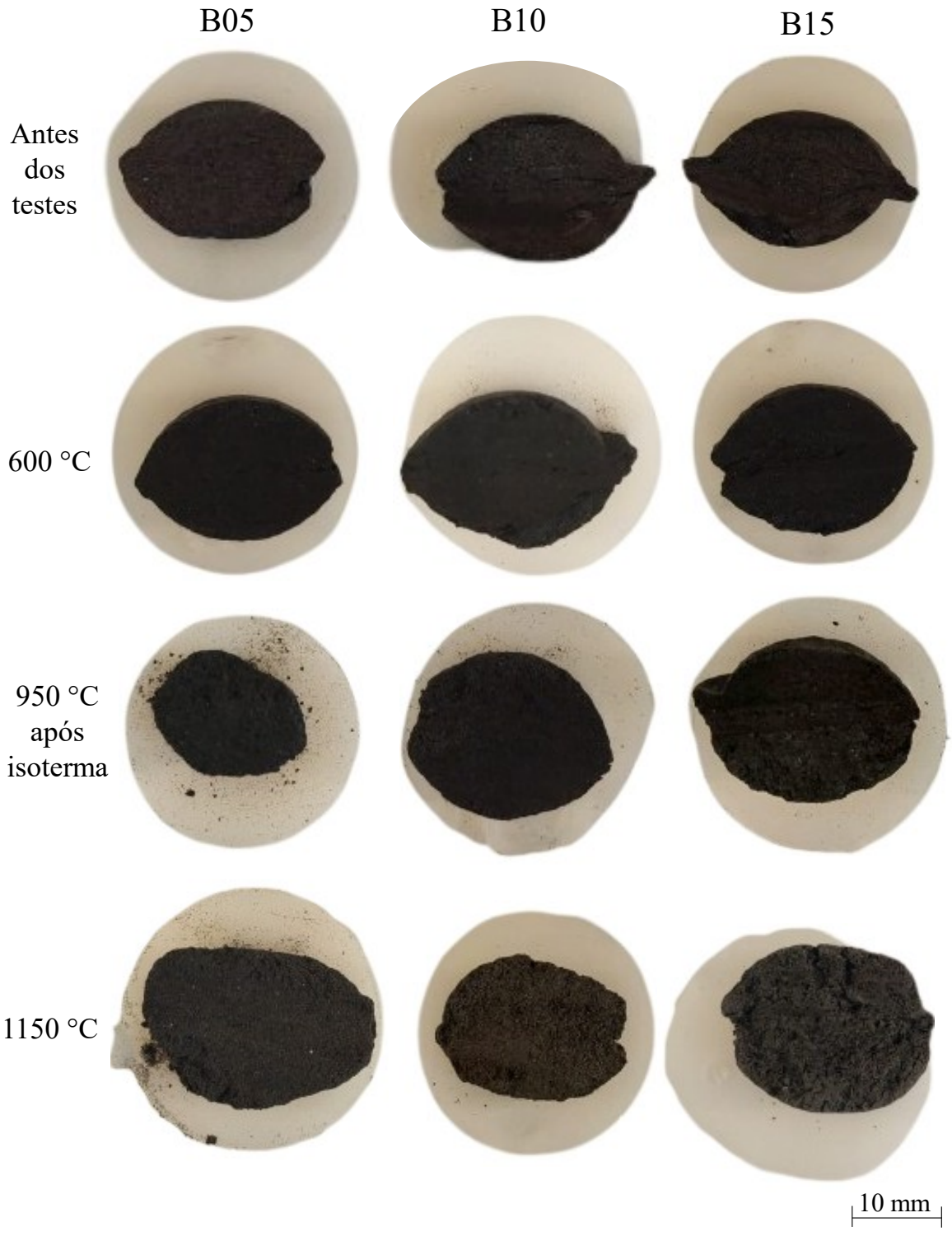

Figura A.1. Aspecto visual da seção transversal dos briquetes antes e após ensaios interrompidos em atmosfera inerte.

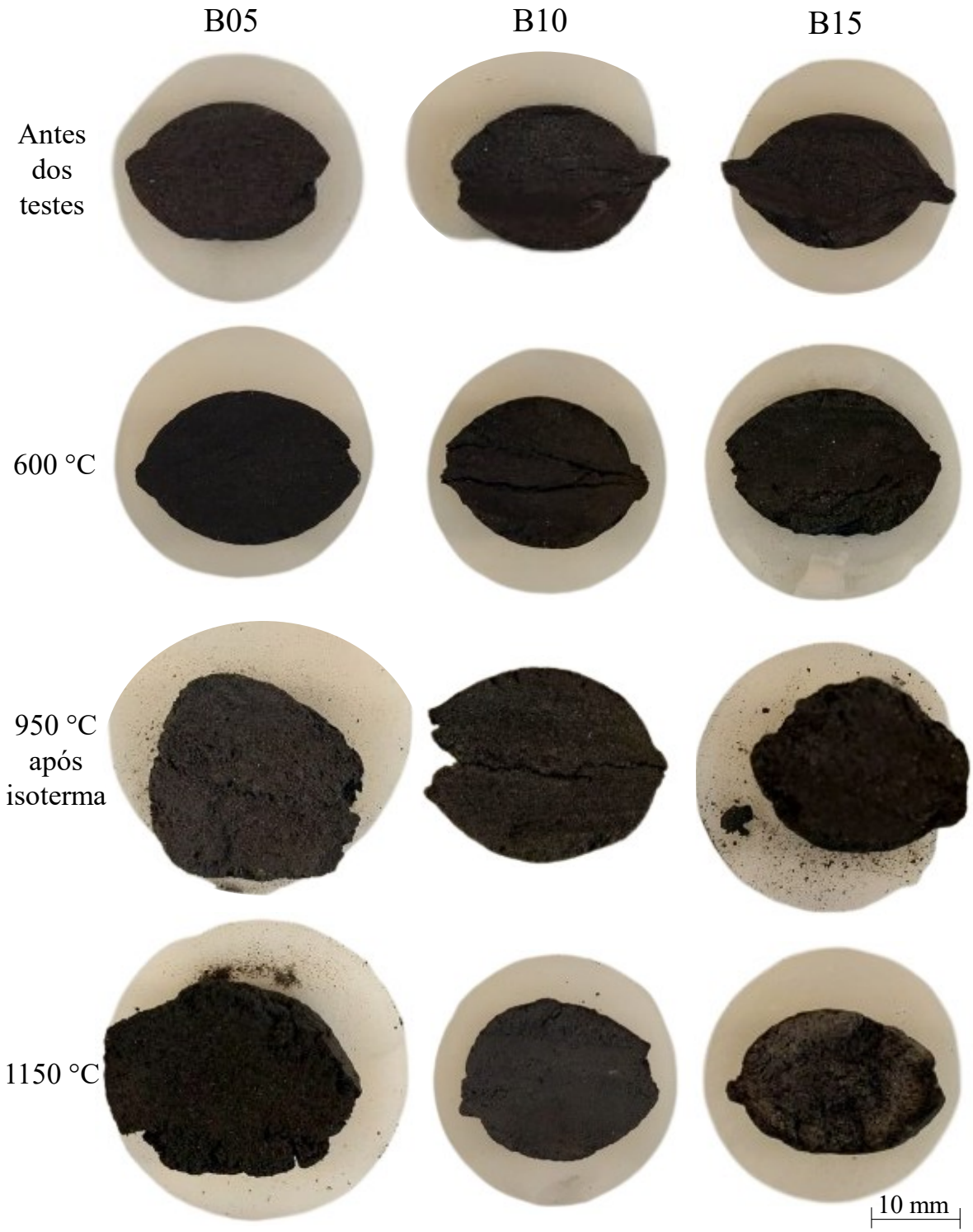

Figura A.2. Aspecto visual da seção transversal dos briquetes antes e após ensaios interrompidos em atmosfera redutora.

APÊNDICE B - Perda de massa teórica e fração reagida

Além das curvas experimentais apresentadas nas Figuras 2.4 e 4.5, a perda de massa total teórica dos briquetes produzidos com biochars pirolisados em diferentes temperaturas (Capítulo 2) e em teores variáveis (Capítulo 4) também é apresentada nas Figuras B.1 e B.2, respectivamente, sendo representada pelas linhas tracejadas correspondentes. A perda de massa teórica foi calculada considerando os fenômenos de desidratação, decomposição dos aglomerantes, desvolatilização e autorredução, conforme detalhado nas Tabelas B.1 e B.2. As contribuições referentes à matéria volátil e ao carbono fixo foram determinadas com base nas Tabelas 2.2 e 4.2, bem como na quantidade de biochar adicionada em cada formulação, enquanto o oxigênio disponível para reação corresponde ao oxigênio associado ao ferro presente no *pellet feed* e à sua fração nos aglomerados. A autorredução foi estimada assumindo-se o consumo completo do carbono fixo e do oxigênio redutível. Essa abordagem possibilitou a comparação direta entre os resultados experimentais e teóricos, fornecendo suporte à interpretação dos comportamentos observados.

Na Figura B.1, os briquetes B250 apresentaram a maior discrepância entre as perdas de massa teórica e experimental, não atingindo o valor máximo estimado. Em temperaturas mais baixas, a maior perda de massa foi atribuída à desvolatilização mais intensa do biochar tratado a 250 °C. Em contrapartida, em temperaturas mais elevadas, os valores experimentais foram significativamente inferiores aos teóricos, indicando a ocorrência de autorredução incompleta. Esse comportamento pode estar associado à limitada disponibilidade de reagentes nesses aglomerados, particularmente ao menor teor de carbono fixo, o que pode ter interrompido as reações de autorredução e, consequentemente, restringido a perda de massa adicional. Por outro lado, os briquetes produzidos com biochars pirolisados a 400 °C (B400) e 550 °C (B550) apresentaram maior concordância entre os resultados teóricos e experimentais, sugerindo maior extensão das reações de autorredução. Contudo, apenas os briquetes B550 atingiram a perda de massa máxima estimada, provavelmente em função da maior quantidade de carbono fixo para reação, evidenciando o papel fundamental do carbono no processo de redução.

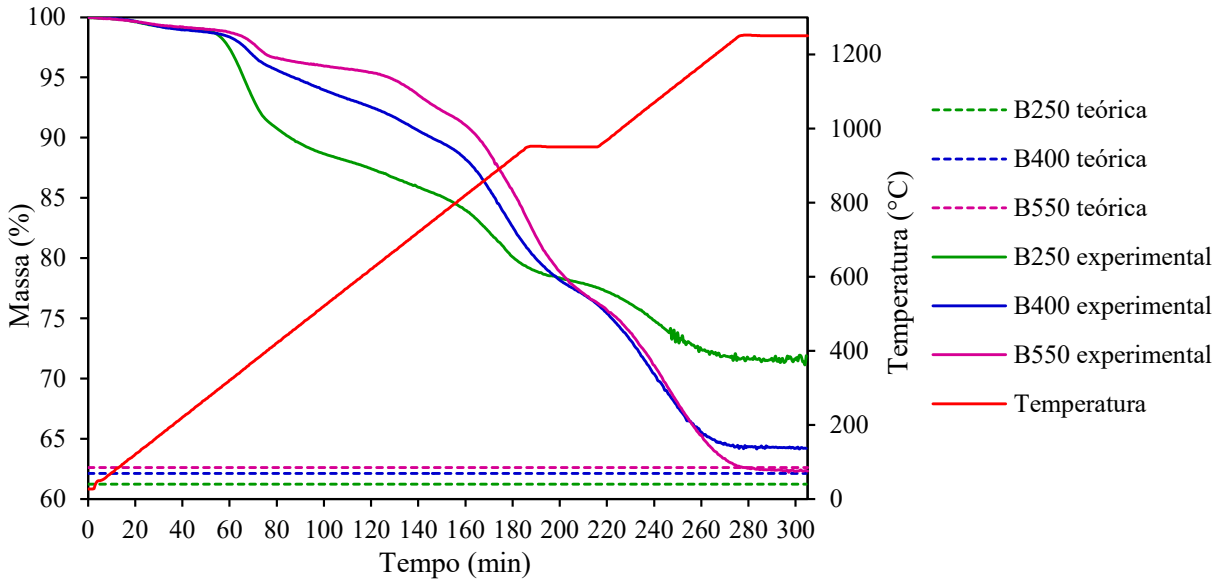

Figura B.1. Perdas de massa experimental e teórica dos briquetes produzidos com biochars pirolisados em diferentes temperaturas.

Tabela B.1. Perda de massa teórica (%) dos briquetes produzidos com biochars pirolisados em diferentes temperaturas.

Briquete	Desidratação	Matéria volátil	Autorredução		Perda de massa total
			Carbono fixo	Oxigênio redutível	
B250	3,80	11,15	3,44	20,38	38,77
B400	3,70	3,96	9,85	20,38	37,89
B550	3,29	2,28	11,43	20,38	37,38

A análise da perda de massa dos briquetes contendo teores variáveis de biochar, apresentada na Figura B.2, indicou que apenas os briquetes B15 (15% de biochar) atingiram a perda de massa total estimada, reforçando o papel crítico do carbono no desempenho desses aglomerados. Em contrapartida, B05 e B10 não alcançaram o valor máximo estimado, o que pode ser atribuído especialmente à quantidade insuficiente de carbono para remover completamente o oxigênio disponível, sugerindo que, nessas formulações, as reações de redução não evoluíram até o seu limite estequiométrico, resultando em conversão parcial dos óxidos de ferro.

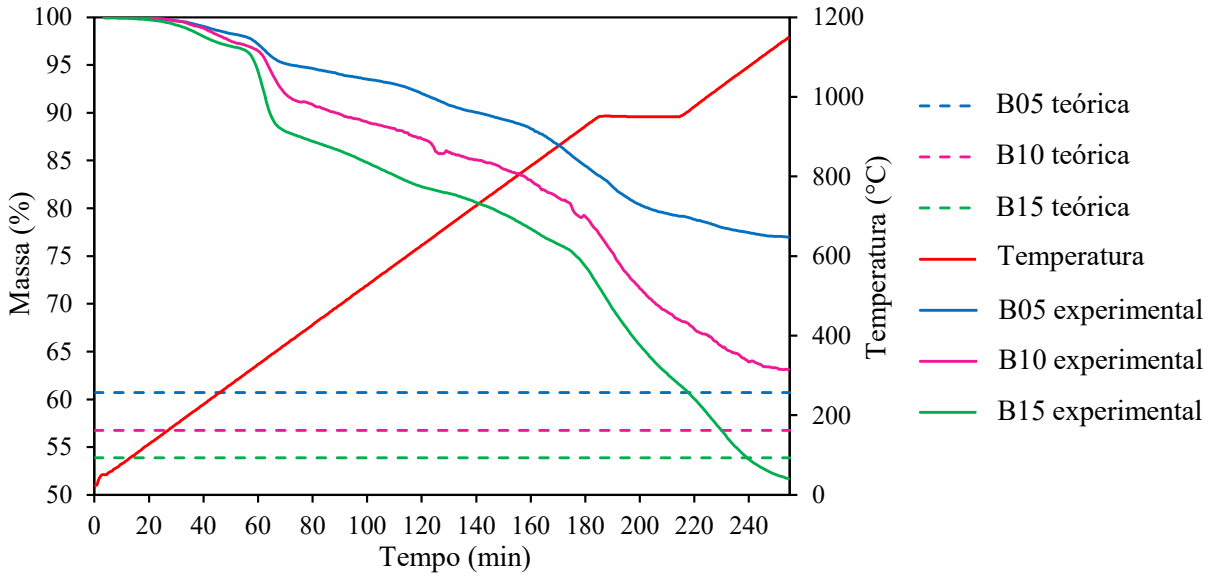

Figura B.2. Perdas de massa experimental e teórica dos briquetes contendo diferentes teores de biochar.

Tabela B.2. Perda de massa teórica (%) dos briquetes contendo diferentes teores de biochar.

Briquete	Desidratação	Decomposição aglomerantes	Matéria volátil	Autorredução		Perda de massa total
				Carbono fixo	Oxigênio redutível	
B05	1,54	8,0	1,44	3,13	25,18	39,29
B10	2,39	8,0	2,88	6,26	23,70	43,23
B15	2,20	8,0	4,32	9,39	22,22	46,13

Uma avaliação mais detalhada dos resultados experimentais de perda de massa possibilitou calcular a fração reagida dos briquetes com diferentes teores de biochar, conforme apresentado na Figura B.3. Com base nos dados obtidos nos ensaios interrompidos, determinou-se a fração reagida máxima em cada intervalo de temperatura, relacionando a perda de massa medida ao valor teórico total estimado para cada formulação. Foram observadas apenas pequenas variações entre as atmosferas avaliadas, refletindo a predominância das reações de autorredução conduzidas pelo carbono sólido derivado do biochar. Embora exista uma competição entre os dois agentes redutores disponíveis (CO fornecido pelo gás de entrada e CO gerado pela gaseificação do carbono sólido), o carbono em contato íntimo com os óxidos de ferro mostrou-se mais eficiente do que a atmosfera redutora externa.

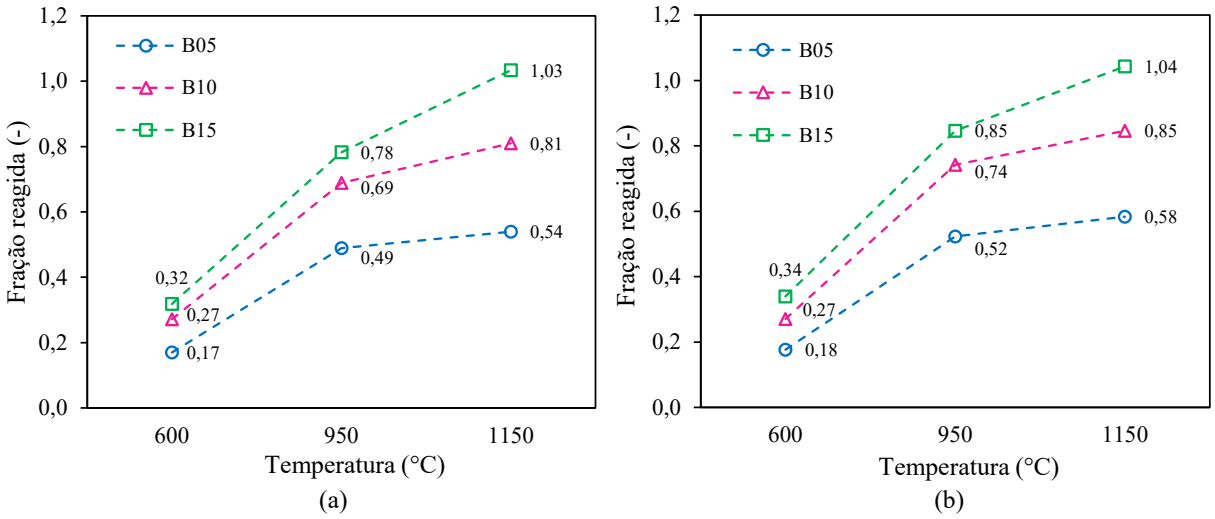

Figura B.3. Fração reagida dos briquetes contendo diferentes teores de biochar após ensaios interrompidos em (a) atmosfera inerte e (b) atmosfera redutora.

APÊNDICE C - Macrotermobalança X Termobalança convencional

Uma análise comparativa entre os dados de perda de massa obtidos nos ensaios em macrotermobalança e aqueles provenientes da análise termogravimétrica convencional foi conduzida a partir dos briquetes produzidos em escala piloto, com diferentes teores de biochar, sob atmosfera inerte de N_2 (Figura C.1). Esses experimentos complementares foram realizados em uma termobalança convencional SDT 650, empregando aproximadamente 11 mg de amostras cominuídas (< 75 µm), aquecidas em um cadinho de alumina a uma taxa de 5 °C/min até 1150 °C sob atmosfera de N_2 e vazão de 100 mL/min. Enquanto a análise convencional exige que as amostras sejam previamente submetidas à cominuição até uma granulometria mais fina, a macrotermogravimetria permite a avaliação dos aglomerados em sua dimensão original. Essa abordagem possibilita a observação de fenômenos que não podem ser capturados em ensaios convencionais, incluindo gradientes de temperatura e de difusão gasosa no interior dos aglomerados, reações químicas que ocorrem ao longo de períodos mais prolongados, colapso estrutural e efeitos de sinterização parcial, além de curvas de perda de massa que representam, de forma mais realista, o comportamento observado em condições industriais.

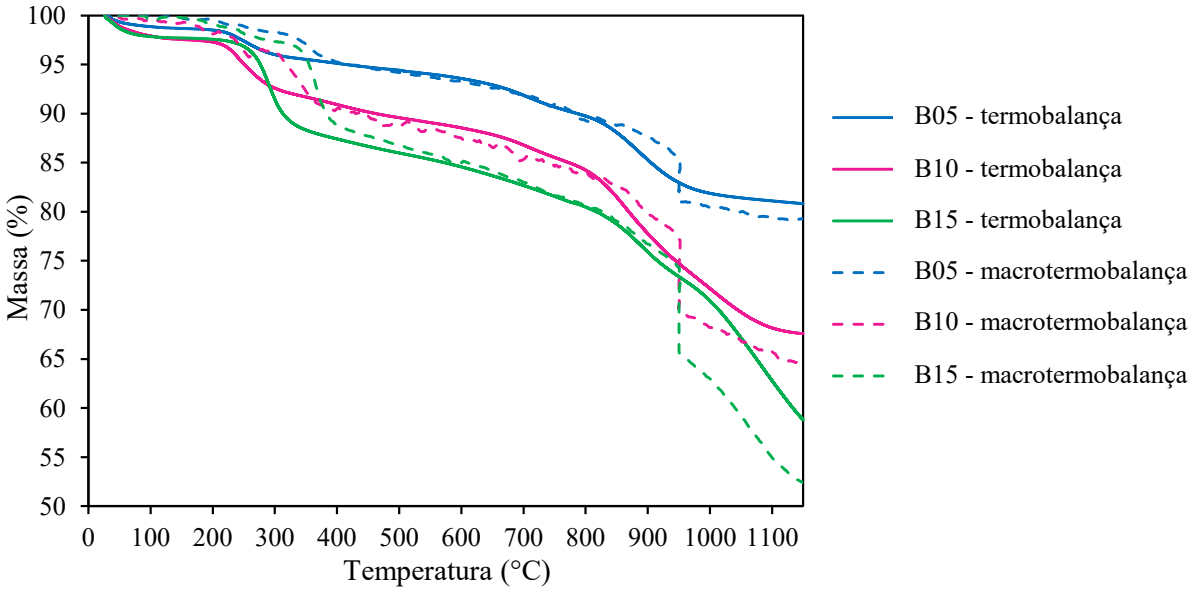

Figura C.1. Comparação entre as curvas de perda de massa dos briquetes obtidas por termogravimetria convencional/termobalança (linhas contínuas) e por macrotermogravimetria/macrotermobalança (linhas tracejadas) sob atmosfera de N_2.

De modo geral, os resultados evidenciaram boa consistência entre as técnicas, indicando que ambas são capazes de captar os principais mecanismos e fenômenos responsáveis pela perda de massa dos briquetes. Conforme esperado, manteve-se a tendência de maior perda de massa nas formulações com maiores teores de biochar, refletindo sua contribuição nas etapas de desvolatilização e de redução. As principais diferenças foram observadas nos estágios iniciais (até 400 °C) e finais (acima de 800 °C) de aquecimento, nos quais a maior área superficial específica, a maior acessibilidade dos gases e a ausência de barreiras difusionais nas amostras de briquetes cominuídas (nos ensaios na termobalança) podem favorecer os fenômenos envolvidos na perda de massa. A maior perda de massa registrada na macrotermobalança em temperaturas superiores a 950 °C é atribuída ao patamar isotérmico aplicado nesses experimentos, o qual não foi empregado nos ensaios termogravimétricos convencionais. Essa condição experimental prolongou o tempo de exposição às reações de autorredução, justificando o desvio característico das curvas tracejadas a partir dessa temperatura.